Università degli Studi di Napoli Federico II

DOTTORATO DI RICERCA IN FISICA

Ciclo XXXVI

Coordinatore: prof. Vincenzo Canale

PHYSICS BEYOND THE STANDARD MODEL AND PRIMORDIAL BLACK HOLES

Settore Scientifico Disciplinare: Fisica Astroparticellare Teorica

Dottorando
Roberta Calabrese

Tutors
Prof. Gennaro Miele
Prof. Stefano Morisi
Dr. Marco Chianese

Anni 2020/2023

Abstract

Of fundamental importance to address the mysteries in cosmology and particle physics is the exploration of the frontiers of physics Beyond the Standard Model. An appealing path to undertake in this fashion is the study of Primordial Black Holes, theoretical Black Holes hypothetically formed shortly after the Big Bang as a byproduct of an array of mechanisms. Depending on their mass, Primordial Black Holes have different impacts on pivotal stages of the Universe's evolution. Thus, information regarding the (non-)existence of Primordial Black Holes may provide valuable insights into these stages. Recently, the topic has been the subject of heated debates, driven by the latest observations of gravitational waves.

This thesis spotlights the sophisticated interaction between Primordial Black Holes and physics Beyond the Standard Model in several contexts. The first part of this manuscript provides a concise review of the state of the art of physics Beyond the Standard Model and Primordial Black Holes, while the second focuses on their interplay in the neutrinos, Dark Matter, and Baryogenesis scenarios. We investigate neutrino and sub-GeV Dark Matter emissions from Primordial Black Hole evaporation and show that they strictly constrain Primordial Black Hole abundance at present. Moreover, while surveying the baryon asymmetry production, we find a peculiar scenario where particle absorption into Primordial Black Holes drives the baryon asymmetry generation. Surprisingly, this scenario works without requiring baryon number violation at the Lagrangian level, violating one of Sakharovs conditions. In the same context, we show a fundamental incompatibility between Primordial Black Holes and thermal Leptogenesis and derive compelling limits in the mixed parameter space.

Dedicated to my parents and siblings.

Remember to look up at the stars and not down at your feet. Try to make sense of what you see and wonder about what makes the universe exist. Be curious. And however difficult life may seem, there is always something you can do and succeed at. It matters that you don't just give up.

STEPHEN W. HAWKING

List of publications

Papers discussed in this thesis

[1] R. Calabrese, M. Chianese, J. Gunn, G. Miele, S. Morisi, and N. Saviano, Phys. Rev. D **107**, 123537 (2023), arXiv:2305.13369 [hep-ph] .

[2] Calabrese, Roberta and Chianese, Marco and Fiorillo, Damiano F. G. and Saviano, Ninetta, Phys. Rev. D **105**, 103024 (2022), arXiv:2203.17093 [hep-ph] .

[3] Calabrese, Roberta and Chianese, Marco and Fiorillo, Damiano F. G. and Saviano, Ninetta, Phys. Rev. D **105**, L021302 (2022), arXiv:2107.13001 [hep-ph] .

[4] Ambrosone, Antonio and Calabrese, Roberta and Fiorillo, Damiano F. G. and Miele, Gennaro and Morisi, Stefano, Phys. Rev. D **105**, 045001 (2022), arXiv:2106.11980 [hep-ph] .

[5] Calabrese, Roberta and Fiorillo, Damiano F. G. and Miele, Gennaro and Morisi, Stefano and Palazzo, Antonio, Phys. Lett. B **829**, 137050 (2022), arXiv:2106.02492 [hep-ph] .

Other papers

[1] R. Calabrese, A. O. M. Iorio, S. Morisi, G. Ricciardi, and N. Vignaroli, (2023), arXiv:2312.02287 [hep-ph] .

[2] R. Calabrese, M. Chianese, J. Gunn, G. Miele, S. Morisi, and N. Saviano, (2023), arXiv:2311.13276 [hep-ph] .

[3] Calabrese, Roberta and Gunn, Jacob and Miele, Gennaro and Morisi, Stefano and Roy, Samiran and Santorelli, Pietro, Phys. Rev. D **107**, 055039 (2023), arXiv:2212.11210 [hep-ph] .

[4] Cacciapaglia, Giacomo and Cagnotta, Antimo and Calabrese, Roberta and Carnevali, Francesco and De Iorio, Agostino and Iorio, Alberto Orso Maria and Morisi, Stefano and Sannino, Francesco, Phys. Rev. D **107**, 055033 (2023), arXiv:2210.07131 [hep-ph] .

[5] Roberta Calabrese, Agostino De Iorio, Damiano F. G. Fiorillo, Alberto Orso Maria Iorio, Stefano Morisi, Gennaro Miele, Phys. Rev. D **104**, 055006 (2021), arXiv:2104.06720 [hep-ph] .

Proceedings

[1] Calabrese, Roberta, J. Phys. Conf. Ser. **2429**, 012033 (2023).

[2] Calabrese, Roberta, J. Phys. Conf. Ser. **2156**, 012127 (2021).

Contents

Introduction

While undertaking a journey into the jungle of particle physics and cosmology, we find ourselves tangled by several captivating enigmas that challenge the boundaries of our comprehension and lead us to delve deeper and deeper into the intricate fabric of our Universe. As we explore the topic, it becomes clear that profound open questions plague the most promising theories describing the foundation of our knowledge. [1].

An elusive and unknown form of matter dominates the matter component of our Universe, stealing the spotlight from ordinary matter. Despite the colossal efforts made by several collaborations spread all over the globe, its true nature remains a riddle.

Furthermore, ordinary matter presents an enigmatic side because of the observed matter/anti-matter asymmetry that defies explanation within the current paradigm.

An intriguing form of energy, the Dark Energy, overshadows the matter component of our Universe and pulls the strings for cosmic expansion.

The undeniable evidence of neutrino oscillations shakes the foundation of the Standard Model minimal formulation that predicts massless neutrinos.

Lastly, the Standard Model presents a fundamental incompatibility with the theory that describes the fabric of the Universe, the general relativity.

One of the possible approaches to address these problems requires a procedure that simultaneously investigates physics Beyond the Standard Model and cosmology. This quest requires us to decipher fundamental elements and relations of particle physics and cosmology under the guiding light provided by physical, astrophysical, and cosmological observations [2].

This thesis seeks to position itself within the collective endeavor dedicated to unveiling the Universe's deepest secrets. In particular, we focus on Primordial Black Holes that serve as an excellent phenomenon that bridges between micro (particle) and macro (cosmology) realms, [2]. They are hypothetical Black Holes formed in the very early Universe, predicted by a landscape of mechanisms [3]. As a result, any observation of Primordial Black Holes can shed light on several aspects of the first phases of our Universe.

In recent years, studies on the topic have skyrocketed because of the gravitational wave observations that suggest that some of the mergers involve Primordial Black Holes [4]. Another pivotal factor contributing to the surging interest in Primordial Black Holes lies in their potential contribution to the Dark Matter abundance. Nonetheless, Hawking radiation imposes a critical cut: only Primordial Black Holes heavier than $\sim 5 \times 10^{14} g$ are viable Dark Matter candidates. Proposed by Hawking in the 1970s as a harmonic combination of quantum xand general relativity effects, this radiation stands out as one of the most intriguing aspects surrounding the physics of Primordial Black Holes that predicts a progressive mass loss associated with the emission of elementary particles from the Primordial Black Holes. Primordial Black Holes served as a fundamental inspiration for the study of this fascinating phenomenon, standing as one of the most significant of the last century because of the intrinsic link between general relativity, quantum mechanics, and thermodynamics despite the persistence of some conceptual challenges. This example illustrates that Primordial Black Holes can lead to profound insights even if their existence remains unproven.

Moreover, Hawking Radiation is crucial in our comprehension of the potential effects of Primordial Black Holes on critical milestones in the evolution of our Universe, including the origin of the baryon asymmetry, Big Bang Nucleosynthesis, and structure formation.

Furthermore, this phenomenon presents an appealing opportunity to explore various extensions of the Standard Model. In this context, the extension may assume a substantial number of new particles, as seen in Supersymmetry, but there are also cases where there is only few new species. For instance, Dark Matter or Right-Handed Neutrino production from the evaporation of Primordial Black Holes are of broad interest. Moreover, Hawking Radiation can survey more intricate extensions involving baroque space-time geometries, as seen in theories like the Extra-dimension.

From the astrophysical perspective, Primordial Black Holes with substantial masses have the potential to serve as seeds for supermassive Black Holes residing in the core of galaxies.

The handful of examples cited are merely instances that lead us to conclude that Primordial Black Holes provide a captivating avenue of research offering an alluring window into the fundamental physics that shape and govern our Universe, whether they exist or not.

We divide this thesis into two Parts. The first part presents the literature on Physics Beyond the Standard Model and Primordial Black Holes. In particular, **Chapter 1** briefly discusses the Standard Model and the open problems that will be discussed later on in the thesis, that are (i) Neutrino masses, (ii) Dark Matter, (iii) the origin of the Baryon asymmetry. **Chapter 2** focuses on the principal features of Primordial Black Holes and their link to the early Universe physics. We will briefly review (i) the formation mechanisms, (ii) how Primordial Black Holes alter the Universe's evolution, (iii) the phenomena contributing to the mass evolution, (iv) the existing constraints on Primordial Black Holes' abundance, and (v) the open problems.

Part II summarizes the papers we published on Primordial Black Holes in the context of Physics Beyond the Standard Model. We organize it as follows. **Chapter 3** focuses on neutrino emitted from primordial black hole evaporation. They can interact via Coherent Elastic neutrino-Nucleus Scattering in Dark Matter direct detection experiments. Here, we obtained forecast constraints on primordial black hole abundance today. The Chapter summarises Ref. [5]. **Chapter 4** portrays the emission of light Dark Matter from evaporating Primordial Black Holes. Recently, light Dark Matter detection gained a lot of attention. Generally, direct detection of sub-GeV Dark Matter is challenging since it induces low recoil energies. The problem is solved by considering light Dark Matter with considerable kinetic energies. Here, we point out that Primordial Black Hole evaporation is a source of boosted light Dark Matter with energies of tens to hundreds of MeV. Considering XENON1T and Super-Kamiokande data, we constrain the mixed parameter space of Primordial Black Holes and sub-GeV Dark Matter. The Chapter sums up Refs.[6, 7]. **Chapter 5** describes a baryogenesis scenario that does not require a Baryon number violation at the Lagrangian level. The mechanism exploits a different absorption of a new particle with Baryon number and its antiparticle into Primordial Black Holes. We identified a region of the parameter space reproducing the correct Baryon asymmetry. The Chapter is based on Ref. [8]. **Chapter 6** discusses the interplay between Leptogenesis and Primordial Black Holes. In particular, we consider Primordial Black Holes evaporating between the sphaleron transitions freeze out and Big Bang Nucleosynthesis. We obtain mutual exclusion limits in the mixed parameter space, and once projected onto the Primordial Black Holes parameter space, they prove to be highly competitive with existing ones despite being model-dependent. The Chapter outlines Ref. [9].

Lastly, Part III summarises Part II's results and illustrates possible outcomes of this thesis.

Part I

CHAPTER 1

Physics Beyond the Standard Model

The Standard Model, often regarded as one of the greatest achievements of modern physics, stands as a stele to our understanding of the fundamental particles and forces governing our Universe [1]. An array of seminal contributions and experimental evidence support this theoretical framework.

Among its achievements, the Standard Model led to the groundbreaking discovery of the Higgs boson, pivotal for determining the mechanisms responsible for the particle's mass. Notably, it also predicted the electron's magnetic moment with astonishing precision with an error of 1 part per 100 billion.

In the forthcoming Section 1.1, we shortly revise the Standard Mode, delving into its core principles.

Currently, searches focus on determining the Standard Model parameters with high precision and, eventually, uncovering signatures for new physics. Indeed, the Standard Model is far from being considered a complete theory but rather an approximation of a theory observable at greater energies. Five main phenomena motivate searches looking for new physics, which are:

- **Neutrino Masses.** The original formulation of the Standard Model assumes neutrinos to be massless. However, several experiments, including the groundbreaking one performed by Super-Kamiokande [10], unequivocally demonstrate that neutrinos oscillate. This discovery raises two questions: (i) Are neutrino Majorana or Dirac particles? (ii) why are neutrino masses so small compared to the other fermions'?

  We revise the topic in Section 1.2.

- **Dark Matter.** Cosmological observations reveal that the Standard Model only accounts for a mere fraction ($\sim 5\%$) of the energy content of the Universe, whereas an unknown form of matter, known as Dark Matter, makes up around 26% [11] of it. The Standard Model fails to provide a valid Dark Matter candidate.

Section 1.3 discusses the evidence, potential candidates, and detection techniques for Dark Matter (see Ref. [12] for a recent review)

- **Matter/anti-matter asymmetry.** The Universe exhibits an asymmetric matter and anti-matter composition, and the reason for this asymmetry remains unanswered. The Standard Model asymmetry predicts an asymmetry order of magnitudes smaller than the observed one [13]. Section 1.4 delves into this topic.

- **Dark Energy.** Dark Energy constitutes the majority of the Universe's energy content ($\sim 69\%$) [11] and it is responsible for our Universe's accelerated expansion [14]. The "*cosmological constant problem*" has been the subject of intense studies since the general relativity formulation, whereas experimental evidence confirmed it around 30 years ago.

- **Gravity.** The Standard Model does not account for gravity and it is incompatible with general relativity [15]. Numerous models, such as string theory, M-theory, and quantum gravity, attempt to connect gravity to the other fundamental interactions.

1.1 Standard Model Unraveled

Particle physics theories should identify fundamental components of our Universe and describe their interactions. Currently, the Standard Model is the most successful theory, excellently describing strong, weak, and electromagnetic interactions up to the electroweak scale ($\Lambda_{EW} \sim 100\,\mathrm{GeV}$). Based on quantum field theory, it regards matters and force with the same formalism, where particles mediate interactions.

The Standard Model Lagrangian is invariant under a local (gauge) transformation under the symmetry group

$$G_{SM} = \mathrm{SU}(3)_c \times \mathrm{SU}(2)_L \times \mathrm{U}(1)_Y\,. \tag{1.1}$$

Each gauge factor describes a different fundamental interaction with fields having various representations under them. In particular, $\mathrm{SU}(3)_c$ characterizes the strong interaction, and $\mathrm{SU}(2)_L \times \mathrm{U}(1)_Y$ the electroweak.

The Standard Model includes 12 fermions, particles of spin $1/2$. We divide them into two categories

- **Quarks:** fermions strongly interacting, meaning that they are triplets under $\mathrm{SU}(3)_c$. Up-type quarks ($u^i = (u, c, t)$) have electric charge $+2/3$, down-type ($d^i = (d, s, b)$) have charge $-1/3$.

	$L_L^i = (\nu^i,\, \ell^i)_L^T$	$Q_L^i = (u^i,\, d^i)_L^T$	ℓ_R^i	u_R^i	d_R^i	$\phi = (\phi^+, \phi^0)^T$
SU(3)$_C$	1	3	1	3	3	1
SU(2)$_L$	2	2	1	1	1	2
Y	$-\frac{1}{2}$	$+\frac{1}{6}$	-1	$+\frac{2}{3}$	$-\frac{1}{3}$	$+\frac{1}{2}$

Table 1.1: Standard Model particle content.

- **Leptons:** do not strongly interact, thus, they are singlets under $\mathrm{SU}(3)_c$. We classify them into charged Leptons ($\ell^i = (e, \mu, \tau)$) with charge ± 1 and neutrinos ($\nu^i = (\nu_e, \nu_\mu, \nu_\tau)$) that are neutral.

Gauge bosons, particles of spin 1, mediate the fundamental interactions. Strong interaction mediators are the gluons (G^a). $W^\pm$ and Z^0 mediate weak interactions and the photon (γ) mediate the electromagnetic one. The weak interaction is chiral, meaning that right- and left-handed fermions transform differently under $\mathrm{SU}(2)_L$. In particular, left-handed fermions are doublet under $\mathrm{SU}(2)_L$, while the right-handed ones are singlets. Consequently, mass terms like $m\bar{\Psi}\Psi$ are not $\mathrm{SU}(2)_L$ invariant, and the Standard Model lagrangian can not accommodate them. Indeed, defining the chiral projector as

$$P_R = \frac{1+\gamma^5}{2}\,, \tag{1.2}$$

$$P_L = \frac{1-\gamma^5}{2}\,, \tag{1.3}$$

$$\tag{1.4}$$

we can write

$$m\bar{\Psi}\Psi = m\bar{\Psi}(P_R + P_L)(P_R + P_L)\Psi = m(\bar{\Psi}_R\Psi_L + \bar{\Psi}_L\Psi_R)\,. \tag{1.5}$$

Furthermore, weak interaction needs Z and $W^\pm$ to be massive. Instead, local Lagrangian invariance requires massless gauge bosons. The Higgs mechanism [16–18] is responsible for the gauge boson masses because of the introduction of a complex scalar field ϕ, with a specific potential invariant under $\mathrm{SU}(2)_L \times \mathrm{U}(1)_Y$ that spontaneously breaks the electroweak symmetry down to $\mathrm{U}(1)_{\mathrm{EM}}$. Fermion masses originate from the Yukawa coupling with the Higgs field. We present more details of the mechanism along with the model's Lagrangian. Table 1.1 reports the Standard Model particle content with their quantum numbers.

In the limit of massless neutrinos, the most general Standard Model Lagrangian features 19 parameters measured experimentally, conveniently summarized in Table 1.2. We divide the Lagrangian into four components

$$\mathcal{L} = \mathcal{L}_B + \mathcal{L}_F + \mathcal{L}_Y - V(\Phi)\,, \tag{1.6}$$

	1	1	1	2	3	10	1
Original	g_s	g	g'	μ, λ	y^{ℓ}_{ij}	y^{q}_{ij}	$\theta_{\rm QCD}$
Measured	α_s	m_W	α	G_F, m_h	$m_{\ell i}$	m_{q^i}, $V_{\rm CKM}$	~ 0

Table 1.2: Standard Model free parameters.

where $\mathcal{L}_B$ and $\mathcal{L}_F$ are bosons and fermions kinetic terms respectively, $\mathcal{L}_Y$ contains the fermions-Higgs interactions (Yukawa terms), and $V(\Phi)$ is the the self-interacting Higgs potential. They are defined as

$$\begin{aligned}
\mathcal{L}_F &= \sum_F i\overline{F}\gamma_\mu \mathcal{D}^\mu F\,, &(1.7)\\
\mathcal{L}_B &= -\frac{1}{4}B^{\mu\nu}B_{\mu\nu} - \frac{1}{4}W^{i\mu\nu}W^i_{\mu\nu} - \frac{1}{4}G^{a\mu\nu}G^a_{\mu\nu} + \frac{1}{2}(\mathcal{D}_\mu\phi)^\dagger\mathcal{D}^\mu\phi\,, &(1.8)\\
\mathcal{L}_Y &= -y^d_{ij}\overline{Q}^i_L\phi d^j_R - y^u_{ij}\overline{Q}^i_L\tilde{\phi}u^j_R - y^\ell_{ij}\overline{L}^i_L\phi\ell^j_R + \text{h.c.}\,, &(1.9)\\
V(\phi) &= \frac{1}{2}\mu^2\phi^2 + \frac{1}{4}\lambda\phi^4\,. &(1.10)
\end{aligned}$$

In Eq. (1.7), the sum is performed over all the fermions, and $\mathcal{D}_\mu$ is the covariant derivative. It is defined as

$$\mathcal{D}_\mu = \partial_\mu + ig_s\frac{\lambda^a}{2}G^a_\mu + ig\frac{\sigma^a}{2}W^a_\mu + ig'\frac{1}{2}YB_\mu\,, \tag{1.11}$$

where g_s, g and g' are $\text{SU}(3)_c$, $\text{SU}(2)_L$, and $\text{U}(1)_Y$ couplings respectively, σ^i (i = 1,2,3) and λ^a are Pauli and Gellamnn matrices (a = 1, ..., 8), and Y is the hypercharge. In Eq. (1.8), we define

$$\begin{aligned}
B_{\mu\nu} &= \partial_\mu B^i_\nu - \partial_\nu B^i_\mu\,, &(1.12)\\
W^i_{\mu\nu} &= \partial_\mu W^i_\nu - \partial_\nu W^i_\mu + g\epsilon^{ijk}W^j_\mu W^j_\nu\,, &(1.13)\\
G^a_{\mu\nu} &= \partial_\mu G^a_\nu - \partial_\nu G^a_\mu + g_s f^{abc}G^b_\mu G^c_\nu\,, &(1.14)
\end{aligned}$$

ϵ^{ijk} and f^{abc} are $\text{SU}(3)_c$ and $\text{SU}(2)_L$ structure constants. W^i_μ and B_μ are the electroweak gauge bosons that can be represented as

$$W^\pm_\mu = \frac{W^1_\mu \mp iW^2_\mu}{\sqrt{2}}\,, \qquad\qquad W^0_\mu = W^3_\mu\,. \tag{1.15}$$

We highlight that W^0_μ and B_μ have the same quantum numbers and can mix. In Eq. (1.9), $\widetilde{\phi} = (\phi^{0\,*}, -\phi^{+\,*})^T$.

We notice that the terms in Eqs.(1.7), (1.8), (1.9), and (1.10) have been constructed to respect the gauge symmetry in Eq.(1.1). Higgs self-interaction in Eq. (1.10) is responsible for $\text{SU}(2)_L \times \text{U}(1)_Y$ symmetry breaking, that occurs when the temperature drops below a critical temperature, causing the quadratic term in Eq.(1.10) to become negative. Consequently, the potential minimum move away from $\phi = 0$.

The fundamental consequence is that Higgs boson acquires a non-zero vacuum expectation value $\langle \phi^0 \rangle = v/\sqrt{2} \simeq 174\,\text{GeV}$[19], that is granted for

$$\left.\frac{\partial V}{\partial \phi^0}\right|_{\langle \phi^0 \rangle = v/\sqrt{2}} = 0 \;\rightarrow \mu^2 = -\lambda v^2\,, \tag{1.16}$$

as long as $\mu^2 < 0$, we notice that the Higgs boson mass is $m_h = \sqrt{|\mu^2|}$.

After the symmetry breaking, particles interacting with the Higgs gain mass. In Eq. (1.8), we get

$$\mathcal{L}_B \supset g^2 \frac{v^2}{8} \left[W^1_\mu W^{1\,\mu} + W^2_\mu W^{2\,\mu} + \left(\frac{g}{g'} B_\mu - W^3_\mu \right) \left(\frac{g}{g'} B^\mu - W^{3\,\mu} \right) \right]\,. \tag{1.17}$$

We observe that the mass matrix is not diagonal because of $\left(\frac{g}{g'} B_\mu - W^3_\mu \right)^2$. From the diagonalization of the boson mass matrix, we obtain the mass eigenstates, that are

$$Z_\mu = \frac{1}{\sqrt{g^2 + g'^2}} \left(g W^3_\mu - g' B_\mu \right) \equiv \cos\theta_W W^3_\mu - \sin\theta_W B_\mu\,, \tag{1.18}$$

$$A_\mu = \frac{1}{\sqrt{g^2 + g'^2}} \left(g' W^3_\mu + g B_\mu \right) \equiv \sin\theta_W W^3_\mu + \sin\theta_W B_\mu\,, \tag{1.19}$$

where θ_W is the Weinberg angle and A_μ indicates the photon. Furthermore, the mass eigenvalues are

$$m_W = g\frac{v}{2}\,, \tag{1.20}$$

$$m_Z = \frac{m_W}{\cos\theta_W}\,, \tag{1.21}$$

$$m_A = 0\,. \tag{1.22}$$

A similar treatment has to be done for Eq. (1.9). In particular, we obtain

$$\mathcal{L}_Y \supset -\frac{v}{\sqrt{2}} \left\{ y^d_{ij} d^{i\,\dagger}_R d^j_L + y^u_{ij} u^{i\,\dagger}_R u^j_L + y^\ell_{ij} \ell^{i\,\dagger}_R \ell^j_L \right\} \text{h.c.}\,. \tag{1.23}$$

In general, Yukawa matrices are not necessarily diagonal in the basis of electroweak and strong interactions eigenstates. As for the bosons, mass eigenstates are obtained diagonalizing the mass matrices. Charged Leptons mixing is formally allowed, it is not experimentally observed.

Quarks mass eigenstates are defined as $u'_L = U_u u_L$ and $d'_L = U_d u_L$, where q and q' are weak interaction and mass eigenstates respectively and U_q is an unitary matrix ($U_q U^\dagger_q = U^\dagger_q U_q = \mathbf{I}$). In terms of the mass eigenstates, the weak interaction takes the form

$$\mathcal{L}_F \supset -\frac{g}{\sqrt{2}} V^{ij}_{\text{CKM}} \overline{u}^{i\,\prime}_L \gamma^\mu W^+_\mu d^{j\,\prime}_L + \text{h.c.} \tag{1.24}$$

$V_{\rm CKM} = U_u^\dagger U_L$ is the Cabibbo-Kobayashi-Maskawa matrix. It is an complex 3×3 matrix that can be parametrized in terms of three mixing angles (θ_{12}, θ_{13}, θ_{23}) and a complex phase (δ), representing the only source of CP-violation in the Standard Model. $V_{\rm CKM}$ is commonly written as

$$V_{\rm CKM} = \begin{pmatrix} 1 & 0 & 0 \\ 0 & c_{23} & s_{23} \\ 0 & -s_{23} & c_{23} \end{pmatrix} \begin{pmatrix} c_{13} & 0 & s_{13}e^{-i\delta} \\ 0 & 1 & 1 \\ -s_{13}e^{i\delta} & 0 & c_{13} \end{pmatrix} \begin{pmatrix} c_{12} & s_{12} & 0 \\ -s_{12} & c_{12} & 0 \\ 0 & 0 & 1 \end{pmatrix}, \tag{1.25}$$

where $c_{ij} = \cos\theta_{ij}$ and $s_{ij} = \sin\theta_{ij}$.

In Table 1.2, we introduce $\theta_{\rm QCD}$ that is responsible for CP violation in strong interactions. At present, its experimental measurement is consistent with zero. Thus, we will not discuss it here. In the same Table, we indicate the Fermi Constant as

$$G_F \equiv \frac{\sqrt{2}}{8}\frac{g^2}{m_W^2} = \frac{\sqrt{2}}{2v^2}\,. \tag{1.26}$$

With the discovery of the Higgs boson in 2012, we measured all the particles predicted by the Standard Model, making it is a complete theory. The Standard Model is exceptionally successful and has withstood decades of precision tests in colliders. Nonetheless, as mentioned at the beginning of the Chapter, the Standard Model is not the final theory because it can not account for several experimental observations.

1.2 Neutrino Masses

Pauli proposed the existence of neutrinos in 1930 as a way to account for the missing energy in the β-decay. They play an essential role as fundamental particles in the Standard Model. Since they are neutral and colorless, left-handed neutrinos only feel weak interaction. Right-handed neutrinos are sterile particles allowed in the Standard Model but not included in its minimal version. For this reason, it considers massless neutrinos (see Eq. (1.9)). Since the neutrino masses are much lighter than the other fermions, this approximation lasted many years. However, the observation of neutrino oscillations provides strong evidence neutrinos are massive. The phenomenon consists of the flavor conversion of neutrinos while propagating because of an underlying mismatch between neutrino mass and interaction eigenstates. The determination of neutrino masses is an active research area. Cosmological observation provides a limit on the total neutrino mass [1]

$$\sum_j \nu_j = 0.14\,\text{eV}\,. \tag{1.27}$$

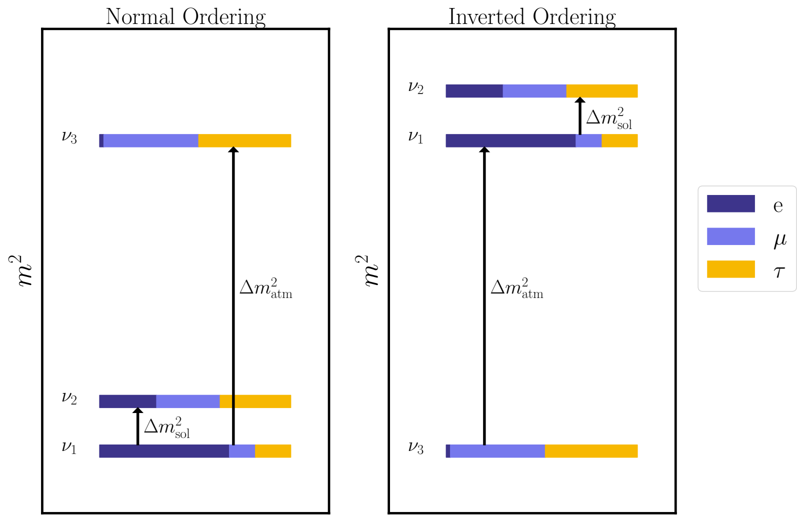

Figure 1.1: **Neutrino mass hierarchy.** Schematic depiction of the probability of measuring ν_α flavor eigenstate in the i-th neutrino mass eigenstate for the normal (left panel) and inverted (right panel) orderings.

KATRIN provides the most stringent limit from direct measurement on neutrino masses up to date by requiring [20]

$$m_\nu < 0.8\,\text{eV at 90\% C.L.}\,. \tag{1.28}$$

However, individual neutrino masses and their ordering are still unknown. Neutrino oscillations experiments can determine the values of the mass-squared differences $\Delta m^2_{ij} \equiv m^2_i - m^2_j$ rather than the individual masses themselves. In particular, experiments determine two mass-squared differences [21]

$$\Delta m^2_{21} \simeq 7.36 \cdot 10^{-5}\,\text{eV}^2\,, \tag{1.29}$$

$$|\Delta m^2_{13}| \simeq 2.485 \cdot 10^{-3}\,\text{eV}^2\,. \tag{1.30}$$

known as the solar and atmospheric mass-squared differences, respectively.

Neutrino mass ordering refers to the hierarchy of the neutrino mass eigenstates in terms of mass. There are two possible mass orderings

- **Normal ordering (NO):** $m_1 \lesssim m_2 \ll m_3$;
- **Inverted ordering (IO):** $m_2 \gtrsim m_1 \gg m_3$.

Experimental measurements of neutrino oscillations do not allow for the determination of the mass ordering, but current data seems to show a mild preference for the normal ordering [22]. In Fig. 1.1, we provide a schematic depiction of the probability of measuring a certain flavor state in the i-th mass eigenstate. If we enrich the Standard Model with right-handed neutrinos,

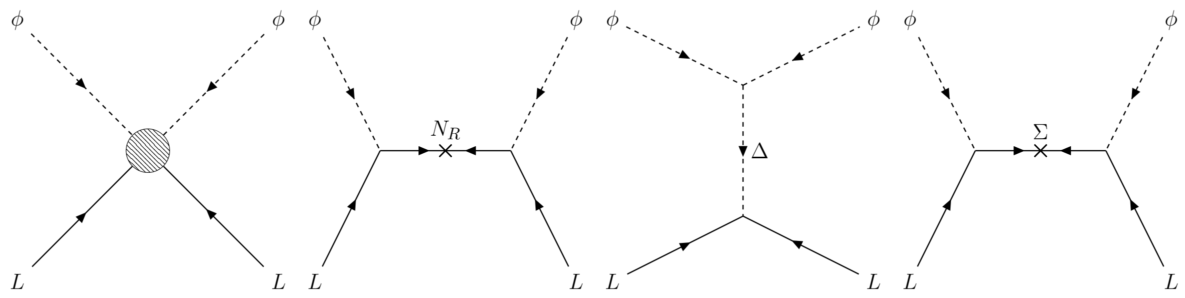

Figure 1.2: **Weinberg operator.** The first diagram represents the effective vertex describing the Weinberg operator. From left to right, the other diagrams illustrate the tree-level diagram from Type I, II, and II seesaw mechanisms where N_R is a singlet Majorana fermion, Δ and Σ are a scalar and fermion triplets under $\mathrm{SU}_L(2)$ with $Y = 1$ and $Y = 0$, respectively.

neutrinos could have the same mass terms as quarks and Leptons (Dirac particles). In such a case, the mass term originates from

$$\mathcal{L} \supset -y^{\nu}_{ij}\overline{L}^{i}_{L}\widetilde{\phi}\nu^{j}_{R} + \text{h.c.}\,. \tag{1.31}$$

This Lagrangian term conserves the flavor Lepton number. To explain neutrino masses, the Yukawa coupling must be $\mathcal{O}(10^{-10})$ or smaller, leading to a fine tuning problem. Conversely, assuming the absence of right-handed neutrinos, we can identify neutrinos with anti-neutrinos (Majorana particles) with mass term given by

$$\mathcal{L} \supset -m_{LL}\overline{\nu}_L\nu^c_L\,. \tag{1.32}$$

However, this term violates $\mathrm{SU}(2)_L \times \mathrm{U}(1)_Y$, but we can derive it from the Weinberg operator [23]

$$\mathcal{L} \supset \frac{1}{\Lambda}\phi\phi L_i L_j + \text{h.c.}\,, \tag{1.33}$$

that is a dimension five non-renormalizable effective operator already included in the Standard Model. Interestingly, it leads to $\Delta\mathrm{L} = 2$ processes not yet observed. We can obtain it from a renormalizable Lagrangian where we have integrated out a heavy mediator. In Fig. 1.2, we picture the effective vertex alongside three examples.

The neutrino masses problem is twofold. From one side, we do not know whether neutrinos are Dirac or Majorana particles. We can study neutrinos' nature by looking at the neutrinoless double β decay, represented in Fig. 1.3. If neutrinos are Majorana particles, we should observe this decay. On the other hand, we need a mechanism explaining why their masses are so small. We recommend Ref. [24] for a comprehensive review.

We divide the Section into three. The first subsection describes neutrino oscillations and consequences. The second subsection presents the seesaw mechanism that simultaneously provides neutrino mass and explains why they are so small compared to the other fermions'.

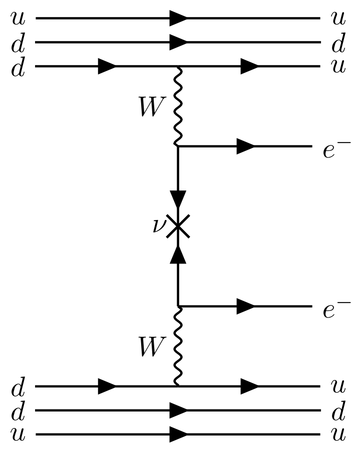

Figure 1.3: Neutrinoless double β decay

Lastly, we detail the Coherent Elastic neutrino-Nucleus Scattering. This interaction provides an insurmountable background in Dark Matter direct detection experiments.

1.2.1 Neutrino oscillations

We define neutrino oscillations as the phenomenon by which a neutrino can change flavor while propagating and represents the most solid evidence of Physics Beyond the Standard Model.

Pontecorvo in 1957 [25, 26] investigated hypothesis of neutrino anti-neutrino oscillations in analogy to $K^0 - \overline{K}^0$ oscillation [27].

Only with the discovery of muon neutrinos the attention shifted on the mixing of massive neutrinos [28, 29] and, a few years later, of neutrino oscillations [30–33]. Refs. [34–36] discuss how the propagation in matter can influence oscillation, a fundamental aspect of our understanding of solar neutrinos.

In 1998, Super-Kamiokande provided the first compelling evidence of neutrino oscillations [10]. However, it was not an unexpected result, as numerous hints had accumulated over the years [37–48].

Since the groundbreaking observation, additional evidence supporting neutrino oscillations has emerged from various sources, including studies of solar [49–54], atmospheric [10, 55, 56], reactor [57, 58], and accelerator [59–61] neutrinos. These findings continue to be a rich source of exploration in the field.

Neutrino oscillations proves that neutrino flavor (ν_α, $\alpha = e,\, \mu,\, \tau$) do not coincide with mass eigenstates (ν_i, $i = 1,\, 2,\, 3$). Hence, we can write the flavor eigenstate as a mixture of the mass

	Normal Ordering		Inverted Ordering	
	best fit $\pm 1\sigma$	3σ **range**	**best fit** $\pm 1\sigma$	3σ **range**
$\sin^2\theta^\ell_{12}/10^{-1}$	$3.03^{+0.13}_{-0.13}$	$[2.63; 3.45]$	$3.03^{+0.13}_{-0.13}$	$[2.63; 3.45]$
$\sin^2\theta^\ell_{23}/10^{-1}$	$4.55^{+0.18}_{-0.15}$	$[4.16; 5.99]$	$5.69^{+0.13}_{-0.21}$	$[4.17; 6.06]$
$\sin^2\theta^\ell_{13}/10^{-2}$	$2.23^{+0.07}_{-0.06}$	$[4.16; 5.99]$	$2.23^{+0.06}_{-0.06}$	$[4.17; 6.06]$
δ^ℓ/π	$1.24^{+0.18}_{-0.13}$	$[0.77; 1.97]$	$1.52^{+0.14}_{-0.15}$	$[1.07; 1.90]$
$\Delta m^2_{12}/10^{-5}\,\mathrm{eV}^2$	$7.36^{+0.16}_{-0.15}$	$[6.93; 7.93]$	$7.36^{+0.16}_{-0.15}$	$[6.93; 7.93]$
$\Delta m^2_{31}/10^{-3}\,\mathrm{eV}^2$	$2.485^{+0.023}_{-0.031}$	$[2.401; 2.565]$	$-2.455^{+0.025}_{-0.030}$	$[-2.541; -2.376]$

Table 1.3: **Three-flavor oscillation parameters**. The first (second) column reports the parameters assuming Normal (Inverted) ordering. We highlight that $\Delta m^2_{31} > 0$ for Normal ordering and $\Delta m^2_{31} < 0$ for Inverted ordering. Note that $\Delta m^2_{\rm sol} \equiv \Delta m^2_{12}$ and $\Delta m^2_{\rm atm} = |\Delta m_{31}|^2$. The experimental data are taken from Ref. [22]. We suggest also Refs. [21, 63].

eigenstates

$$\begin{pmatrix} \nu_e \\ \nu_\mu \\ \nu_\tau \end{pmatrix} = U_{\rm PMNS} \begin{pmatrix} \nu_1 \\ \nu_2 \\ \nu_3 \end{pmatrix} \tag{1.34}$$

where $U_{\rm PMNS}$ is the Pontecorvo-Maskawa-Nagasaki-Sasaka matrix. The standard parametrization is

$$U_{\rm PMNS} = \begin{pmatrix} U_{e1} & U_{e2} & U_{e3} \\ U_{\mu 1} & U_{\mu 2} & U_{\mu 3} \\ U_{\tau 1} & U_{\tau 2} & U_{\tau 3} \end{pmatrix} \begin{pmatrix} e^{i\alpha_1/2} & 0 & 0 \\ 0 & e^{i\alpha_2/2} & 0 \\ 0 & & 1 \end{pmatrix} \equiv UV \tag{1.35}$$

where

$$U = \begin{pmatrix} 1 & 0 & 0 \\ 0 & c^\ell_{23} & s^\ell_{23} \\ 0 & -s^\ell_{23} & c^\ell_{23} \end{pmatrix} \begin{pmatrix} c^\ell_{13} & 0 & s^\ell_{13} e^{-i\delta^\ell} \\ 0 & 1 & 0 \\ -s^\ell_{13} e^{i\delta^\ell} & 0 & c^\ell_{13} \end{pmatrix} \begin{pmatrix} c^\ell_{12} & s^\ell_{12} & 0 \\ -s^\ell_{12} & c^\ell_{12} & 0 \\ 0 & 0 & 1 \end{pmatrix} \tag{1.36}$$

where $c^\ell_{ij} = \cos\theta^\ell_{ij}$, $s^\ell_{ij} = \sin\theta^\ell_{ij}$. δ is the Dirac CP-violating phase, α_1 and α_2 are the Majorana complex phases. While Dirac phases can be reabsorbed in the field definition, Majorana phases can not because of the less degrees of freedom [62]. In Table 1.3, we report the experimental measurement for fundamental quantities describing the phenomenon.

Two flavor oscillation

We start with the simple example of two-flavor oscillation between ν_e and ν_μ. Eq. (1.35) simplifies as

$$
\begin{aligned}
|\nu_e\rangle &= \cos\theta\,|\nu_1\rangle + \sin\theta\,|\nu_2\rangle \ , && (1.37)\\
|\nu_\mu\rangle &= -\sin\theta\,|\nu_1\rangle + \cos\theta\,|\nu_2\rangle \ . && (1.38)
\end{aligned}
$$

We can express the oscillation as

$$
|\nu_j(t)\rangle = |\nu_j(0)\rangle\, e^{-E_j t} \, . \tag{1.39}
$$

where E_j is the neutrino energy. According to this notation, we can write transition from ν_e to ν_μ as

$$
P(\nu_e \to \nu_\mu; t) = |\langle \nu_\mu(0)|\nu_e(t)\rangle|^2 = \frac{1}{2}\sin^2 2\theta\,[1 - \cos(E_1 - E_2)t] \ . \tag{1.40}
$$

We can write this expression in terms of the neutrino masses m_i, by using

$$
E_2 - E_1 = \sqrt{p^2 + m_2^2} - \sqrt{p^2 + m_1^2} \overset{(p \gg m_i)}{\simeq} \frac{m_2^2 - m_1^2}{2E} \equiv \frac{\Delta m_{21}^2}{2E} \ . \tag{1.41}
$$

We highlight that from neutrino oscillations, we can deduce the squared mass splitting $\Delta m_{12}^2 = m_1^2 - m_2^2$. We will see that the same results apply to the case with three neutrinos.

Three flavor oscillation

Similarly to what we have done in the previous paragraph, the transition probability from ν_α to ν_β is given by

$$
\begin{aligned}
P(\nu_\alpha \to \nu_\beta; t) &= |\langle|\nu_\beta|\nu_\alpha(t)\rangle|^2 = \left|\sum_j U_{\alpha j}^* U_{\beta j} e^{-iE_j t}\right|^2 && (1.42)\\
&= \sum_{i,j} U_{\alpha j}^* U_{\beta j} U_{\alpha k} U_{\beta k}^* \exp\{-i(E_j - E_k)t\} && (1.43)\\
&= \sum_j |U_{\alpha j}|^2\,|U_{\beta j}|^2 + \sum_{j \neq k} U_{\alpha j}^* U_{\beta j} U_{\alpha k} U_{\beta k}^* \exp\{-i(E_j - E_k)t\} \, . && (1.44)
\end{aligned}
$$

By using the unitarity condition and approximating $E_j \simeq p + m_j^2/2p$, we obtain

$$
\begin{aligned}
P(\nu_\alpha \to \nu_\beta; t) &= \delta_{\alpha\beta} + \sum_{j \neq k} U_{\alpha j}^* U_{\beta j} U_{\alpha k} U_{\beta k}^* \exp\{-i(E_j - E_k)t\} && (1.45)\\
&\simeq \delta_{\alpha\beta} + \sum_{j > k} \Big(-4\mathrm{Re}\left[U_{\alpha j}^* U_{\beta j} U_{\alpha k} U_{\beta k}^*\right] \sin^2 X_{ij} + && (1.46)\\
&+ 2\mathrm{Im}\left[U_{\alpha j}^* U_{\beta j} U_{\alpha k} U_{\beta k}^*\right] \sin 2X_{ij} \Big) \ ,
\end{aligned}
$$

where $X_{ij} = (m_j^2 - m_k^2)/4E$. From CPT and T transformations, we obtain the oscillation probability for anti-neutrinos

$$P(\overline{\nu}_\alpha \to \overline{\nu}_\beta; t, \delta) = P(\nu_\alpha \to \nu_\beta; t, -\delta)\,. \tag{1.47}$$

We can write the CP-violation as

$$\Delta_{\alpha\beta}^{CP} = \frac{1}{2}\left[P(\nu_\alpha \to \nu_\beta) - P(\overline{\nu}_\alpha \to \overline{\nu}_\beta)\right] = 2\sum_{j>k} \mathrm{Im}\left[U_{\alpha j}^* U_{\beta j} U_{\alpha k} U_{\beta k}^*\right] \sin 2X_{ij}\,. \tag{1.48}$$

For $\alpha = \beta$, we have no CP violation.

Lastly, we mention the MikheyevSmirnovWolfenstein effect, a phenomenon describing the alteration of neutrino oscillations as they travel in matter with varying density [34, 35]. The effect stems from the interaction between electrons and electron neutrinos that induces an effective potential changing the Hamiltonian of the system, $H_0 \to H_0 + V$, where H_0 is the Hamiltonian in vacuum. Therefore, neutrino mass eigenvalues and eigenstates change. Consequently, propagation in matter alters the neutrino oscillations probabilities because they depend on the neutrino mass square differences.

1.2.2 Seesaw Mechanism

The seesaw mechanism explains the smallness of neutrino masses by introducing heavy neutrino singlets. Here, we present type I seesaw [64]. For a complete review on all the possible mechanism, we recommend Ref. [65].

Type I seesaw

We consider the following Lagrangian

$$-\mathcal{L} \supset -i\overline{N}_i \partial\!\!\!/ N_i + \frac{1}{2} M_{ij} \overline{N^c}_i N_j + Y_{ij} \overline{L}_i \tilde{\phi} N_j + \text{h.c.}\,. \tag{1.49}$$

where N are n right-handed singlets neutrinos, $M_{ij} = \mathrm{diag}(M_1, M_2, ..., M_n)$ is orders of magnitude larger than the electroweak scale. We highlight that this Lagrangian contains vertices violating the Lepton number. After the spontaneous symmetry breaking, the relevant Lagrangian terms are

$$\mathcal{L} \supset -\overline{\nu}_L m_D N - \frac{1}{2}\overline{N^c} M N + \text{h.c.}\,, \tag{1.50}$$

where

$$m_D = Y\frac{v}{\sqrt{2}} \tag{1.51}$$

In the matrix form, Eq. 1.50 is

$$\mathcal{L} \supset \begin{pmatrix} \overline{\nu}_L & \overline{N^c} \end{pmatrix} \begin{pmatrix} 0 & m_D \\ m_D^T & M \end{pmatrix} \begin{pmatrix} \nu_L^c \\ N \end{pmatrix} \tag{1.52}$$

If we assume the right-handed neutrinos originated from a Grand Unified Theory, $M \gg m_D$. Thus, we obtain the effective Majorana masses for the left-handed fermions from the diagonalization of the mass matrix as

$$m_\nu = -m_D M^{-1} m_D^T \,. \tag{1.53}$$

We can see that m_ν are suppressed from M^{-1}. For instance if we take $m_D \sim m_W$ and $M \sim M_{GUT}$, $m_{LL} \sim 10^{-3}$ eV. In particular, we block-diagonalize the matrix as follows

$$\begin{pmatrix} -m_D M^{-1} m_D^T & 0 \\ 0 & M \end{pmatrix} \simeq \mathcal{U}^T \begin{pmatrix} 0 & m_D \\ m_D^T & M \end{pmatrix} \mathcal{U} \tag{1.54}$$

where

$$\mathcal{U} = \begin{pmatrix} U_{\mathrm{PMNS}} & m_D^* M^{*\,-1} \\ -M^{-1} m_D^T & \mathbf{I}_{n\times n} \end{pmatrix} \equiv \begin{pmatrix} U_{\mathrm{PMNS}} & \alpha \\ -\alpha^\dagger & \mathbf{I}_{n\times n} \end{pmatrix} . \tag{1.55}$$

Therefore, the Majorana left-handed neutrino is $\tilde{\nu}_L^i = \nu_L^i + \alpha_{ij} N_j^c$. Being $\alpha_{ij} \ll 1$, we can disregard the small right-handed component.

Assuming to have three right-handed heavy neutrinos, we recast Y according to the Casas-Ibarra-parametrization [66]

$$Y = \frac{1}{v}\sqrt{M} R \sqrt{\hat{m}_\nu} U_{\mathrm{PMNS}}^\dagger \,, \tag{1.56}$$

where $\hat{m}_\nu = \mathrm{diag}(m_1, m_2, m_3)$, m_i are the light neutrino masses, and R is an arbitrary complex orthogonal matrix ($R^T R = R R^T = \mathbf{I}$). According to the Lagrangian in Eq. (1.49), we can write m_ν as

$$m_\nu \simeq -v^2 Y \cdot \frac{1}{\hat{M}} \cdot Y^T \,. \tag{1.57}$$

1.2.3 Coherent Elastic Neutrino Nucleus Scattering

Coherent Elastic Neutrino Nucleus Scattering (CEνNS) [67] is a phenomenon with interesting implications not only in high-energy physics, but also astrophysics, nuclear physics, and beyond. It is a flavor-blind neutral-current interaction between the nucleus and (anti-)neutrino, where the nucleus recoils as a single particle. The cross-section scales approximately as the atomic number (A) square. In the Standard Model, the Z boson mediates the process (see

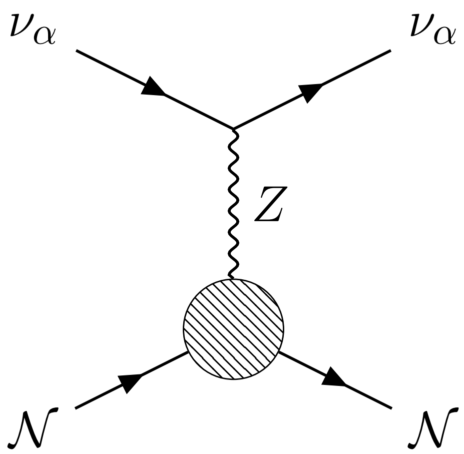

Figure 1.4: Coherent Neutrino nucleus scattering process.

Fig. 1.4).

The process occurs when the transferred momentum (q) is smaller than the inverse of the nucleus's radius ($R \simeq 1.2A^{1/3}$ [68]).

Coherent Elastic Neutrino Nucleus Scattering is of high interest because it allows the measurement of low energies neutrinos ($E_\nu < 100\,\mathrm{MeV}$), fundamental for astrophysical and reactor neutrinos detection [69]. Additionally, it provides a good test bench for neutrino properties and the Standard Model. Indeed, COHERENT collaboration [70] measurements are sensitive to new physics coupling with quarks and Leptons [71, 72].

In the Standard Model, Coherent Elastic Neutrino-Nucleus Scattering differential cross-section is [67]

$$\frac{\mathrm{d}\sigma_{\nu\mathcal{N}}}{\mathrm{d}E_r} = \frac{\mathrm{G}_\mathrm{F}^2 m_\mathcal{N}}{4\pi} Q_w^2 \left(1 - \frac{m_\mathcal{N} E_r}{2E_\nu}\right) F^2(q)\,, \tag{1.58}$$

where $\mathrm{G_F}$ is the Fermi constant, $E_r = q^2/(2\,m_\mathcal{N})$ is the recoil energy, and $m_\mathcal{N}$ is the nucleus mass. The recoil energy takes value in $[0, E_r^{\max} = 2E_\nu^2/(m_\mathcal{N}+2E_\nu)]$. $Q_w = [N - Z(1 - 4\sin^2\theta_W)]$ is the weak vector nuclear charge, N and Z are the nucleus number of proton and neutrons respectively, and $\sin^2\theta_W = 0.231$ [73] is the Weinberg angle. $F^2(q)$ is the nuclear form factor defining the loss of coherence for $qR > 1$. According to the Helm parametrisation [74]

$$F(q) = \frac{3j_1(qR_0)}{qR_0} e^{-q^2 s^2/2}\,, \tag{1.59}$$

where $j_1(x)$ is the spherical Bessel function of order one, $R_0 = \sqrt{R^2 - 5s^2}$, and $s \approx 0.5\,\mathrm{fm}$ [68] is the skin factor. The nucleon distribution is obtained by convoluting of a uniform density of radius R_0 and a Gaussian profile of thickness s [75]. In general, analyses use the prescription provided in Ref. [76].

As mentioned in Refs. [77, 78], additional processes like quasi elastic and deep inelastic scattering contribute to the total cross-section for energies above $\sim 100\,\mathrm{MeV}$.

1.3 Dark Matter

Dark Matter is a fundamental ingredient in modern cosmology, but astronomers and cosmologists acknowledge its existence only in the 1980s. The Standard Model does not contain a viable Dark Matter candidate, necessitating the exploration of Physics Beyond the Standard Model to address this issue. The relevant development of Dark Matter happened simultaneously with the paradigm shifts in cosmology and particle physics. Indeed, Dark Matter has been the subject of intense debates since the end of the IXX century (see Ref. [79] for a historical overview). Among the earliest recognized evidence for the existence of Dark Matter, we can cite the observation made by F. Zwicky on the Coma cluster, who noticed that eight Galaxies of the cluster present a large scatter in the apparent velocities [80, 81]. Using the virial theorem, he inferred that the cluster mass was ~ 400 times larger than the mass of the visible matter. In 1970, K. Ford and V. Rubin used spectroscopic observation of Andromeda [82], confirming and refining the results of M. Roberts from radio observation [83].

From the 80s, more and more evidence supporting the existence of Dark Matter appeared. Examples are the data from weak and strong lensing by clusters of background object [84, 85], the Bullet cluster [86], hot gas in clusters [87], large structure formation [88], Big Bang Nucleosynthesis [89], cosmic microwave background [90], and more [91, 92].

The literature presents several Dark Matter candidates with masses spanning more than 90 orders of magnitude [12]. Viable Dark Matter candidate must be neutral, stable on cosmological scale, and weakly interacting. Furthermore, it has to be sufficiently non-relativistic at present. We can divide Dark Matter candidates into particles and Astrophysical objects. For instance, particle Dark Matter candidates are axions and axion-like-particles [93], Wimpzillas [94], Sterile Neutrinos [95], Fuzzy Dark Matter [96], and Asymmetric Dark Matter [97]. Astrophysical objects that can be Dark Matter candidates are Massive Compact Halo Objects [98] and Primordial Black Holes [99]. We discuss in Section 1.3.1 the most accredited model, the Weakly Interacting Massive Particles (WIMPs) [100]. Weakly coupling particles with masses around the weak scale would naturally leave the correct relic abundance [101]. In the last few years, experimental collaborations deployed numerous techniques for its detection. So far, we have detected no particles outside the Standard Model. Alternatively to the Dark Matter hypothesis, several papers discuss the possibility of Modified Newtonian dynamics (MOND) to account for the experimental evidence of Dark Matter [102].

1.3.1 Weakly Interacting Massive Particles

In the natural version, they cover the mass range from $10\,\mathrm{GeV}$ to $1\,\mathrm{TeV}$, interact with the W and Z bosons but not with photons (electrically neutral) and gluons (colorless). The naturalness principle lost its charm since we did not observe either Supersymmetry or the natural WIMPs. Since then, we have extended the WIMPs range to $m_\chi \in [1\,\mathrm{MeV} - 1\,\mathrm{TeV}]$.

WIMPs stand out among the other Dark Matter candidates because of a remarkable feature: their thermal relic abundance is naturally compatible with the observed value [103–106]. The literature often denominates this phenomenon as the "*WIMP miracle*" to further underline the elegance of WIMPs as the solution to the Dark Matter problem. The progressive cooling down and expansion of the extremely hot and dense initial stage of the Universe has a profound implication on the abundance and behavior of the particles within it: particles gradually move farther apart and lose energy. Consequently, their ability to interact with the surrounding bath diminishes significantly. If the expansions prevail on the interaction, the number of particles effectively reaches a stable, unchanging level, giving rise to a relic population that persists over time, the so-called "*freeze out*". This concept is of fundamental importance for WIMPS because, without freeze-out, these particles would have been subject to Boltzmann suppression (e^{-m_χ/T_U}) for temperatures of the Universe T_U below the WIMPs mass m_χ. The following Boltzmann equation well describes this phenomenon

$$\frac{\mathrm{d}n_\chi}{\mathrm{d}t} = -3Hn_\chi - \langle\sigma_A v\rangle \left(n_\chi^2 - n_\chi^{\mathrm{eq}\,2}\right) , \tag{1.60}$$

where n_χ is χ number density, n_χ^{eq} is χ thermal equilibrium number density, $\langle\sigma_A v\rangle$ is the the thermally averaged annihilation cross-section. H is the Hubble parameter defined as

$$H^2 \equiv \left(\frac{1}{a}\frac{\mathrm{d}a}{\mathrm{d}t}\right)^2 = \frac{8\pi}{3\mathrm{M}_{\mathrm{Pl}}^2}\rho_{\mathrm{tot}} , \tag{1.61}$$

where a is the cosmological scale factor and ρ_{tot} is the total energy density. n_χ^2 in Eq.(1.60) originates from $\chi\chi \to \mathrm{SM\,SM}$, while $n_\chi^{\mathrm{eq}\,2}$ arises from the opposite process.

We can roughly estimate the freeze-out temperature when $\langle\sigma_{A\chi}v\rangle\, n_\chi = H$. Thus, the final abundance is

$$n_\chi^f \sim (m_\chi T_U^f)^{3/2} e^{-m_\chi/T_U^f} = \frac{g_s^0}{g_s^f}\frac{T_U^{f\,2}}{\mathrm{M}_{\mathrm{Pl}}\,\langle\sigma_{A\chi}v\rangle} , \tag{1.62}$$

where the index f indicates the quantities at freeze-out. We define $z_f \equiv m_\chi/T_U^f$. We obtain

$$\Omega_\chi|_o = \left.\frac{\rho_\chi}{\rho_{\mathrm{cr}}}\right|_o = \frac{m_\chi n_\chi^o}{\rho_{\mathrm{cr}}^o} \sim \frac{z_f T_{U\,o}^3}{\rho_{\mathrm{cr}}\mathrm{M}_{\mathrm{Pl}}}\langle\sigma_{A\chi}v\rangle^{-1} . \tag{1.63}$$

where ρ_{cr} and ρ_χ are the critical and χ energy densities respectively, the index o indicates the present day value. The cross-section is

$$\sigma_{A\chi} v = k \frac{g^4}{16\pi^2 m_\chi^2} \cdot \begin{cases} 1 & \text{for S-wave annihilation}\,, \\ v^2 & \text{for P-wave annihilation}\,, \end{cases} \tag{1.64}$$

where $g \simeq 0.65$ is the weak coupling constant, k quantifies the deviation from this estimation. We can determine k as a function of m_χ. Considering $k \in [0.5 - 2]$, the range $m_\chi \in [100\,\text{GeV} - 1\,\text{TeV}]$ can compose all of the observed Dark Matter, while $m_\chi \in [30 - 300]\,\text{GeV}$ can compose 10% of it [107]. In summary, weakly Interacting particles with masses around the electroweak scale are attractive Dark Matter candidates.

1.3.2 Dark Matter detection

Assuming that the Dark Matter interacts with Standard Model particles, we can identify three detection techniques

- **Production:** [108–110] Colliders can produce Dark Matter in pair via SM SM $\to \chi\,\chi$. We can extract information of χ only through the missing transverse energy, as for neutrinos.
- **Indirect Detection:** After the freeze-out, the effect of annihilation ($\chi\,\chi \to$ SM SM) on the relic abundance is negligible. Despite that, the process is still present and can have observable effects. Numerous indirect detection facilities focused on different signatures exist. For instance, they look at γ ray [111–116], neutrinos [117–121], and cosmic rays [122–125] signals. Each experiment has different systematic uncertainties and difficulties in determining the background. Furthermore, indirect detection can help us in mapping Dark Matter distribution. This line of search is complementary to the gravitational information obtained since 1920s.
- **Direct Detection:** [126–154] We can directly detect Dark Matter via scattering processes like χ SM $\to \chi$ SM. WIMP scattering can be spin-independent ($\overline{\chi}\chi\overline{q}q$) or spin-dependent ($\overline{\chi}\gamma^\mu\gamma^5\chi\overline{q}\gamma_\mu\gamma^5 q$). The requirements are low background, achieved by building these experiments underground, and high sensitivity because the recoil energies are at most $\sim 100\,\text{keV}$. Moreover, these experiments are sensitive only to weakly interactive Dark Matter because, otherwise, the atmosphere would stop it.

Direct detection experiments suffer two main problems. On the one hand, Astrophysical neutrinos constitute a background for WIMPs detection, the so-called neutrino floor, discussed in detail in the next Section. On the other hand, experiments looking for the nuclear and electron recoil energy associated with the scattering with Dark Matter present a sharp decrease in sensitivity at low recoil energies. It causes the constraints on Dark matter to weaken for masses

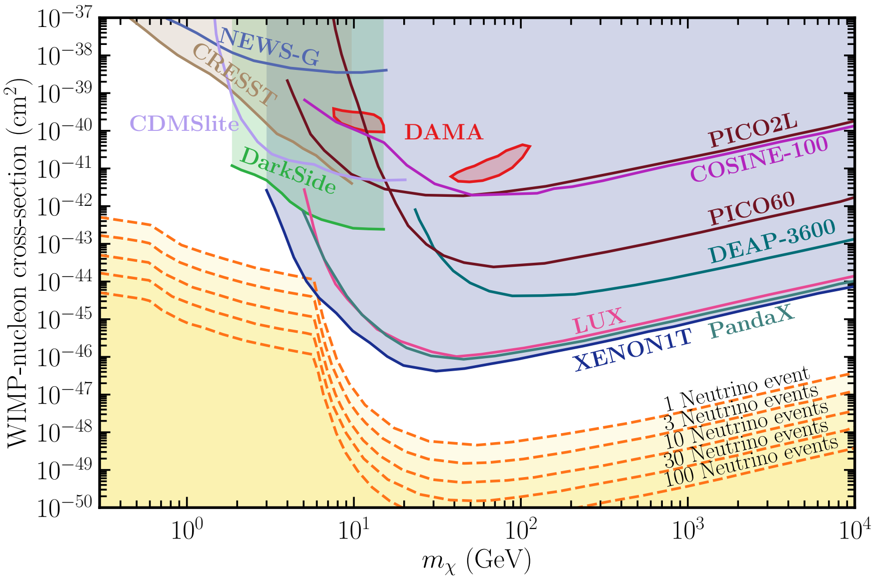

Figure 1.5: **Standard Neutrino floor.** The Figure shows the neutrino isoevent contour lines obtained for $\rho_0 = 0.3\,\mathrm{GeV\,cm^{-3}}$ (orange dashed lines) from Ref [77]. The continuous lines represent the exclusion limit on the spin-independent WIMP-nucleon cross section from several experiments [141, 144, 177–189].

below 1 GeV (1 MeV) for Dark Matter-nucleon (electron) interactions. Thus, direct detection experiments poorly probe light Dark Matter candidates. We can circumvent this problem by considering highly relativistic (boosted) Dark Matter. Several mechanisms [155–157] can boost a fraction of the Dark Matter abundance to velocities higher than the virial one. For instance, the collision with cosmic rays up-scatter to (semi-)relativistic velocities light Dark Matter [158–163]. In Chapter 4, we discuss the possibility of having boosted Dark Matter from Primordial Black Holes. Nonetheless, the literature is flooded with complementary approaches. For instance, parameter space arguments [164, 165] and structure formation [166] constrain fermionic Dark Matter lighter than 0.1 keV. Astrophysical, cosmological, and collider observations further constrain the parameter space [167–176].

Neutrino Floor

Several Dark Matter direct detection experiments look for the signals generated from the scattering between Dark Matter and nuclei [190, 191]. The process they look for is similar to Coherent Elastic neutrino-Nucleus Scattering [67, 192, 193]. For this reason, in the upcoming future, these facilities will measure the signals produced by astrophysical neutrinos. Solar, atmospheric, and Diffuse Supernovae neutrino background can limit Dark Matter direct detection. Indeed, the recoil signatures from different neutrino sources mimic the Dark Matter signal in disparate mass and cross-section ranges [194]. In what follows, we summarize the prescription of Ref. [77] to quantify the limitation for WIMPs searches in direct detection facilities, the Neutrino Floor. The first step consists in estimating the WIMP-induced nuclear recoil event rate. According to Ref. [76], the differential event rate is defined as

$$\frac{\mathrm{d}R_\chi}{\mathrm{d}E_R} = N_T \frac{\rho_0 \sigma_0}{2 m_\chi m_r^2} F^2(q) \int_{v_{\rm min}} \frac{f(\vec{v})}{v} \mathrm{d}\vec{v} \tag{1.65}$$

where N_T is the detector's number of target nuclei, $\rho_\odot$ is the local Dark Matter distribution, σ_0 is the normalized to nucleus cross-section, m_χ and $m_r = m_\chi m_\mathcal{N}/(m_\chi + m_\mathcal{N})$ are the WIMP mass and the WIMP-nucleus reduced mass respectively. $f(\vec{v})$ is WIMP velocity distribution in the Earth frame. Assuming the Maxwell-Boltzmann model [76], the velocity distribution is

$$f(\vec{v}) = \begin{cases} \frac{1}{N_{\rm esc}(2\pi\sigma_v^2)^{3/2}} \exp\left\{\left[-\frac{(\vec{v}+\vec{V}_{\rm lab})^2}{2\sigma_v^2}\right]\right\} & \text{if } |\vec{v}+\vec{V}_{\rm lab}| < v_{\rm esc} \\ 0 & \text{if } |\vec{v}+\vec{V}_{\rm lab}| \geq v_{\rm esc} \end{cases}, \tag{1.66}$$

where $\sigma_v = v_0/\sqrt{2}$ is the WIMP velocity dispersion, $v_0 = 220\,\mathrm{km/s}$, $V_{\rm lab} = 232\,\mathrm{km/s}$ and $v_{\rm esc} = 544\,\mathrm{km/s}$ are respectively the local circular, laboratory and escape velocities in the Galactic frame, $N_{\rm esc}$ is a correction factor that accounts for the velocity cutoff.

The first step to calculate the Neutrino-induced background in the WIMP-nucleon cross-section - WIMP mass plane is to generate background-free exclusion limits with varying recoil energy thresholds in the range $[0.001 - 100]\,\mathrm{keV}$ defined as isovalues of WIMPs events (2.3 at 90% C.L.) with exposure fixed so that background consists of only one neutrino. For fixed m_χ we consider the minimum WIMP-nucleon cross-section measurable as

$$\sigma_{\chi-n}(m_\chi) = 2.3 \min_{E_r^{\rm th}} \frac{\int_{E_r^{\rm th}} \mathrm{d}E_r \frac{\mathrm{d}R_\nu}{\mathrm{d}E_r}}{\int_{E_r^{\rm th}} \mathrm{d}E_r \frac{\mathrm{d}R_\chi}{\mathrm{d}E_r}}, \tag{1.67}$$

where $\mathrm{d}R_\nu/\mathrm{d}E_r$ is the neutrino background event rate defined as

$$\frac{\mathrm{d}R_\nu}{\mathrm{d}E_r} = N_T \times \int \mathrm{d}E_\nu \frac{\mathrm{d}\sigma_{\nu\mathcal{N}}}{\mathrm{d}E_r} \frac{\mathrm{d}\phi_\nu^{\rm bck}}{\mathrm{d}E_\nu} \Theta(E_r^{\rm max} - E_r)\,. \tag{1.68}$$

$\phi_\nu^{\rm bck}$ is the background neutrino flux, and Θ is the Heaviside function. We notice that Eq. (1.67) is independent of N_T because the event rates in Eqs. (1.65), (1.68) are proportional to it. According to this procedure, we obtain the best background-free sensitivity by adjusting the recoil energy depending on the WIMP mass. The orange line in Fig. 1.5 shows the isocurvature limits obtained with this procedure in Ref. [77]. Fig. 1.5 illustrates also the present exclusion limit on the spin-independent WIMP-nucleon cross-section assuming the same coupling to neutron and proton (see caption for more details). Any additional neutrino astrophysical source can modify the standard neutrino floor. In Chapter 3, we show how neutrinos evaporated from Primordial

Black Holes modify the neutrino floor.

1.4 Baryon asymmetry

Baryons represent the fundamental constituent of all the structures, galaxies, and stars. This statement naturally prompts us to question where all the anti-matter, which initially balanced the matter in our Universe, has disappeared to.

Numerous experimental observations reveal a conspicuous absence of anti-matter structure at the present time. A compelling piece of evidence is the absence of anti-matter bodies within the solar systems. Moreover, when examining cosmic rays, we find that the ratio of protons to anti-protons is approximately

$$\frac{n_p}{n_{\overline{p}}} \sim 10^{-4}\,, \tag{1.69}$$

compatible with antiproton production as secondary particles in $pp \to 3p + \overline{p}$ interactions. Similarly, experimental observations imply that $n_{^4He}/n_{^4\overline{He}} \sim 10^{-5}$.

The non-observation of the expected γ-radiation produced by nucleon/anti-nucleon annihilation rules out the possibility of having structure and anti-structure coexist in the same cluster of galaxies.

One could contemplate the possibility of a symmetric Universe with large isolated asymmetric regions. In such a scenario, we expect the annihilation to unfold in the interfaces separating these domains. Since we do not observe the expected diffuse γray background or disruption in the Cosmic Microwave Background, we conclude that the typical size of these domains should be large. However, numerical analyses show that the Universe is entirely made of matter up to the Hubble size. At even larger scales, there is scant evidence.

This persistent prevalence of matter over anti-matter raises profound questions about the mechanism responsible for the transition from an initially symmetric Universe to the present time asymmetric one. Unfortunately, the Standard paradigms fail to provide a valid explanation for this phenomenon. The line of search inquiring about this topic is known as Baryogenesis (see Ref. [195] for a comprehensive review), but despite the large array of proposed mechanisms, we still do not know how the asymmetry originated.

The Baryon number density is not constant during the Universe's evolution, scaling as a^{-3}. Hence, we conveniently indicate the Baryon asymmetry as [19]

$$\mathrm{Y}_{\mathrm{B}}^{\mathrm{obs}} \equiv \left.\frac{n_{\mathrm{B}} - n_{\overline{\mathrm{B}}}}{s}\right|_o = (8.61 \pm 0.09) \times 10^{-11}\,, \tag{1.70}$$

$$\eta_{\mathrm{B}}^{\mathrm{obs}} \equiv \left.\frac{n_{\mathrm{B}} - n_{\overline{\mathrm{B}}}}{n_\gamma}\right|_o = (6.12 \pm 0.04) \times 10^{-10}\,. \tag{1.71}$$

where s is the entropy density, n_{B}, $n_{\overline{\mathrm{B}}}$, and n_γ are the Baryon, anti-Baryon, and photon number densities respectively, and the subscript o means “at present time”. We note that $\mathrm{Y_B}$ and η_B are not independent quantities but are connected by the relationship between the entropy density and the photon number density. Specifically, at present, we have $s \simeq 7.02 n_\gamma$ [196].

At present, we regard Baryon-violating processes as the leading candidates responsible for generating the Baryon asymmetry. However, their mere existence is insufficient to account for the observed excess. In his seminal work [197], Sakharov identified three conditions necessary to generate the observed Baryon asymmetry. These conditions are

- **Baryon number violation:** If the Universe is symmetric at the beginning ($\mathrm{B}(t_i) = 0$), it can not evolve in a state with $\mathrm{B} \neq 0$ if there are no processes violating the Baryon number. In particular, if the Baryon number is conserved, then the Hamiltonian $\mathcal{H}$ commutes with the Baryon number, $[B, \mathcal{H}] = 0$. Thus, $B(t) \propto \int_{t_i}^{t} \mathrm{d}t' \, [B, \mathcal{H}] = 0$.

- *C* **and** *CP* **violation:** Assuming that C is an exact symmetry, the rate of the processes $i \to f$ and $\bar{i} \to \bar{f}$ would be the same, resulting in a cancellation of the Baryon asymmetry generated by the first process with that from the second one. We emphasize that weak interactions maximally violate C.

  Furthermore, assuming CP invariance, results in time-invariance because of the CPT theorem. Under this assumption, we obtain that

$$\Gamma\left(i\left(\mathbf{r}_i\,, \mathbf{p}_i\,, \mathbf{s}_i\right) \to f\left(\mathbf{r}_j\,, \mathbf{p}_j\,, \mathbf{s}_j\right)\right) = \Gamma\left(f\left(\mathbf{r}_j\,, -\mathbf{p}_j\,, -\mathbf{s}_j\right) \to i\left(\mathbf{r}_i\,, -\mathbf{p}_i\,, -\mathbf{s}_i\right)\right)\,, \tag{1.72}$$

  where Γ indicates the process rate. The integration over the spin and momenta leads to a vanishing Baryon asymmetry.

- **Departure from thermal equilibrium:** In thermal equilibrium, processes and the reverse processes happen at the same rate (no arrow of time). If there is no departure from the equilibrium, we can not have the origination of the Baryon asymmetry. To understand this requirement, let us consider a specie X and $\overline{X}$ with a non-zero Baryon number in thermal equilibrium. Their number densities are

$$n_X \simeq g_X (m_X T_U)^{3/2} \exp\left(\frac{\mu_X - m_X}{T_U}\right)\,, \tag{1.73}$$

$$n_{\overline{X}} \simeq g_X (m_X T_U)^{3/2} \exp\left(\frac{\mu_{\overline{X}} - m_X}{T_U}\right)\,. \tag{1.74}$$

  where μ_X ($\mu_{\overline{X}}$) is X ($\overline{X}$) chemical potential.

  For any process in chemical equilibrium, the final and initial total chemical potentials are equal. Considering the process $X\overline{X} \to \gamma\gamma$ and the fact that $\mu_\gamma = 0$, we obtain that

$\mu_X = -\mu_{\overline{X}}$. As a consequence, contribution from X and $\overline{X}$ to the Baryon asymmetry is

$$B \propto n_X - n_{\overline{X}} = 2\gamma_X (m_X T_U)^{3/2} e^{-m_X/T_U} \sinh\left(\frac{\mu_X}{T_U}\right) . \tag{1.75}$$

From the B-violating process $XX \to \overline{XX}$, we obtain $\mu_X = 0$. Hence, we require processes out of thermal equilibrium to have a non-vanishing Baryon asymmetry.

If the scenario fails to meet these requirements, it can not generate a Baryon asymmetry. It is fundamental to underscore that these are necessary conditions but do not guarantee the realization of the observed asymmetry.

For instance, while the Standard Mode satisfies these requirements, it fails to explain the asymmetry observed. In particular, (i) Baryon number violation results from sphaleron processes (detailed in Section 1.4.1) stemming from the triangle anomaly. These processes have a negligible effect at low temperatures, but the transitions are unsuppressed in the early Universe. (ii) The Kobayashi-Maskawa mechanism [198] violates C and CP. We may need additional CP sources to enhance the Baryon asymmetry. (iii) The electroweak phase transition assures the departure from thermal equilibrium. However, this transition is not first order, which is necessary for a successful baryogenesis mechanism. Hence, the problem of the Baryon asymmetry generation represents a hint for physics beyond the Standard Model.

The literature presents a broad spectrum of mechanisms for achieving the correct asymmetry. Some of the most famous baryogenesis mechanisms include

- **GUT Baryogenesis:** [199–208] The Baryon asymmetry originates from the decay of heavy bosons predicted by Grand Unified Theories (GUTs). Generally, these theories violate $(\mathrm{B}+\mathrm{L})$ and conserve $(\mathrm{B}-\mathrm{L})$. Standard Model sphaleron transitions would destroy the asymmetry. Furthermore, the non-observation of proton decay leads to a lower limit on the boson's mass. It causes the reheat temperature after inflation to be too high to be explained by simple inflationary models. We show a simple examples in Section 1.4.2.

- **Leptogenesis:** [196, 209–218] It is a class of mechanisms where the Baryon asymmetry derives from a Lepton asymmetry obtained from the decay of sterile neutrinos. It simultaneously explains neutrino low masses. The Majorana masses of sterile neutrinos violate the Lepton number. This asymmetry is partially transferred into the Baryon sector via sphaleron processes [219]. The details of Leptogenesis depend on the seesaw mechanism and the oscillation observation. In Section 1.4.3, we present thermal Leptogenesis.

- **Electroweak Baryogenesis:** [220–225] These models modify the scalar potential so that the electroweak phase transition becomes of the first order and provide new CP violation sources. In Section 1.4.4, we present a simple example of Electroweak Baryogenesis.

We organize the next few subsections as follows. The first discusses the sphaleron processes, the sole source of Baryon and Lepton number violation in the Standard Model. The second subsection describes a simple example of GUT baryogenesis. Afterwards, we present Thermal Leptogenesis originating from type I seesaw (see Section 1.2.2) with right-handed neutrinos with masses above 10^{10} GeV. Finally, we depict a basic example of Electroweak Baryogenesis

1.4.1 Sphaleron Processes

Here, we describe the Baryon and Lepton number violations within the Standard Model. At the classical level, the Standard Model conserves Baryon and Lepton numbers separately. Indeed, its Lagrangian is invariant under global Abelian symmetries $\mathrm{U}(1)$ associated with the Baryon and Lepton symmetries. Consequently, it does not contain processes at the tree level or any perturbative order violating B and L. However, non-perturbative effects give rise to processes violating $\mathrm{B}+\mathrm{L}$, but not $\mathrm{B}-\mathrm{L}$ [226]. As discussed below, these processes are suppressed today but were relevant in the very early Universe. The first step to understanding where this anomaly arises consists in writing down the vector-like currents

$$j^\mu_{\mathrm{B}} \equiv \sum \frac{1}{2}\bar{q}\gamma^\mu q = \sum \frac{1}{4}\left[\bar{q}\gamma^\mu(1-\gamma^5)q + \bar{q}\gamma^\mu(1+\gamma^5)q\right] , \tag{1.76}$$

where the sum is over all the colors and flavors. A similar expression holds for Leptons. Quantum effect cause the axial current ($\overline{\psi}\gamma^\mu\gamma^5\psi$) to be anomalous [227, 228]. The axial part is fundamental for calculating the divergence of j^μ_{B}. The divergence of the Baryon and Lepton numbers is [229]

$$\partial_\mu j^\mu_{\mathrm{B}} = \frac{n_f}{32\pi^2}\left(g^2 W^a_{\mu\nu}\widetilde{W}^{a\mu\nu} - g'^2 B_{\mu\nu}\widetilde{B}^{\mu\nu}\right) , \tag{1.77}$$

$$\partial_\mu j^\mu_{\mathrm{L}} = \frac{n_f}{32\pi^2}\left(g^2 W^a_{\mu\nu}\widetilde{W}^{a\mu\nu} - g'^2 B_{\mu\nu}\widetilde{B}^{\mu\nu}\right) , \tag{1.78}$$

where n_f is the number of families, and $\widetilde{W}^{a\mu\nu} = 1/2\varepsilon^{\mu\nu\rho\sigma}W^a_{\rho\sigma}$, $\widetilde{B}^{\mu\nu} = 1/2\varepsilon^{\mu\nu\rho\sigma}B^a_{\rho\sigma}$. It implies the violation of Lepton and Baryon numbers at the quantum level [226]. We notice that both the Lepton number and Baryon number currents satisfy the same relation, leading to the conservation of $\mathrm{B}-\mathrm{L}$ in the Standard Model. This is a consequence of any gauge theory including the Higgs mechanism. We can recast Eq. (1.77) and (1.78) as

$$\partial_\mu j^\mu_{\mathrm{B}} = \frac{n_f}{32\pi^2}\left(g^2\partial_\mu K^\mu - g'^2\partial_\mu k^\mu\right) , \tag{1.79}$$

where

$$K^\mu = \varepsilon^{\mu\nu\rho\sigma}\left(W^a_{\nu\rho}W^a_\sigma - \frac{1}{3}g\varepsilon^{abc}W^a_\nu W^b_\rho W^c_\sigma\right), \tag{1.80}$$

$$k^\mu = \varepsilon^{\mu\nu\rho\sigma}B_{\nu\rho}B_\sigma\,. \tag{1.81}$$

Furthermore, we highlight that the anomaly has a structure with multiple vacua. At the beginning and the end of transitions between vacua, the average values of the filed strengths are zero. Being $\partial_\mu k^\mu$ proportional to the field strength of an Abelian gauge theory, we can ignore this term. We can write the change in the Baryon number from $t = 0$ to $t = t_f$ as

$$\Delta\mathrm{B} = \mathrm{B}(t_f) - \mathrm{B}(0) \equiv \int_0^{t_f} \mathrm{d}t \int \mathrm{d}^3x\partial_\mu j^\mu_\mathrm{B} = n_f\left[N_\mathrm{CS}(t_f) - N_\mathrm{CS}(0)\right] \equiv \Delta N_\mathrm{CS}\,, \tag{1.82}$$

where N_CS are the Chern-Simons number. Neglecting the spatial component $\int \mathrm{d}^3x\vec{\nabla}\cdot\vec{K}$, they are defined as

$$N_\mathrm{CS} = \frac{n_f}{32\pi^2}\int \mathrm{d}^3x g^2 K^0\,. \tag{1.83}$$

For instance, this approximation holds if $\vec{K}$ vanishes at spatial infinity or assuming periodic boundary conditions. We notice that while N_CS are not gauge invariant, ΔN_CS is [229]. The transition between vacua leads to the production of fermions. These transitions are classically forbidden because B is an exact global symmetry. A barrier obtained as the static solution of equations of motion separates adjacent vacua. The saddle points with half-integer Chern-Simons number are the Sphalerons. They are the configuration of maximum energy in the minimum energy path connecting two vacua. The Spahalerons are unstable and localized in space. The transition from two vacua can happen only via quantum tunneling for temperatures lower than the barrier's height. Instead, if the temperature is higher than the barrier, thermal fluctuation can classically cause the transition. In particular, the tunneling transition probability is of the order

$$\exp\left\{-\frac{16\pi^2}{g^2}\right\} \sim 10^{-170}\,, \tag{1.84}$$

that is too small to have observable effects. The sphaleron solution in the temporal gauge $W^a_0 = 0$ is

$$W^a_i = \frac{2i}{g}\left(\varepsilon_{iaj}\frac{x_j}{r^2}\right)f(\xi)\,, \tag{1.85}$$

$$\phi = \frac{n_f}{\sqrt{2}}i\frac{\vec{\sigma}\cdot\vec{x}}{r}\begin{pmatrix}0\\1\end{pmatrix}h(\xi) \tag{1.86}$$

where $f(0) = h(0) = 0$, $f(\infty) = h(\infty) = 1$, $r = |\vec{x}|^2$, $\xi = r/r_0 = rgn_f$. In this case, the probability transition is

$$P \sim \exp\left\{-\frac{M_{\text{sph.}}}{T_U}\right\}, \qquad\qquad M_{\text{sph.}} = 8\pi\frac{m_W}{g^2}\,. \tag{1.87}$$

We can interpret the sphaleron as an unstable particle of mass $M_{\text{sph.}}$.

Near the thermal equilibrium, we can describe the evolution of the Chern-Simons numbers in terms of the sphaleron rate [230]

$$\Gamma_{\text{sph.}} = \lim_{V,t\to\infty}\frac{\langle[N_{\text{CS}}(t) - N_{\text{CS}}(0)]^2\rangle}{Vt}\,, \tag{1.88}$$

where $V \sim a^3$ is the spatial volume. In Ref. [231–233], the authors estimate $\Gamma_{\text{sph.}} \approx (25 \pm 2)\alpha_W^5 T_U^4$ in a pure $\mathrm{SU}(2)$ gauge theory. We can use the sphaleron rate to calculate when the sphaleron processes go out of the equilibrium and freeze-out as [234]

$$\Gamma_{\text{sph.}}(T_{\text{sph.}})/T^3_{\text{sph.}} = \tilde{\alpha}H(T_{\text{sph.}})\,, \tag{1.89}$$

where $\tilde{\alpha} \approx 0.105$ is a function of the Higgs vacuum expectation value. In a radiation dominated universe $H^2(T_U) = \pi^2 g_* T^4/(90\mathrm{M_{Pl}})$, therefore $T_{\text{sph.}} = (131.7 \pm 2.3)\,\mathrm{GeV}$.

In the following we estimate the equilibrium relation between B and L. We follow the prescription of Ref. [235]. We consider temperatures above the electroweak phase transition, we can approximate all the species as ultra-relativistic. The excess of particle over antiparticle number density is

$$n_i - n_{\bar{i}} = \frac{g_i T_U^3}{6}\begin{cases} \frac{\mu_i}{T_U} & \text{fermions} \\ 2\frac{\mu_i}{T_U} & \text{bosons}\end{cases}\,, \tag{1.90}$$

where μ_i and g_i are the chemical potential and the degrees of freedom of the i-th specie. The relevant fields in this context are N left-handed quarks and Leptons ($u_{i\,L}$, $u_{i\,L}$, $\nu_{i\,L}$, $\ell_{i\,L}$, $i = 1, ..., N$), N right-handed quarks and charged Leptons ($u_{i\,R}$, $u_{i\,R}$, $\ell_{i\,R}$, $i = 1, ..., N$), $W^{\pm}$, and m complex Higgs doublets (ϕ_i^+, ϕ_i^0, ϕ_i^-, $\phi_i^{o\,*}$, $i = 1, ..., m$). We can neglect W^0, B^0, G since they have vanishing chemical potential. Furthermore, having a vanishing chemical potential for the gluons guarantees the same chemical potential for all quark's colors. We denote with μ_W, $W^{\pm}$, μ_0 (μ_-) , $\mu_{u\,L}$ ($\mu_{u\,R}$) , $\mu_{d\,L}$ ($\mu_{d\,R}$), $\mu^i_{\ell\,L}$ ($\mu^i_{\ell\,R}$), μ_i are the chemical potential for $W^{\pm}$, the neutral (charged) Higgs fields, the left-(right-)handed up quarks, the left-(right-)handed down quarks, the left-(right-)handed charged Leptons quarks, and neutrinos respectively. Fast electroweak interactions in the early Universe impose the same relations [235]

$$\begin{aligned}
W^- \longleftrightarrow \phi^- + \phi^0 \quad &\Longrightarrow \quad \mu_W = \mu_- + \mu_0\,, && (1.91)\\
W^- \longleftrightarrow \overline{u}_L + d_L \quad &\Longrightarrow \quad \mu_{d\,L} = \mu_{u\,L} + \mu_W\,, && (1.92)\\
W^- \longleftrightarrow \overline{\nu}^i_L + \ell^i_L \quad &\Longrightarrow \quad \mu^i_{\ell\,L} = \mu_i + \mu_W\,, && (1.93)\\
\phi^0 \longleftrightarrow \overline{u}_L + u_R \quad &\Longrightarrow \quad \mu_{u\,R} = \mu_0 + \mu_W\,, && (1.94)\\
\phi^0 \longleftrightarrow \overline{d}_L + d_R \quad &\Longrightarrow \quad \mu_{d\,R} = -\mu_0 + \mu_W + \mu_{u\,L}\,, && (1.95)\\
\phi^0 \longleftrightarrow \overline{\ell}^i_L + \ell^i_R \quad &\Longrightarrow \quad \mu^i_{\ell\,R} = -\mu_0 + \mu_W + \mu_i\,. && (1.96)
\end{aligned}$$

These relations allow recasting the chemical potentials in terms of μ_W, μ_0, $\mu_{u\,L}$, and $\mu = \sum_i \mu_i$. As long as the sphaleron interactions are rapid, it must be true that

$$N(\mu_{u\,L} + 2\mu_{dL}) + \mu = 3N\mu_{u\,L} + 2N\mu_W + \mu = 0\,. \tag{1.97}$$

We then can write the Baryon, Lepton, charge, and $\mathcal{I}_3$ number densities as

$$\begin{aligned}
\mathrm{B} &\equiv N(\mu_{u\,L} + \mu_{u\,R}) + N(\mu_{d\,L} + \mu_{d\,R}) = 4N\mu_{u\,L} + 2N\mu_W\,, && (1.98)\\
\mathrm{L} &\equiv \sum_i (\mu_i + \mu^i_{\ell\,L} + \mu^i_{\ell_R}) = 3\mu + 2N\mu_W - N\mu_0\,, && (1.99)\\
Q &\equiv N(\mu_{u\,L} + \mu_{u\,R}) - 2N(\mu_{d\,L} + \mu_{d\,R} - \sum_i (\mu^i_{\ell\,L} + \mu^i_{\ell_R}) - 4\mu_W - 2\mu_- \\
&= 2\mu_{u\,L} - 2\mu - (4N + 2m + 4)\mu_W + (4N + 2m)\mu_0\,, && (1.100)\\
Q_3 &\equiv \frac{3N}{2}(\mu_{u\,L} - \mu_{d\,L}) + \frac{1}{2}\sum_i (\mu_i - \mu^i_{\ell\,L}) - 4\mu_W - m(\mu_0 + \mu_-)\\
&= -(2N + m + 4)\mu_W\,. && (1.101)
\end{aligned}$$

Let us consider $T_{\text{sph.}} < T_{\text{EW}}$, where $T_{\text{EW}} = (159 \pm 1)$ GeV is the temperature of the electroweak phase transition. In this case, Q and Q_3 must be equal to zero, implying that $\mu_W = 0$. Having $Q = 0$ allows expressing B and L in terms of $\mu_{u\,L}$ [235]

$$\begin{aligned}
\mathrm{B} &= 4N\mu_{u\,L}\,, && (1.102)\\
\mathrm{L} &= -\frac{14N^2 + 9Nm}{2N + m}\mu_{u\,L}\,. && (1.103)
\end{aligned}$$

Since $(\mathrm{B} - \mathrm{L})$ is conserved, we recast these equation as

$$\begin{aligned}
\mathrm{B} &= \frac{8N + 4m}{22N + 13m}(\mathrm{B} - \mathrm{L})\,, && (1.104)\\
\mathrm{L} &= -\frac{14N + 9m}{22N + 13m}(\mathrm{B} - \mathrm{L})\,. && (1.105)\\
& && (1.106)
\end{aligned}$$

	$X \to qq$	$X \to \overline{q}\overline{\ell}$	$\overline{X} \to \overline{q}\overline{q}$	$\overline{X} \to \ell q$
	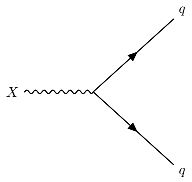	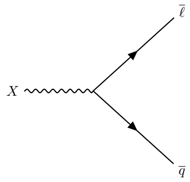	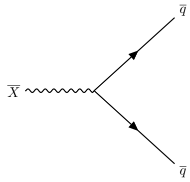	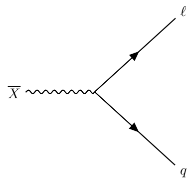
BR	r	$1-r$	$\overline{r}$	$1-\overline{r}$
$\not{B}$	$\frac{2}{3}$	$-\frac{1}{3}$	$-\frac{2}{3}$	$+\frac{1}{3}$
$\not{L}$	0	-1	0	1

Table 1.4: Decay rate, Baryon and Lepton number violation for the relevant processes.

Conversely, if we consider $T_{\rm sph.} < T_{\rm EW}$, Q_3 can be different from zero because $\mathrm{SU}(2)_L$ is broken. $Q = 0$ still holds. Furthermore, μ_0 must be equal to zero because of the vacuum condensate of ϕ^0. In this case, we we have [235]

$$\mathrm{B} = \frac{8N^2 + 4N(m+2)}{m+2}\mu_{u\,L}\,, \tag{1.107}$$

$$\mathrm{L} = -\frac{16N^2 + 9N(m+2)}{m+2}\mu_{u\,L}\,. \tag{1.108}$$

In terms of $(\mathrm{B}-\mathrm{L})$ they read as

$$\mathrm{B} = \frac{8N + 4(m+2)}{24N + 13(m+2)}(\mathrm{B}-\mathrm{L})\,, \tag{1.109}$$

$$\mathrm{L} = -\frac{14N + 9(m+2)}{24N + 13(m+2)}(\mathrm{B}-\mathrm{L})\,. \tag{1.110}$$

$$\tag{1.111}$$

Considering the Standard Model with $N = 3$, $m = 1$, we have

$$\mathrm{B} = \begin{cases} \frac{28}{79}(\mathrm{B}-\mathrm{L}) & T_{\rm sph.} > T_{\rm EW} \\ \frac{12}{37}(\mathrm{B}-\mathrm{L}) & T_{\rm sph.} < T_{\rm EW} \end{cases} \tag{1.112}$$

In conclusion, the rapid sphaleron transition do not lead to a zero value for $(\mathrm{B}+\mathrm{L})$ if $(B-L) \neq 0$ before the processes go out of equilibrium and the relationship between B and L depends on when the sphaleron freeze-out occurs.

1.4.2 Baryogenesis in Grand Unified Theories.

Grand Unified Theories predict the unification of the three fundamental forces at high scales into one described with a single coupling. These theories maintain the invariance under the Standard Model gauge group, recovered at lower energies after several symmetry breakings. Grand Unified theories typically consider an extended scalar and boson sector. Notably, if they do not extend the fermion sector, they do not violate $\mathrm{B}-\mathrm{L}$ [195].

In the following, we consider $\mathrm{SU}(5)$ theory, the smallest group containing the Standard Model. It embeds each generation of the Standard Model into an anti-quintuplet and a decouplet (an antisymmetric rank-2 tensor)

$$\mathbf{10}:\begin{pmatrix} 0 & (u_b^i)^c & -(u_g^i)^c & (u_r^i)^c & d_r^i \\ -(u_b^i)^c & 0 & (u_r^i)^c & u_g^i & d_g \\ (u_g^i)^c & -(u_r^i)^c & 0 & u_b^i & d_b^i \\ -u_r^i & -u_g^i & -u_b^i & 0 & (\ell^i)^c \\ -d_r^i & -d_g^i & -d_b^i & -(\ell^i)^c & 0 \end{pmatrix}, \qquad \mathbf{\bar{5}}:\begin{pmatrix} (d_r^i)^c \\ (d_g^i)^c \\ (d_b^i)^c \\ \ell^i \\ \nu_i \end{pmatrix}, \tag{1.113}$$

where g, b, r are the color indices. The gauge sector of the theory consists of 24 gauge bosons, organized as follows

$$V_\mu = \left(\begin{array}{c|cc} G_\mu & X_\mu/\sqrt{2} & Y_\mu/\sqrt{2} \\ \hline X_\mu^\dagger/\sqrt{2} & \multicolumn{2}{c}{\multirow{2}{*}{$W_\mu/\sqrt{2}$}} \\ Y_\mu^\dagger/\sqrt{2} & & \end{array}\right) + B_\mu\sqrt{\frac{3}{5}}\left(\begin{array}{c|c} -\mathbf{I}_{3\times3}/3 & 0 \\ \hline 0 & \mathbf{I}_{2\times2}/2 \end{array}\right), \tag{1.114}$$

where V_μ is a 5×5 matrix, G_μ, W_μ, and B_μ are the Standard Model gauge bosons, lastly X_μ and Y_μ are new Leptoquark gauge bosons linking quarks and Leptons.

In the following, we consider the heavy boson X that can decay in qq or $\bar{q}\bar{\ell}$ pairs. The first process leads to a Baryon number violation of $2/3$, and the second of $-1/3$. Similarly, $\overline{X}$ decays into $\overline{qq}$ or $q\ell$. CPT invariance implies the equality of the total decay rates, $\Gamma_X = \Gamma_{\overline{X}}$. However, C and CP violation means that $\mathrm{BR}(X\to qq)\equiv r$ and $\mathrm{BR}(\overline{X}\to\overline{qq})\equiv\bar{r}$ are not necessarily equal. Table 1.4 conveniently encapsulates the branching ratio (BR) and the Baryon and Lepton number violation of the relevant processes.

For temperatures close to the decay temperature $T_D \lesssim m_X$, the specie goes out of thermal equilibrium because the inverse decays are negligible ($\Gamma_X/H \ll 1$). In particular, the Baryon asymmetry is the one produced by the out-of-equilibrium decay at T_D

$$\mathrm{Y_B} = \mathrm{Y}_X^* \left(\mathrm{B}_X - \mathrm{B}_{\overline{X}}\right) , \tag{1.115}$$

where B_X and $\mathrm{B}_{\overline{X}}$ are the net Baryon number generated by X and $\overline{X}$ decay, $Y_X^* = Y_X(T_D) \simeq Y_{\overline{X}}(T_D)$. The net Baryon number produced by X and $\overline{X}$ are

$$\mathrm{B}_X = +\frac{2}{3}r - \frac{1}{3}(1-r) = r\,, \tag{1.116}$$
$$\mathrm{B}_{\overline{X}} = -\frac{2}{3}\overline{r} + \frac{1}{3}(1-\overline{r}) = -\overline{r}\,. \tag{1.117}$$

We parametrize the CP violation as $\epsilon = r - \overline{r}$. Then, we write the final Baryon asymmetry produced as

$$\mathrm{Y_B} = \mathrm{Y}_X^* \epsilon = \frac{\epsilon}{g_*}\,. \tag{1.118}$$

where we obtained the last equality considering that $n_\gamma \simeq n_X$, $s \simeq g_* n_\gamma$. We conclude that we need small C and CP violations to achieve the observed Baryon asymmetry. However, we simultaneously produce

$$\mathrm{Y_L} = \mathrm{Y}_X^* \epsilon\,, \tag{1.119}$$

causing the sphaleron processes to wash out the asymmetry attained.

1.4.3 Thermal Leptogenesis

The conservation of $\mathrm{B-L}$ and violation of $\mathrm{B+L}$ open the possibility of generating the observed Baryon asymmetry from a Lepton asymmetry. The mechanism relies on the partial conversion of the Lepton number into the Baryon sector via sphaleron processes. Here, we focus on the simplest Leptogenesis realization.

Thermal Leptogenesis is a simple model generating the Baryon asymmetry from the decay of right-handed neutrinos. It implements the type I seesaw mechanism (see Section 1.2.2 for more details) with a hierarchical mass spectrum for the right-handed neutrinos ($M_1 < M_2 < M_3$). Thermal scatterings after inflation produce the lightest one N_1. The subsequent out-of-equilibrium decay generates the Lepton asymmetry if the Yukawa couplings Y (see Eq.(1.56)) violate CP. In the following, we consider a normal ordering for the left-handed neutrinos ($m_1 < m_2 < m_3$). Furthermore, we assume $m_1 \equiv m_l \lesssim m_2 \ll m_3 \equiv m_h$.

Fundamental for thermal Leptogenesis is the CP violation in N_1 decay. The CP violation stems from the interference of the diagrams in Fig. 1.6. We define

$$\epsilon_{\alpha\alpha} = \frac{\Gamma(N_1 \to \ell_\alpha\,\phi) - \Gamma(N_1 \to \overline{\ell}_\alpha\,\overline{\phi})}{\Gamma(N_1 \to \ell_\alpha\,\phi) + \Gamma(N_1 \to \overline{\ell}_\alpha\,\overline{\phi})}\,, \tag{1.120}$$

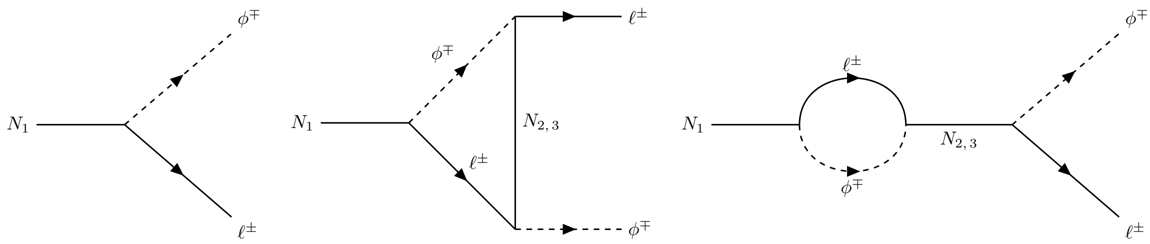

Figure 1.6: N_1 decay diagrams contributing to the CP violation.

where Γ indicates the decay with of the process. At temperatures higher than $\sim 10^{12}$ GeV, the charged Lepton Yukawa interactions are slower than the Hubble rate. Thus, if the asymmetry originates at higher temperatures, Leptogenesis is flavor blind [196]. Assuming $M_1 \ll M_2,\, M_3$, we obtain [214]

$$\epsilon = \sum_{\alpha} \epsilon_{\alpha\alpha} = -\frac{3}{16\pi} \sum_{j=2,\,3} \frac{M_1}{M_j} \frac{\mathrm{Im}(YY^{\dagger})_{1j}}{(YY^{\dagger})_{11}} \,. \tag{1.121}$$

From the expression of Y in Eq. (1.56), we highlight that U_{PMNS} drops out. Thus, there is no connection between the low-scale Dirac CP violation and high-scale CP asymmetry. Indeed, ϵ depends only on the complex mixing angles in R. As per the assumptions made so far, Ref. [211] shows that the only relevant rotation is described as

$$R = \begin{pmatrix} \cos(x+iy) & 0 & \sin(x+iy) \\ 0 & 1 & 0 \\ -\sin(x+iy) & 0 & \cos(x+iy) \end{pmatrix} . \tag{1.122}$$

where x and y are real parameters. We can then express ϵ as

$$|\epsilon| = \frac{3M_1}{16\pi v^2} \frac{|\Delta m^2_{\mathrm{atm}}|}{m_h + m_l} \frac{|\sin(2x)\sinh(2y)|}{\cosh(2y) - f\cos(2x)} \tag{1.123}$$

where $f = (m_h - m_l)/(m_h + m_l)$. ϵ controls both N_1 thermal production and decay with the same magnitude but in opposite sign. If we start from a vanishing N_1 abundance, the inverse decay produce an initial "anti-asymmetry" in the Lepton sector. When $T_U = M_1$, the thermal population will decay as long as $\Gamma/H|_{T_U=M_1} > 1$, where Γ is the decay rate. It is equivalent to [196, 212, 214]

$$K \equiv \frac{\tilde{m}_1}{m^*} > 1 \,, \tag{1.124}$$

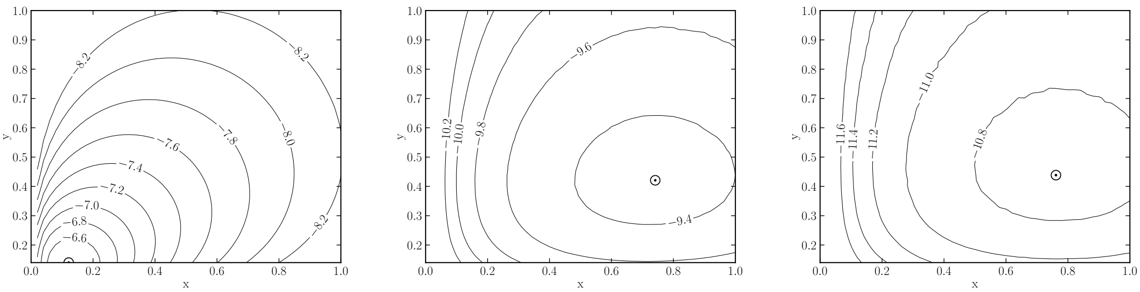

Figure 1.7: The plot illustrates the Baryon asymmetry $\log_{10} \mathrm{Y_B}$ as a function of x, y for $m_h = \sqrt{m^2_{\rm atm}} \approx 0.05$ eV (left panel), $m_h = 0.1$ eV (middle panel) and $m_h = 0.2$ eV (right panel), with $M_1 = 2.0 \times 10^{13}$ GeV. In each plot, we indicate with $\odot$ the point maximizing $\mathrm{Y_B}$. We took the Figures from Ref. [9].

where

$$
\begin{aligned}
m^* &\equiv \frac{8\pi v^2}{M_1^2} H(T_U = M_1)\,, && (1.125)\\
\tilde{m}_i &\equiv \sum_\alpha \frac{|Y_{\alpha\, i}|^2 v^2}{M_1}\,. && (1.126)
\end{aligned}
$$

The right-handed neutrino out of equilibrium decay would cancel out the initial "anti asymmetry" if it were not for the washout processes. This is called "strong washout" regime. We can divide the washout processes into two categories $\Delta \mathrm{L} = 1$ and $\Delta \mathrm{L} = 2$. The first category includes the inverse decay ($\ell^\pm \phi^\mp \to N_1$) that is Boltzmann suppressed at temperatures lower than M_1. The second category comprises scattering processes as $\ell^\pm\phi^\mp \to \ell^\mp \phi^\pm$ that are mediated by N_1. They are not Boltzmann suppressed since an off-shell N_1 can be the mediator. For $K > 1$, N_1 decays when the processes are effective. The washout cancels out the initial "anti asymmetry". It leads to a non-zero Lepton asymmetry. Conversely, for $K < 1$, N_1 decay is slower than the Hubble parameter meaning that it decays when the washout processes are too weak. This is called "*weak washout*" regime. It requires additional mechanisms to produce an initial population of right-handed neutrinos [196]. Moreover, when examining the definition of K, it becomes evident that the weak washout regime necessitates m_h really close to $\sqrt{\Delta m^2_{\rm atm}}$, the lower limit allowed by oscillation data. It implies that the parameter space where this regime holds is exceptionally narrow. In the following, we consider the strong washout regime only. Reason for which we present an analysis limited to $|y| > 0.14$. Additionally, the washout suppresses any asymmetry produced by $N_{2,3}$.

Since the sphaleron processes conserve $\mathrm{B} - \mathrm{L}$, we track its number density. In doing so, we need to understand also the evolution of N_1 number density. In the following, we account for

- **1 → 2 N₁ decay**. In particular, we look for $N_1 \to \ell\phi^+$ and its CP conjugate $N_1 \to \bar{\ell}\phi^-$.

The total rate is proportional to N_1 number density and Γ_{N_1}. The depletion of N_1 abundance source $\mathrm{B}-\mathrm{L}$ asymmetry.

- **2 → 1 inverse decay** $\ell^{\pm}\phi^{\mp} \to \mathbf{N_1}$. We relate the inverse decay to the decay rate as $\Gamma^{\mathrm{ID}} = \Gamma_{N_1} n_{N_1}^{\mathrm{eq}}/n_{\ell}^{\mathrm{eq}}$, where n_i^{eq} si the equilibrium number density of the specie i. These processes produce N_1 abundance and wash out the asymmetry.

- **2 → 2 scatterings mediated by $\mathbf{N_1}$.**Processes like $\phi^{\pm}\ell^{\rightarrow}\phi^{\mp}\ell^{\pm}$ do not contribute to the asymmetry but are a fundamental component of the washout. We neglect the scattering involving gauge bosons and top quarks. This approximation is justified because these processes are $\mathcal{O}(Y^2 h_t)$, where h_t is the top quark Yukawa coupling.

Furthermore, we neglect the effects of 3-body decay because they are numerically small [236]. The Boltzmann equation for N_1 and $\mathrm{B}-\mathrm{L}$ in term of $\alpha = \log_{10} a$, where a is the cosmological scale factor, reads as

$$\begin{aligned}
\frac{\mathrm{d}\mathcal{N}_{N_1}}{\mathrm{d}\alpha} &= \ln(10)\frac{\Gamma_{N_1}^{\mathrm{th.}}}{H}(\mathcal{N}_{N_1}^{\mathrm{eq.}} - \mathcal{N}_{N_1})\,, && (1.127)\\
\frac{\mathrm{d}\mathcal{N}_{\mathrm{B-L}}}{\mathrm{d}\alpha} &= \frac{\ln(10)}{H}\left[\epsilon\Gamma_{N_1}^{\mathrm{th.}}(\mathcal{N}_{N_1} - \mathcal{N}_{N_1}^{\mathrm{eq.}}) + \left(\frac{1}{2}\frac{\mathcal{N}_{N_1}^{\mathrm{eq.}}}{\mathcal{N}_{\ell}^{\mathrm{eq.}}}\Gamma_{N_1}^{\mathrm{th.}} + \gamma\frac{a^3}{\mathcal{N}_{\ell}^{\mathrm{eq.}}}\right)\mathcal{N}_{\mathrm{B-L}}\right]\,, && (1.128)
\end{aligned}$$

where $\mathcal{N}_i \equiv a^3 n_i$ is the comoving number density of i, $H = (\mathrm{d}a/\mathrm{d}t)/a$ is the Hubble parameter. $\Gamma_{N_1}^{\mathrm{th.}}$ is the thermally averaged three level N_1 decay rate, defined as

$$\Gamma_{N_1}^{\mathrm{th.}} = \langle\frac{M_1}{E_{N_1}}\rangle\frac{(Y^{\dagger}Y)_{11}M_1}{8\pi} \tag{1.129}$$

where $\langle M_1/E_{N_1}\rangle \approx K_1(z)/K_2(z)$, where K_i is the n^{th} order modified Bessel function of the second kind and $z \equiv M_1/T$. γ asseses the contribution to the washout originating from $\Delta\mathrm{L} = 2$ processes. Ref. [237] shows that

$$\gamma = \frac{3T_U^6}{4\pi^5 v^4}\mathrm{Tr}[m_{\nu}^{\dagger}m_{\nu}]\,. \tag{1.130}$$

Being $M_1 \gg T_{\mathrm{EWPT}}$, the Lepton asymmetry is produced long before the sphaleron processes freeze out. The final Baryon asymmetry freezes when the sphaleron processes go out of equilibrium at $T_{\mathrm{sph.}}$. Thus, we quantify the final Baryon asymmetry as

$$\mathrm{Y_B} = \frac{12}{37}\frac{\mathcal{N}_{\mathrm{B-L}}(T_{\mathrm{sph.}})}{\mathcal{S}}\,. \tag{1.131}$$

In a standard cosmological scenario $\mathcal{S} = 2\pi^2 g_*(Ta)^3/45$. For $T \gtrsim 300\,\mathrm{GeV}$, $g_* = 106.75$ [238]. We stress that the relevant quantities in Eqs. (1.127), (5.19) are defined in the four dimensional parameter space $(x,\, y,\, M_1,\, m_h)$. In Fig. 1.7, we show the behaviour of $\log_{10}\mathrm{Y_B}$ as a function of $x,\, y$ for $M_N = 2.0{\cdot}10^{13}\,\mathrm{GeV}$ and $m_h = 0.05\,\mathrm{eV}$ (left plot), $m_h = 0.1\,\mathrm{eV}$ (middle plot), $m_h = 0.2\,\mathrm{eV}$

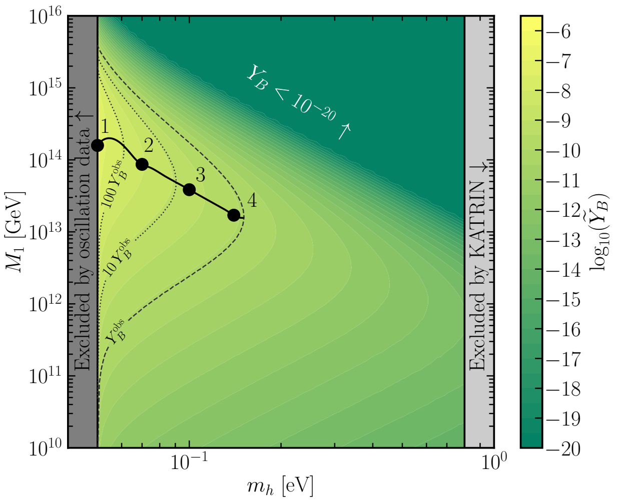

	m_h [eV]	M_1 [GeV]	$\widetilde{\rm Y}_{\rm B}$
1	0.05	1.5×10^{14}	1.5×10^{-6}
2	0.07	1.0×10^{14}	3.6×10^{-9}
3	0.10	4.0×10^{13}	5.5×10^{-10}
4	0.14	2.0×10^{13}	1.2×10^{-10}

Figure 1.8: **Maximum Baryon asymmetry generated as a function of m_h and M_1.** The dashed and dotted contours show constant $\log_{10}(\widetilde{\rm Y}_{\rm B}/{\rm Y}_{\rm B}^{\rm obs})$ reported in the labels. The absolute maximum is achieved for $m_h = 0.05\,{\rm eV}$, $M_1 = 1.5 \cdot 10^{14}\,{\rm GeV}$ and we indicate with dot 1. The black line connect the points maximizing $\widetilde{\rm Y}_{\rm B}$ for fixed M_1. The grey bands picture experimental bounds. The black dots are four benchmark cases for $m_h = 0.05\,{\rm eV}$, $0.07\,{\rm eV}$, $0.1\,{\rm eV}$, $0.14\,{\rm eV}$, whose values are reported in the Table. We will refer to them in Chapter 6. We took this Figure from Ref. [9].

(right plot). We indicate with $\odot$ the $(x,\, y)$ maximizing ${\rm Y}_{\rm B}$. We notice that for $m_h \gg \sqrt{m^2_{\rm atm}}$ the maximum is achieved for $x \simeq \pi/4$, $y \simeq 0.44$ [237].

We want to show the parameter space region that can reproduce the observed Baryon asymmetry. We consider the parameter space region in

$$0 < \quad x \quad < \pi\,, \tag{1.132}$$

$$0.14 < \quad y \quad < \pi\,, \tag{1.133}$$

$$\sqrt{\Delta m^2_{\rm atm}} < \quad m_h \quad < 0.8\,{\rm eV}\,, \tag{1.134}$$

$$10^{10}\,{\rm GeV} < \quad M_1 \quad < 10^{16}\,{\rm GeV}\,. \tag{1.135}$$

We fix x and y to maximize the asymmetry. In this way, we reduce our parameter space to $(M_1,\, m_h)$. We notice that $y = 0.44$ and $x = \pi/4$ maximize ${\rm Y}_{\rm B}$ if $m_h \gg \sqrt{\Delta m^2_{\rm atm}}$ [237]. We define

$$\widetilde{\rm Y}_{\rm B}(m_h,\, M_1) = \max_{x,\,y} {\rm Y}_{\rm B}(x,\, y,\, m_h,\, M_1) \tag{1.136}$$

and show its behaviour in Fig. 1.8. The lower limit on m_h stems from oscillation data, while the upper limit comes from KATRIN [20].

We show the interplay between Thermal Leptogenesis and Primordial Black Holes in Chapter 6.

1.4.4 Electroweak Baryogenesis

We define Electroweak Baryogenesis as any mechanism where the Baryon asymmetry originates at the Electroweak Phase transition. Differently from the prevous cases, we do not attain the departure from thermal equilibrium with the decay of a particle, but with a first order phase transition.

Here, we summarize the shared features characterizing the Electroweak Baryogenesis scenarios. For instance, they all assume a radiation-dominated Universe with a symmetric content of Baryons and a manifest $\mathrm{SU}(2)_L \times \mathrm{U}(1)_Y$ symmetry. When the Universe reaches $T_U \lesssim 100\,\mathrm{GeV}$, the Higgs acquires a non-zero vacuum expectation value breaking the electroweak symmetry. The generation of the Baryon asymmetry happens during this phase transition. The fundamental requirement is that this phase transition is *strongly first-order*. In a first order phase transition, the Higgs vacuum expectation value becomes different from zero abruptly at a critical temperature $T_{\mathrm{cr.}}$ and an energy barrier separates the two minima. Conversely, a transition is second order when the vacuum expectation value changes continuously as the temperature crosses $T_{\mathrm{cr.}}$ with no energy barrier between the two minima. We schematically depict the two the two phase transitions in Fig. 1.10. A first order phase transition induces the formation of bubbles, leading to the coexistence of symmetric and broken phases, two different thermodynamical states in equilibrium (see the left panel of Fig. 1.9 for a schematic representation). In particular, the Higgs has a non-zero vacuum expectation value inside (true vacuum) the bubble and zero outside (false vacuum). As the temperature decreases, the bubbles percolate, leaving the Universe in a broken phase. Outside the bubble, sphaleron processes are active, generating and reprocessing the asymmetry leading to a zero neat asymmetry. If the transition is *strongly first-order*, the Sphaleron processes can not reprocess the asymmetry if it ends inside the bubble, where they are negligible. The mechanism is successful if the interactions of fermions with the bubble walls violate CP. Since the CP violation in the Standard Model is insufficient to produce the observed asymmetry, a successful electroweak baryogenesis mechanism must provide new CP violation sources.

The electroweak phase transition in the Standard Model is not *strongly first-order*. Thus, all the electroweak baryogenesis mechanisms need to extend the Standard Model scalar sector to verify this requirement.

We can schematize the mechanism as follows (see also the right panel of Fig. 1.9) [239]:

- CP violating scattering of the particles in the plasma with the Bubble wall generate CP and C asymmetries in particle abundance.
- Outside the bubble, the sphaleron transitions produce a neat Baryon asymmetry from the asymmetries generated by the scatterings.

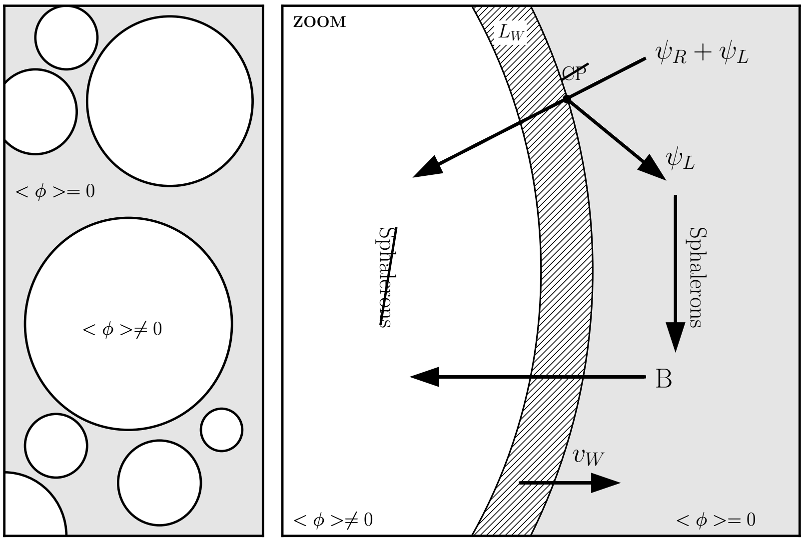

Figure 1.9: In the left panel, we show the bubble with a broken phase expanding in the plasma with an electroweak-symmetric phase. The right panel shows the production of the Baryon asymmetry near the bubble walls. We start with an equal number of left-handed particles and right-handed antiparticles outside the bubble (for simplicity we show only ψ_R and ψ_L). We highlight that left-handed antiparticles and right-handed particles do not participate in sphaleron processes. CP violating scattering, the bubble wall segregates the particles generating a chiral asymmetry, later converted to the Baryon sector thanks to the sphaleron processes. The expanding bubble swallows this asymmetry before the sphaleron processes re-even the asymmetry.

- A fraction of the Baryon asymmetry ends inside the expanding bubble. Here, the sphaleron processes are suppressed and cannot wash out the asymmetry.

Here, we focus on the renormalized finite-temperature effective potential of the Higgs boson and show why the transition is not fist order for m_H observed. The effective potential at one-loop order is [240]

$$V_{\text{eff}}(\phi,\, T_U) = V(\phi) + V_1(\phi) + \Delta V_1(\phi,\, T_U)\,. \tag{1.137}$$

where $V(\phi)$ is the Higgs potential at tree level shown in Eq. (1.10). $V_1(\phi)$ is the effective potential at one loop for $T_U = 0$ defined as [241]

$$V_1(\phi) = \sum_i \frac{n_i(-1)^{2s_i}}{4(4\pi)^2} m_i^4(\phi) \left[\ln\left(\frac{m_i(\phi)}{\mu^2}\right) + \mathcal{C}_i\right]\,, \tag{1.138}$$

where the sum is performed over all the particles of the theory. m_i, n_i, and s_i are the mass, number of degrees of freedom, and spin of the i-th specie. μ is a mass independent renormalizarion scale and $\mathcal{C}_i$ are scheme-dependent constants. $\Delta V_1(\phi,\, T_U)$ contains the correction of

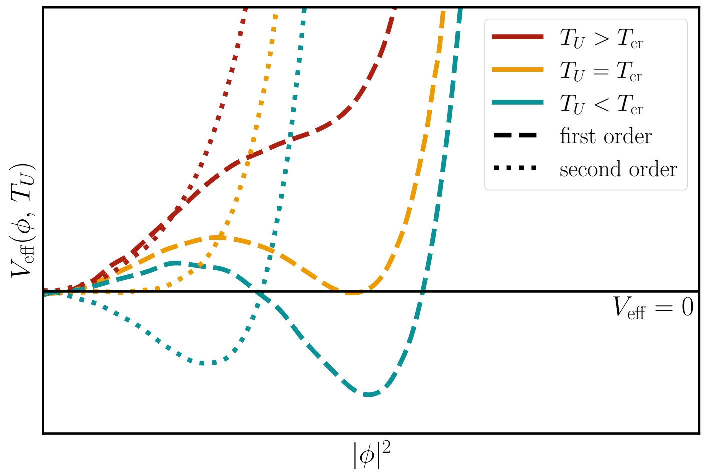

Figure 1.10: The plot shows the profile of the effective potential for a first- (second-) order phase transition with dashed (dotted) lines for three temperatures. The red, yellow, and blue lines indicate $T_U > T_{\rm cr.}$, $T_U = T_{\rm cr.}$, and $T_U < T_{\rm cr.}$ respectively.

the effective potential at one loop at finite temperature and is defined as [240]

$$\Delta V_1(\phi, T_U) = \sum_{i=boson} n_i \frac{T^4}{2\pi^2} J_b\left(\frac{m_i^2}{T_U^2}\right) - \sum_{i=fermion} n_i \frac{T^4}{2\pi^2} J_f\left(\frac{m_i^2}{T_U^2}\right), \tag{1.139}$$

where [242]

$$J_f(x^2) \simeq \begin{cases} -\frac{7\pi^4}{360} - \frac{\pi^4}{24}x^2 - \frac{1}{32}x^4 \ln\left(\frac{x^2}{a_f}\right) + \mathcal{O}(x^3) & x \ll 1 \\ \left(\frac{x}{2\pi}\right)^{3/2} e^{-x}\left(1 + \frac{15}{8x} + \mathcal{O}(x^{-2})\right) & x \gg 1 \end{cases}, \tag{1.140}$$

$$J_f(x^2) \simeq \begin{cases} -\frac{\pi^4}{45} + \frac{\pi^2}{12}x^2 - \frac{\pi}{6}x^3 - \frac{1}{32}x^4 \ln\left(\frac{x^2}{a_f}\right) \mathcal{O}(x^3) & x \ll 1 \\ \left(\frac{x}{2\pi}\right)^{3/2} e^{-x}\left(1 + \frac{15}{8x} + \mathcal{O}(x^{-2})\right) & x \gg 1 \end{cases}, \tag{1.141}$$

where $\ln a_f \simeq 5.4076$ and $\ln a_b \simeq 2.6351$. To better understand the thermal correction to the Higgs potential, we rewrite the potential in the following approximated form valid at high temperatures [242]

$$V_{\rm eff}(\phi, T_U) \simeq D(T_U^2 - T_0^2) - ET\phi^3 + \frac{\overline{\lambda}}{4}\phi^4, \tag{1.142}$$

where D and $\overline{\lambda}$ are independent of ϕ, but slowly depends on T_U.

For $E = 0$, at $T_U = T_0$ we have a second order phase transition. For $T_U < T_0$, the Higgs

Lattice	4D Isotropic [244]	4D Anisotropic [245]	3D Isotropic [246]	3D isotropic [247]
$m_H <$	(80 ± 7) GeV	(72.4 ± 1.7) GeV	(72.3 ± 0.7) GeV	(72.4 ± 0.9) GeV

Table 1.5: Upper limit on the Higgs mass to have a first order phase transition

vacuum expectation value is

$$\langle \phi \rangle = T_0 \sqrt{\frac{2D}{\bar{\lambda}} \left(1 - \frac{T_U^2}{T_0^2}\right)} \tag{1.143}$$

If E is different than zero, we have a first-order phase transition. We have the formation of a second minimum originates for

$$T_1 = T_0 \sqrt{\frac{8\bar{\lambda}D}{8\bar{\lambda}DT_0^2 - 9E^2}}\Bigg|_{T=T_1} , \tag{1.144}$$

The Universe reaches $T_{\text{cr.}}$ when the second minimum is degenerate with the origin.

We characterize the degree to which the transition is first-order with the following ratio

$$\frac{\phi_{\text{cr.}}}{T_{\text{cr.}}} = \frac{2E}{\bar{\lambda}} . \tag{1.145}$$

where $\phi_{\text{cr.}}$ is the location of the second minimum at $T_{\text{cr.}}$. A transition is *strongly first order* when $\phi_{\text{cr.}}/T_{\text{cr.}} \gtrsim 1$ [243]. If the electroweak transition is not *strongly first order* the sphaleron processes can wash out the Baryon asymmetry [243]. In Table 1.5, we report the maximum Higgs mass allowed to have a first order phase transition from some lattice studies.

In the following, we show how to estimate the final asymmetry by focusing on a single bubble and integrating the Baryonic density over radial coordinate perpendicular to the bubble wall. We approximate the bubble to be planar with thickness L_W that expands with velocity v_W.

We consider a coordinate system comoving with the bubble wall with the origin in the middle of it. We denote with z the direction perpendicular to the wall. In this way, the electroweak phase is broken for $z < 0$. The wall reflects or transmits a particle depending on the interaction. CP violating processes cause left- and right-handed to interact differently with the wall. Thus, the reflection and transmission probabilities depend on the chirality leading to a chiral asymmetry inside and outside the bubble. Weak sphaleron processes convert the left-handed fermion excess outside the bubble into a Baryon asymmetry.

The Baryon yield is [248]

$$\mathrm{Y_B} = \frac{135 N_f}{4\pi^2 v_W g_* T_U} \int_{-\infty}^{+\infty} \mathrm{d}z \Gamma_{WS} \mu_L \exp\left\{-\frac{3\mathcal{A}}{2v_W} \int_{-\infty}^{z} \mathrm{d}z \Gamma_{WS}\right\} , \tag{1.146}$$

where $\Gamma_{WS} = 10^{-6} T_U \exp\{-a\phi(z)/T_U\}$ is the weak sphaleron rate, $a = 37$, $\mathcal{A} = 15/2$, $N_f = 3$ is the number of flavour, μ_L is left-handed density excess outside the bubble wall. The fermion transport through the wall determines μ_L.

CHAPTER 2

Primordial Black Holes physics

Primordial Black Holes are Black Holes formed in the early Universe through mechanisms different than stellar collapse. Positive observations of Primordial Black Holes can potentially probe early Universe physics, high energy physics, and quantum gravity. Zel'dovic and Novikov discussed the concept of Primordial Black Holes for the first time in Ref. [249], and a few years later, Hawking and Carr proposed the first solid works in Refs. [250–252]. Hawking realization that Black Holes evaporate while emitting elementary particles, the Hawking radiation [253, 254] further consolidated the importance of investigating Primordial Black Holes. While the effect is negligible for stellar Black Holes, Primordial Black Holes with masses $\mathrm{M_{PBH}} \lesssim 10^{15}\,\mathrm{g}$ can produce observable effects. It is one of the reasons for the popularity of Primordial Black Holes.

Primordial Black Hole evaporation can explain several observations, such as the presence of antimatter in cosmic rays [255], Galactic [256] and Extra-Galactic [257] γ-ray background, the reionization of the pregalactic medium [258], the annihilation line radiation from the Galactic Centre [259], and short-period γ-ray bursts [260]. However, it is worth noting that Primordial Black Holes are not the sole explanation for these phenomena.

Heavier Primordial Black Holes can have astrophysical consequences, such as serving as seeds for the formation of Supermassive Black Holes [261], contributing to the formation of large-scale structure [262], and modifying the thermal and reionization history of the Universe [263].

Cosmologists soon realized that Primordial Black Holes could be excellent Dark Matter candidates [251, 264], as they are non-luminous, non-relativistic, and almost collisionless. Furthermore, several papers discuss the possibility of having particle Dark Matter produced from Primordial Black Holes [265–274]. In recent years, many studies investigated the simultaneous solution of Dark Matter and Baryon asymmetry problems with Primordial Black Holes [275–278].

Accretion disks typically surround massive Primordial Black Holes. The coexistence of Primordial Black Holes and WIMPs would amplify the expected WIMP detection signature because of the enhanced annihilation rate. Thus, this scenario is heavily constrained to the extent that the simultaneous existence of solar-mass Primordial Black Holes and WIMPs are incompatible [279, 280].

Primordial Black Holes' presence across the first stages of our Universe can alter or provide information on fundamental mechanisms such as Baryogenesis [201, 281–287], structure formation [288], Big Bang Nucleosynthesis [289], and the nature of cosmic phase transitions [290]. We summarize the principal features of Primordial Black Holes, depending on the mass range, in Table 2.1.

Interestingly, Primordial Black Holes are a natural byproduct of most inflationary scenarios, offering a precious link to the physics of inflation. The recent gravitational waves observation by LIGO and VIRGO [291–293] rekindled interest in studying Primordial Black Holes.

Primordial Black Holes can provide an explanation to several phenomena, including: (i) Planet-mass objects produce microlensing effects towards the Galactic bulge. The estimated abundance of these objects is larger than the expected for free-floating planets [294]. (ii) Microlensing of quasar [295] It includes the cases where the probability that a star caused the lensing is very low. (iii) Dark objects in the range $[2-5]\mathrm{M}_\odot$, incompatible with Black Holes of stellar origin [296], produce several microlensing events towards the Galactic bulge [297]. (iv) The correlation between cosmic infrared background fluctuation and source subtracted X-ray [298]. (v) The unexplained absence of ultra-faint dwarfs below a certain radius [299]. (vi) The existence of Galaxies for redshift $z \in [10-18]$ [300], in tension with standard cosmology. (vii) The Supernova population following the distribution of white dwarf-Dark Matter interaction [301]. (iix) The recent measurements of mass, spin, and coalescent rates of Black Holes by LIGO and Virgo [302], especially the events involving Black Holes with masses unexplained by stellar evolution. (ix) The link between the Galaxy's mass and the Black Holes in its center. Ref. [303] points out that the thermal history of the Universe can explain most of the enigma mentioned above.

This Chapter introduces the fundamental elements of Primordial Black Hole physics and is organized as follows. The first Section discusses Primordial Black Holes formation mechanisms, where we start with an overview of the most famous scenarios and examine a simple example. The second Section reviews Primordial Black Holes' mass evolution. It depends on three competing factors: Accretion, Merging, and Evaporation. Here, we present Hawking's calculation and the particle emission from Primordial Black Holes. The third Section examines how Primordial Black Holes alter standard Cosmology by analyzing Friedmann Equations. Finally, the fourth Section overviews the existing constraints on Primordial Black Holes abundance.

<table>
<tr><th>Mass Range</th><th>DM</th><th>Features</th></tr>
<tr><td>$\mathrm{M_{PBH}} \lesssim 10^{15}\,\mathrm{g}$</td><td>No*</td><td>*If the evaporation leaves stable relics, they contribute to ρ^0_{DM} [304–314]

They can affect the early Universe physics. For instance, they can
∘ inject entropy [99].
∘ modify Baryogenesis [283, 315–318] and/or Nucleosynthesis [319].
∘ generate neutrinos [320, 321], gravitinos [322], etc [323, 324].
∘ swallow monopoles [325, 326].
∘ remove the domain wall [322].
∘ contribute to the Universe's reionization [327, 328].</td></tr>
<tr><td>$\mathrm{M_{PBH}} \sim 10^{15}\,\mathrm{g}$</td><td>Yes</td><td>They are evaporating today

They can contribute to
∘ the cosmological γ-ray background [319].
∘ the Galactic γ-ray background [256, 329].
∘ antiprotons or positrons in cosmic rays [281, 330, 331].

They might generate γ-ray bursts [332], radio bursts [333], and annihilation-line radiation coming from center of the Galaxy [259, 320].

They can unveil the physics of the final explosive phase of Black Hole evaporation [334].</td></tr>
<tr><td>$\mathrm{M_{PBH}} \gtrsim 10^{15}\,\mathrm{g}$</td><td>Yes</td><td>They can be detected via gravitational effects

There are almost no constraints for $\mathrm{M_{PBH}}$ in $[10^{20} - 10^{26}]\,\mathrm{g}$ [305, 335, 336] and $[10^2 - 10^4]\mathrm{M}_\odot$ [337–339].

Large Primordial Black Holes can
∘ influence large-scale structure [262, 340–343].
∘ be seeds for Supermassive Black Holes [261, 344–346].
∘ generate background gravitational waves [347–351].
∘ produce x rays through accretion [263].</td></tr>
</table>

Table 2.1: **Primordial Black Holes classification.** For each mass range (first column) we report if they are Dark Matter Candidate (second column) and the main information for detection and constraints (third column). The table summarizes the classification provided in Ref. [319].

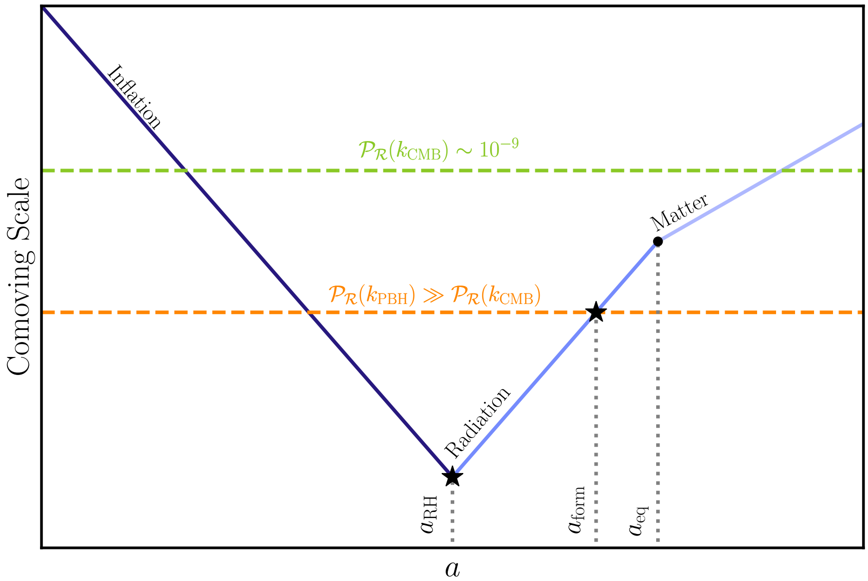

Figure 2.1: Primordial Black Hole formation scheme. From the darkest to the lightest violet shade, we indicate the inflationary, radiation dominated and matter dominated periods. $a_{\rm RH}$, $a_{\rm form}$, $a_{\rm eq}$ indicate the reheating, Primordial Black Holes formation, and radiation-matter equality comsic scales. The horizontal lines represent $k_{\rm PBH}^{-1}$ (orange) and $k_{\rm CMB}^{-1}$ (green).

2.1 Formation Mechanisms

This Section serves as an overview of Primordial Black Holes formation mechanisms, all of which require the existence of sizable inhomogeneities in the early Universe. The most famous class of formation mechanisms involves quantum effects during inflation to generate overdensity fluctuations that subsequently undergo gravitational collapse. Some mechanisms predict that fluctuations decrease at bigger scales so that the formation of Primordial Black Holes happens shortly after reheating [304, 352–354]. Other scenarios predict that the fluctuations power spectrum peaks at a fixed scale [305, 335–337, 355–365]. Alternatively, Refs. [366–373] investigate the scenarios where the fluctuations amplitude increases on lower scales with a non-trivial power law. Furthermore, more complex inflationary scenarios are viable in literature [338, 374–379], offering additional avenues for Primordial Black Holes formation as a consequence of inflation.

Additionally, several mechanisms can alter Primordial Black Holes formation. Examples include the sudden pressure drop associated with the QCD era [380–382], a “dustlike” period caused by a matter-dominated period [383], and a slow reheating [352].

Moreover, phase transition can generate inhomogeneities or enhance Primordial Black Holes formation. Examples of phase transition that can lead to Primordial Black Holes formation include Bubble collisions [384–389], cosmic String collapse [390–398], domain [399, 400] and necklace wall [401–406].

We expect Primordial Black Holes mass, denoted with $\mathrm{M_{PBH}}$, to be around the Hubble mass

$$\mathrm{M_{PBH}} = \gamma_{\mathrm{PBH}} \frac{c^3 t}{G_N} \approx \gamma_{\mathrm{PBH}} 10^{15} \left(\frac{t}{10^{-23}\,\mathrm{s}} \right) \mathrm{g}\,. \tag{2.1}$$

where γ_{PBH} depends on the gravitational collapse details. Primordial Black Holes mass range is wide, with potential formation occurring between the Planck time (10^{-43} s) and $t = 1\,\mathrm{s}$, resulting in $\mathrm{M_{PBH}} \in [10^{-5} - 10^{38}]\,\mathrm{g}$. By comparison, Black Holes originating from stellar collapse can not be lighter than $1\,M_\odot$. It is worth noting that inflation exponentially dilutes Primordial Black Holes formed with masses $\mathrm{M_{PBH}} \lesssim 1\,\mathrm{g}$. In a radiation dominated era, analytical calculations show that $\gamma_{\mathrm{PBH}} = c_s^3 \simeq 0.2$ [252, 407], where $c_s^2 = 1/3$ is the sound speed. Eq. (2.1) suggests that Primordial black Holes formed at a specific time should have an almost monochromatic mass distribution ($\delta\mathrm{M_{PBH}} \sim \mathrm{M_{PBH}}$). However, some mechanisms predict an extended formation period, leading to an extended mass distribution.

Assuming Primordial Black Holes form in a radiation-dominated Universe and using Eq. (2.1), we estimate they form when the Universe temperature is

$$T_{\mathrm{in}} = \frac{1}{2} \left(\frac{5}{g_* \pi^3} \right)^{1/4} \sqrt{\frac{3\gamma_{\mathrm{PBH}} \mathrm{M_{Pl}^3}}{\mathrm{M_{PBH}}}}\,. \tag{2.2}$$

Most PBH formation mechanisms require the presence of inhomogeneities and overdense regions that stop expanding and recollapse. This condition demands that the fluctuations in these regions be larger than the Jeans length at maximum expansion. The Jeans length is $\sqrt{\omega} ct$ for an equation of state $p = \omega \rho c^2$, where p and ρ are the pressure and the energy density of the Universe. For relativistic matter, $\omega = 1/3$.

When the overdensity δ re-enters the horizon must be higher than a critical value $\delta_{\mathrm{cr.}}$ to collapse. $\delta_{\mathrm{cr.}}$ depends on the formation period and the shape of the density perturbation. For instance, Ref.[408] focused on a wide shape range, obtaining $\delta_{\mathrm{cr.}} \in [0.41 - 0.67]$. For broader shapes, the role of the pressure gradient is negligible, leading to a lower critical value. In a radiation-dominated Universe, the perturbation might collapse and form a Primordial Black Hole if the overdensity overcomes the radiation pressure, meaning that $\delta_{\mathrm{cr.}} \approx c_s^2$.

Primordial Black Holes formation is an example of a critical phenomenon, and several studies suggest that the mass function has an upper cut-off around the Hubble mass, M_H, and a lower limit. The Primordial Black Hole mass depends on the amplitude of fluctuation originating it as [409, 410]

$$\mathrm{M_{PBH}} = \kappa M_H (\delta - \delta_{\mathrm{cr.}})^\gamma\,, \tag{2.3}$$

The perturbation shape and the background equation of state determine γ and κ.

In the following, we describe Primordial Black Hole formation in a radiation-dominated

Universe from overdensities generated during inflation. Our goal is to show the relation of the information on the Primordial Black Hole population with the primordial curvature fluctuation.

Before discussing the formation mechanism, we set the stage with all the fundamental ingredients. Since Primordial Black Hole energy density is not constant ($\rho_{\rm PBH} \sim a^{-3}$), we refer to Primordial Black Holes abundance at formation for definiteness. We indicate it with

$$\beta \equiv \left.\frac{\rho_{\rm PBH}}{\rho_{\rm cr.}}\right|_{\rm in}, \tag{2.4}$$

$$\beta' \equiv \gamma_{\rm PBH}^{1/2}\left(\frac{g_*(T_{\rm in})}{106.5}\right)^{-1/4}\left(\frac{h}{0.67}\right)^{-2}\beta\,, \tag{2.5}$$

where $h = 0.67$ [411] is related to the Hubble constant, $\rho_{\rm cr.}$ is the critical energy density of the Universe. The second definition is the most commonly used because β often appears multiplying $\gamma_{\rm PBH}^{1/2} g_*^{-1/4} h^{-2}$. Alternatively, if Primordial Black Holes survive until today, they can (partially) comprise Dark Matter and we express their abundance as

$$f_{\rm PBH} \equiv \left.\frac{\rho_{\rm PBH}}{\rho_{\rm DM}}\right|_{o}. \tag{2.6}$$

We can relate β to the fraction of the energy density budget of the Universe composed of Primordial Black initial abundance as [319]

$$\Omega^o_{\rm PBH} \equiv \left.\frac{\rho_{\rm PBH}}{\rho_{\rm cr.}}\right|_{o} = \beta\Omega^o_{\rm rad}(1+z) \approx 10^{18}\beta\left(\frac{{\rm M_{PBH}}}{10^{15}\,{\rm g}}\right)^{-1/2} \tag{2.7}$$

where $1+z = a_o/a_{\rm in}$ is the redshift and $\Omega_{\rm rad} = \rho_{\rm rad}/\rho_{\rm cr.}$. If Primordial Black Holes were to compose Dark Matter ($\Omega_{\rm PBH} = \Omega_{\rm DM} \approx 0.25$), β must extremely small. Nonetheless, there exist scenarios providing naturally small initial Primordial Black Hole abundance [319].

Primordial Black Hole formation is a causal process because gravity needs to "communicate" the presence of an overdensity to initiate its collapse. Thus, we need to understand the concept of causality in an expanding universe. The Hubble rate H indicates the expansion rate of our Universe. We refer to H^{-1} as the Hubble distance. It measures the distance that light travels in one Hubble time. We can consider it a time-dependent length sizing the causally connected region of the Universe. We are interested in knowing the behavior in time of the comoving Hubble horizon $1/(aH)$. The time derivative of the comoving Hubble horizon is

$$\frac{{\rm d}}{{\rm d}t}\left(\frac{1}{aH}\right) = -\frac{{\rm d}^2 a}{{\rm d}t^2}\frac{1}{a^2H^2}\,. \tag{2.8}$$

By considering the second Friedmann equation

$$\frac{1}{a}\frac{\mathrm{d}^2 a}{\mathrm{d}t^2} = -\frac{1}{6\mathrm{M}_{\mathrm{Pl}}^2}(3P+\rho)\,, \tag{2.9}$$

and the continuity equation

$$P(t) = \omega\rho(t)\,, \tag{2.10}$$

we obtain that

$$(aH)^{-1} = H_0^{-1} a^{(1+3\omega)/2}\,. \tag{2.11}$$

During inflation $\omega = -1$, thus $1/aH$ decreases with time, whereas for radiation- (matter-)dominated Universe, $\omega = 1/3$ ($\omega = 0$), meaning that $1/aH$ is a crescent function.

We study the statistical properties of the fluctuation in Fourier space where we express each perturbation mode in terms of a comoving length scale k^{-1}. The gravitational collapse of the perturbation needs its comoving length comparable to the casual distance $k_{\mathrm{PBH}}/aH \simeq 1$. We define a perturbation as super-Horizon (sub-Horizon) when its wavelength is $k < aH$ ($k > aH$). The initial (quantum) fluctuations live inside the Horizon ($k > aH$). Since $1/aH$ grows during inflation, the fluctuation becomes sub-Horizon at a certain point. After the reheating, the Universe is radiation-dominated, and $1/aH$ increases again (see Fig. 2.1 for a schematic depiction). The perturbation exits the Horizon at smaller scales for smaller k, but it takes longer to re-enter the Horizon.

At the end of the inflation, the mode associated with k_{PBH} becomes the seeds for the overdensity fluctuation

$$\mathcal{P}_{\mathcal{R}}(k_{\mathrm{PBH}})^{1/2} \sim \frac{\delta\rho}{\rho} \equiv \delta\,. \tag{2.12}$$

If $\delta \geq \delta_{\mathrm{cr.}}$, the gravitational interaction leads to the formation of Primordial Black Holes from the collapse of the overdensity.

According to the Press-Schecter model of gravitational collapse, we have [412]

$$\beta \equiv \int_{\delta_{\mathrm{cr.}}}^{+\infty} P(\delta)\mathrm{d}\delta\,, \tag{2.13}$$

where $P(\delta)$ describes the probability of having an overdensity δ. Assuming a Gaussian distribution, we want to show how to get a large Primordial Black Hole population today. The fundamental quantity is the variance of the distribution σ. Indeed, for fixed mean value μ, having greater σ results in a wider distribution, which leads to increased integration in $[\delta_c; +\infty]$. Assuming $\mu = 0$, we have

$$\beta = \int_{\delta_{\mathrm{cr.}}}^{+\infty} \frac{\mathrm{d}\delta}{\sqrt{2\pi}\sigma} \exp\left\{-\frac{\delta^2}{2\sigma^2}\right\} = \frac{1}{2}\left(1 - Erf\left(\frac{\delta_{\mathrm{cr.}}}{\sqrt{2}\sigma}\right)\right) \simeq \frac{\sigma}{\sqrt{2\pi}\delta_{\mathrm{cr.}}} \exp\left\{-\frac{\delta_{\mathrm{cr.}}}{2\sigma^2}\right\} \tag{2.14}$$

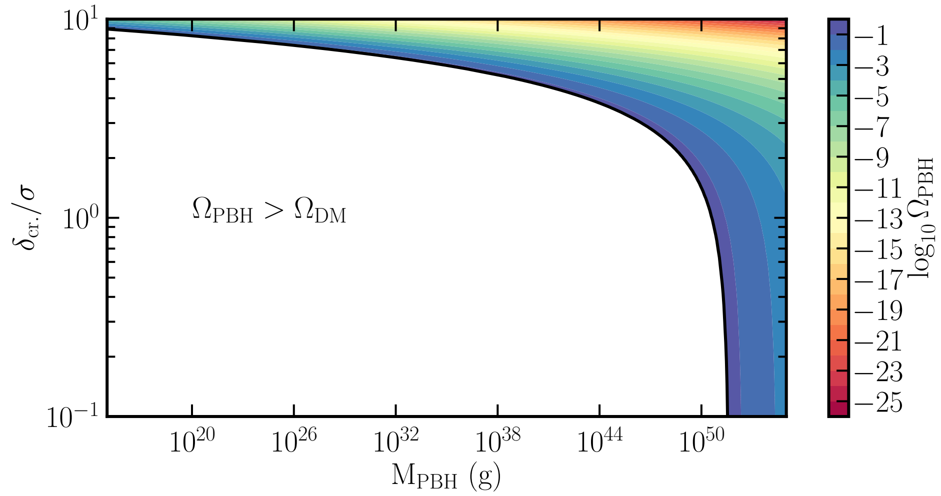

Figure 2.2: In color we show $\log_{10}\Omega_{PBH}$ as a function of $\rm M_{PBH}$ and $\delta_{\rm cr}/\sigma$. The black contour illustrates when $\Omega^o_{\rm PBH} = \Omega^o_{\rm DM}$, while the region in white corresponds to Primordial Black Holes with an abundance greater than Dark Matter today.

where $Erf(x)$ is the error function. The second equality is true for $\delta_{\rm cr.} \gg \sigma$. By combining this result with Eq. (2.7), we can estimate $\delta_{\rm cr.}/\sigma$ so that $\Omega^o_{\rm PBH} = \Omega^o_{\rm DM}$. For instance,

$$\rm M_{PBH} = 10^{-12} M_\odot, \qquad \Omega^o_{\rm PBH} = \Omega^o_{\rm DM} \Longrightarrow \delta_{\rm cr.}/\sigma \simeq 7.9\,. \tag{2.15}$$

In Fig. 2.2, we show in color the behaviour of $\Omega_{\rm PBH}$ as a function of $\rm M_{PBH}$ and $\delta_{\rm cr}/\sigma$. The white region corresponds to $\Omega_{\rm PBH} > \Omega_{\rm DM}$, while the black line represents the equality.

To connect the amplitude of the comoving curvature perturbation $\mathcal{R}$ [413, 414], we expand at the leading order δ and obtain [408]

$$\delta(\vec{x},t) \simeq \frac{2(1+\omega)}{5+3\omega}\frac{\nabla^2\mathcal{R}(\vec{x})}{(aH)^2} + \mathcal{O}(\mathcal{R}^\in) \Longrightarrow \delta_k \simeq -\frac{4}{9}\left(\frac{k}{aH}\right)^2 \mathcal{R}_k\,. \tag{2.16}$$

where the second equality holds for a radiation dominated Universe $\omega = 1/3$. We define the power spectrum as

$$\langle X_k X_{k'}\rangle = \frac{2\pi^2}{k^3}\mathcal{P}_X(k)\delta^{(3)}\left(k-k'\right)\,, \tag{2.17}$$

The power spectrum of overdensity and the curvature perturbation relation is

$$P_\delta(k) \simeq \frac{16}{81}\left(\frac{k}{aH}\right)^4 \mathcal{P}_\mathcal{R}\,. \tag{2.18}$$

We define a window function $\mathcal{W}$ to smooth δ on scales relevant for Primordial Black Hole formation $R \approx k^{-1} \approx 1/aH$. The relation between the variance of the density contrast and the

spin	0	1	3/2	2	1/2 (neutral)	1/2 (charged)
f	0.267	0.060	0.020	0.007	0.147	0.142

Table 2.2: Contributions per degree of freedom to $f(\mathrm{M}_{\mathrm{PBH}})$ depending on the particle spin [417].

power spectrum is[415, 416]

$$\sigma^2(R) \equiv \langle \delta^2 \rangle_R = \int_0^{+\infty} \mathrm{d}\ln q\, \mathcal{W}^2(q,R)\mathcal{P}_\delta(q) \simeq \frac{16}{81}\int_0^{+\infty} \mathrm{d}\ln q\, \mathcal{W}^2(q,R)(qR)^2\mathcal{P}_\mathcal{R}(q)\,, \tag{2.19}$$

By considering $\mathcal{P}_\delta$ peaked at $k = k_{\mathrm{PBH}}$, we obtain $\sigma^2 \sim \mathcal{P}_\delta(k_{\mathrm{PBH}})$. From Eq. (2.18) and that $k \simeq aH$ at formation, we obtain

$$\mathcal{P}_\mathcal{R} \sim 5\sigma^2\,, \tag{2.20}$$

To better understand that Primordial Black Holes require large amplification of the curvature spectrum, we want to compare it with the one associated with the Cosmic Microwave Background ($\mathcal{P}_\mathcal{R}(k_{\mathrm{CMB}}) \sim 10^{-9}$). Recalling the example in Eq.(2.15) and assuming $\delta_{\mathrm{cr.}} = 0.4$, we obtain

$$\frac{\mathcal{P}_\mathcal{R}(k_{\mathrm{PBH}})}{\mathcal{P}_\mathcal{R}(k_{\mathrm{CMB}})} \sim 10^7\,. \tag{2.21}$$

Considering lighter Primordial Black Holes leads to similar results. From Eqs. (2.14) and (2.20), we obtain that

$$\mathcal{P}_\mathcal{R} \sim \frac{5}{2}\frac{\delta^2_{\mathrm{cr.}}}{\ln(1/\beta)}\,. \tag{2.22}$$

Thus, we obtain that $\mathcal{P}_\mathcal{R}$ logaritmically dependent on β. Conversely, we observe that β depends exponentially on $\mathcal{P}_\mathcal{R}$ and $\delta_{\mathrm{cr.}}$.

2.2 Mass evolution

This Section illustrates the evolution of Primordial Black Hole mass from the competition of accretion and evaporation. The phenomenon is sensible to the sound speed in the cosmological fluid, the energy density of the accreted component, and the Primordial Black Hole's parameters (mass, spin, and charge). For simplicity, we focus on neutral and non-rotating Primordial Black Holes unless otherwise specified. We organize the Section as follows. First, we discuss evaporation and the related particle flux on Earth. Then, we briefly discuss the accretion.

2.2.1 Evaporation

In the seminal papers Ref. [253, 254], Hawking investigated the quantum properties of Black Holes, prompted by the observation that very light Primordial Black Holes could form in the very early Universe. Combining quantum mechanics, general relativity, and thermodynamics, he realized that Primordial Black Holes are not perfectly "black". Indeed, they emit elementary particles with a black body-like spectrum with a temperature proportional to the gravity surface s,

$$\mathcal{T}_{\rm PBH} \equiv \frac{s}{2\pi}\,. \tag{2.23}$$

We define this emission as "Hawking Radiation" and is a semiclassical effect that can be roughly understood as follows. Due to quantum fluctuation, pairs of particles and antiparticles appear and disappear continuously. When such a phenomenon happens near the horizon of a Primordial Black Hole, one of them can fall behind the horizon while the other escapes and is measurable at spatial infinity.

As mentioned above, the emission is black body-like, thus

$$\frac{{\rm d}^2 N_\chi}{{\rm d}E_\chi {\rm d}t} = \frac{g_\chi}{2\pi}\frac{\Gamma^\chi(E_\chi, \mathcal{T}_{\rm PBH})}{\exp\{E_\chi/\mathcal{T}_{\rm PBH}\} - (-1)^{2s_\chi}} \tag{2.24}$$

where g_χ, s_χ, E_χ are χ degrees of freedom, spin and energy. Γ is the grey-body factor that describe the discrepancy between the Primordial Black Hole emission and the black body one. We define it as

$$\Gamma^\chi \equiv \left|\frac{Z_\infty}{Z_{\rm hor.}}\right|^2 \tag{2.25}$$

where Z_∞ and $Z_{\rm hor.}$ are the amplitudes of a plane wave evolved from the Primordial Black Hole horizon to the spatial infinity. The grey-body factors depend on the particle mass, spin, and charge of the particle and the Primordial Black Hole. We mention that particles emitted from Primordial Black Hole evaporation can decay or interact, generating a secondary flux.

As the Primordial Black Hole emits Hawking Radiation it looses mass. We can determine the mass loss as follows

$$\kappa({\rm M}_{\rm PBH}, J) \equiv -{\rm M}^2_{\rm PBH}\frac{{\rm dM}_{\rm PBH}}{{\rm d}t} = {\rm M}^2_{\rm PBH}\sum_\chi \int_0^{+\infty} {\rm d}E_\chi \frac{{\rm d}^2 N_\chi}{{\rm d}E_\chi {\rm d}t} E_\chi\,, \tag{2.26}$$

where J is the Primordial Black Hole momentum and we perform the sum over all the particles emitted ($m_\chi \lesssim \mathcal{T}_{\rm PBH}$). We can do the same for the momentum loss. We can recast Eq. (2.26) as

$$\frac{{\rm dM}_{\rm PBH}}{{\rm d}t} = -\frac{\kappa}{{\rm M}^2_{\rm PBH}}\,. \tag{2.27}$$

In the following, we consider neutral and non-rotating (Schwarzschild) Primordial Black Holes. Quantum emission causes the loss of angular momentum and charge on a shorter timescale [418], justifying our assumption. We emphasize that this reasoning can fail at the

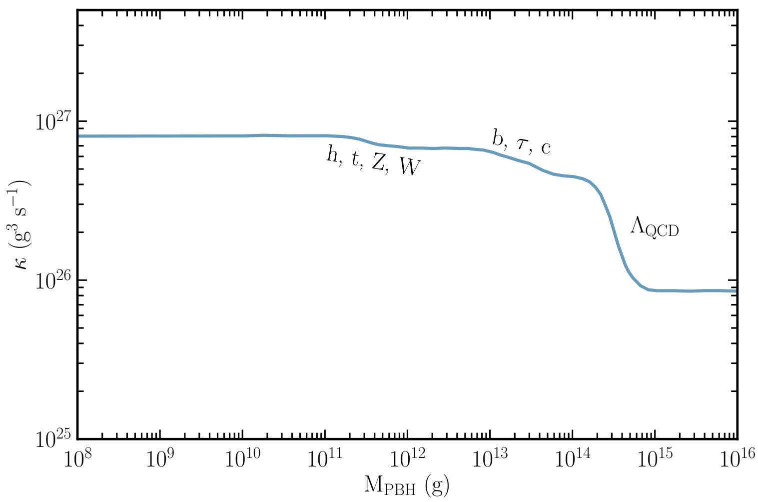

Figure 2.3: The plot shows the behaviour of κ as a funciton of $\mathrm{M_{PBH}}$. Primordial Black Holes can emit a certain particle when $\mathcal{T}_{\rm PBH}$ crosses its mass. We indicate with a label the particle responsible for the threshold. We highlight that Primordial Black Holes radiate quarks and gluons only if $\mathcal{T}_{\rm PBH} \gtrsim \Lambda_{\rm QCD}$.

Planck scale [418]. In such a case, the temperature reads as

$$k_{\rm B}\mathcal{T}_{\rm PBH} = \frac{\hbar c^3}{8\pi \mathrm{M_{PBH}}} \simeq 1.06 \left(\frac{10^{16}\,\mathrm{g}}{\mathrm{M_{PBH}}}\right) \mathrm{MeV}\,. \tag{2.28}$$

Moreover, in this scenario, we can approximate κ as

$$\kappa = 5.34 \times 10^{15}\,\mathrm{g^2\,s^{-1}}\, f(\mathrm{M_{PBH}})\,. \tag{2.29}$$

where $f(\mathrm{M_{PBH}})$ accounts for the number of particles emitted per specie and degrees of freedom (see Table 2.2 for the numerical values). We define it so that it is normalized to unity for Primordial Black Holes with $\mathrm{M_{PBH}} \gtrsim 10^{17}\,\mathrm{g}$. Indeed, they emit only particles that are (effectively) massless, like photons, neutrinos, and gravitinos. In Fig 2.3, we report the behaviour of κ as a function of the Primordial Black Hole mass.

By integrating over the cosmic time Eq.(2.27), we obtain that the Primordial Black Hole lifetime

$$\tau \approx 407 \left(\frac{f(\mathrm{M_{PBH}})}{15.35}\right)^{-1} l \left(\frac{\mathrm{M_{PBH}}}{10^{10}\,\mathrm{g}}\right)^3 \mathrm{s}\,. \tag{2.30}$$

We define $\mathrm{M_{PBH}^{cr.}}$ as the critical mass for which Primordial Black Holes lifetime equals the

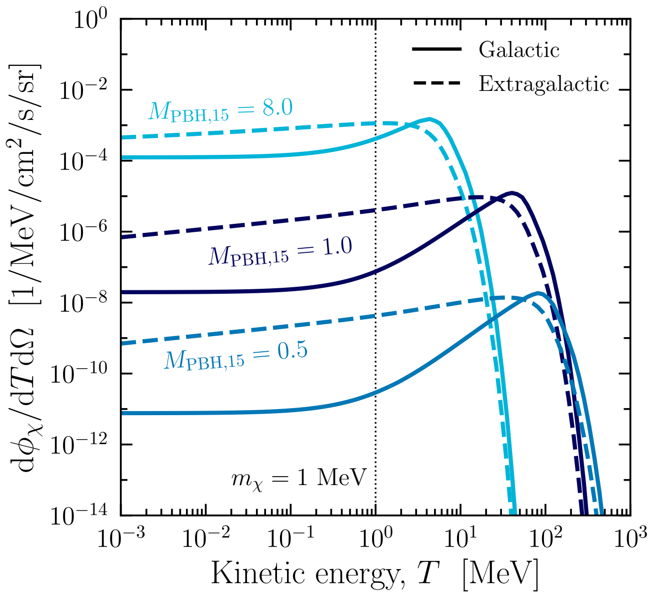

age of the Universe (13.8 Gyr). It is equal to

$$\mathrm{M}_{\mathrm{PBH}}^{\mathrm{cr.}} \approx 1.02 \times 10^{15} \left(\frac{f(\mathrm{M}_{\mathrm{PBH}}^{\mathrm{cr.}})}{15.35}\right)^{1/3} \mathrm{g} \approx 5.1 \times 10^{14}\,\mathrm{g} \tag{2.31}$$

Particle flux on Earth

In this Section, we show how to calculate the flux of a specie emitted from Primordial Black Holes that are still evaporating today. We suppose the particle χ to be weakly interacting like neutrinos and Dark Matter. In this way, there is no need to compute deflection effects. For clarity, we consider a monochromatic Primordial Black Hole mass distribution. We divide χ flux into two components. One results from the Extra-Galactic (ϕ_{EG}) Primordial Black Holes, and one from Primordial Black Holes in our Galaxy (ϕ_{MW}). The differential Extra-Galactic flux contribution is

$$\frac{\mathrm{d}\phi^{\mathrm{EG}}}{\mathrm{d}T_\chi} = \frac{f_{\mathrm{PBH}}\rho_{\mathrm{DM}}}{4\pi \mathrm{M}_{\mathrm{PBH}}} \int_{t_{\min}}^{t_{\max}} \mathrm{d}t\,[1+z(t)] \left.\frac{\mathrm{d}^2 N_\chi}{\mathrm{d}T\mathrm{d}t}\right|_{E_s} \tag{2.32}$$

where T_χ is χ kinetic energy, $z(t)$ is the redshift and $E_s = \sqrt{\left(E_\chi^2 - m_\chi^2\right)(1+z(t))^2 + m_\chi^2}$ is χ redshifted energy. f_{PBH} is the fraction of Dark Matter comprised of Primordial Black Holes

$$f_{\mathrm{PBH}} = \frac{\rho_{\mathrm{PBH}}}{\rho_{\mathrm{DM}}} \leq 1\,. \tag{2.33}$$

The integral in Eq. (2.32) is performed from the matter-radiation equality ($t_{\min}$) up to $t_{\max} = \min[\tau_{\mathrm{PBH}}, \tau_{\mathrm{univ.}}]$, where τ_{PBH} and $\tau_{\mathrm{univ.}}$ are respectively Primordial Black Holes lifetime and the Universe's age. The Extra-Galactic component is assumed isotropic.

The Galactic component is

$$\frac{\mathrm{d}\phi^{\rm MW}}{\mathrm{d}T_\chi} = \frac{f_{\rm PBH}}{4\pi \mathrm{M}_{\rm PBH}} \frac{\mathrm{d}^2 N_\chi}{\mathrm{d}T_\chi \mathrm{d}t} \int_0^{\ell_{\max}} \mathrm{d}\ell \rho_{\rm DM}^{\rm NFW}(r) \tag{2.34}$$

where $r(\ell,\phi)$ is the Galactometric distance defined as

$$r(\ell,\phi) = \sqrt{r_\odot^2 - 2\ell r_\odot cos\theta + \ell^2}\,, \tag{2.35}$$

$$\ell_{\max} = \sqrt{r_h^2 - r_\odot^2 \sin^2\theta} + r_\odot cos\theta\,, \tag{2.36}$$

where $r_h = 200\,\mathrm{kpc}$ is the halo radius. $\rho_{\rm DM}^{\rm NFW}(r)$ is the Navarro-Frenk-White defined as [419]

$$\rho_{\rm DM}^{\rm NFW}(r) = \rho_\odot \left(\frac{r_\odot}{r}\right) \left(\frac{1 + r_\odot/r_s}{1 + r/r_s}\right)^2 \tag{2.37}$$

where $\rho_\odot = 0.4\,\mathrm{GeV\,cm^{-3}}$ is the local Dark Matter density, $r_\odot = 8.5\,\mathrm{kpc}$ and $r_h = 20\,\mathrm{kpc}$ are the distance between the Sun and the Milky Way center and the scale radius respectively. We notice that the total flux, given by the sum of Eqs. (2.32)-(2.34), is proportional to $f_{\rm PBH}/\mathrm{M}_{\rm PBH}$. Therefore, lower masses lead to higher fluxes.

Fig. 2.2.1 shows the Galactic and Extra-Galactic χ flux in solid and dashed lines. We consider χ a Dirac fermion ($g_\chi = 4$) and $m_\chi = 1\,\mathrm{MeV}$. The colors illustrate different $[\mathrm{M}_{\rm PBH}, f_{\rm PBH}]$ benchmarks. The vertical line indicates $T_\chi = m_\chi$. The kinetic energy distribution peaks at higher energies for smaller $\mathrm{M}_{\rm PBH}$. The Galactic distribution flattens for T_χ smaller than χ mass since the particles are produced almost at rest.

2.2.2 Accretion

Accretion may alter the evolution of Primordial Black Holes and impact several observables (see Refs [420–422] for comprehensive reviews). The phenomenon consists of the gravitational capture of matter by Primordial Black Holes. The infalling matter heats up until it ionizes and emits high-energy radiation. Accretion owes its complexity to its dependence on the physical parameters of the cosmic fluids and the convoluted relation between the accretion rate and the geometry of the accretion flow. Additionally, Primordial Black Hole mass, sound speed, and the energy density of the accreted region strongly influence the phenomenon.

Roughly speaking, we can identify two cases: isolated Primordial Black Holes or in a binary system. In the latter, the binary system generates a deeper gravitational, requiring a precise estimation of the deviation of the mean gas density.

If Primordial Black Holes entirely comprise the Dark Matter abundance, Baryonic matter surrounds them. Instead, assuming the coexistence of Primordial Black Holes and a secondary Dark Matter component, we should also account for the formation of dark halos.

The key objective of the sub-Section is to quantify Primordial Black Hole mass variation due to accretion in the isolated case. In the following, we do not discuss the radiation emitted during accretion, which is crucial for the constraints from the Cosmic Microwave Background observations [423–426].

In the following, we describe the accretion of an isolated Primordial Black Hole surrounded by matter. We describe the surrounding medium with hydrogen gas with a number density

$$n_{\rm gas} = 200\,{\rm cm}^{-3}\left(\frac{1+z}{1000}\right)^3 . \tag{2.38}$$

The mass evolves according to the Bondi-Hoyle rate [263, 420]

$$\left(\frac{{\rm dM_{PBH}}}{{\rm d}t}\right)_{\rm acc} = 4\pi\lambda m_H n_{\rm gas} v_{\rm eff} r_B^2 \,, \tag{2.39}$$

where $v_{\rm eff} = \sqrt{v_{\rm rel}^2 + c_s^2}$, $v_{\rm rel}$ is the relative velocity between the Primordial Black Hole and the gas and c_s is the sound speed

$$c_s = 5.7\,{\rm km/\,s}\left(\frac{1+z}{1000}\right)^{1/2}\left[\left(\frac{1+z_{\rm dec}}{1+z}\right)^{\iota} + 1\right]^{-1/2\iota} , \tag{2.40}$$

with $\iota = 1.72$ and $z_{\rm dec} \simeq 130$. r_B is the Bondi-Hoyle radius

$$r_B \equiv \frac{\rm M_{PBH}}{v_{\rm eff}} \simeq 1.3\times 10^{-4}\,{\rm pc}\left(\frac{\rm M_{PBH}}{\rm M_\odot}\right)\left(\frac{v_{\rm eff}}{5.7\,{\rm km/\,s}}\right)^{-2} \tag{2.41}$$

λ accounts for the gas viscosity, the Hubble expansion, and the coupling of the Cosmic Microwave Background radiation to the gas via Compton Scattering. Ref. [420] defines it as

$$\lambda = \exp\left\{\frac{9/2}{3+\hat{\iota}^{0.75}}\right\} x_{\rm cr.}^2 . \tag{2.42}$$

where

$$x_{\rm cr.} \equiv \frac{r_{\rm cr.}}{r_B} = \frac{-1+\sqrt{1+\hat{\iota}}}{\hat{\iota}} \tag{2.43}$$

and

$$\hat{\iota} = \left(\frac{\rm M_{PBH}}{10^4{\rm M_\odot}}\right)\left(\frac{1+z}{1000}\right)^{3/2}\left(\frac{v_{\rm eff}}{5.74\,{\rm km/\,s}}\right)^{-3}\left[0.257 + 1.45\left(\frac{x_e}{0.01}\right)\left(\frac{1+z}{1000}\right)^{5/2}\right] \tag{2.44}$$

It is a function of the redshift z, the effective velocity, and the ionization of the cosmic gas x_e.

Scenario with a Dark Matter halo

Primordial Black Holes may comprise a small fraction of the Dark Matter energy density. The presence of another Dark Matter component in the Universe can form a dark halo around Primordial Black Holes. Since the dark halo intensifies the gravitational attraction of the gas to the system, it acts like a catalyst enhancing the gas accretion rate. We stress that the infall of the surrounding Dark Matter component is negligible [420].

We denote with M_h the dark halo mass truncated at a radius r_h. We assume the dark halo to have a power law density profile ($\rho_h \sim e^{-\alpha}$, $\alpha \simeq 2.25$). As long as the Primordial Black Holes are isolated and until they are still accreting Dark Matter, M_h and r_h grow according to [280, 339]

$$\mathrm{M}_h = 3\mathrm{M}_{\mathrm{PBH}} \left(\frac{1+z}{1000}\right)^{-1} , \tag{2.45}$$

$$r_h = 0.019\,\mathrm{pc} \left(\frac{\mathrm{M}_{\mathrm{PBH}}}{\mathrm{M}_\odot}\right)^{1/3} \left(\frac{1+z}{1000}\right)^{-1} , \tag{2.46}$$

Primordial Black Holes accrete all the Dark Matter when

$$3 f_{\mathrm{PBH}} \left(1 + \frac{z}{1000}\right)^{-1} = 1\,. \tag{2.47}$$

The Bondi radius can be smaller or larger than the Bondi radius. In the first case, we can describe this scenario with Eq. (2.39), where we substitute $\mathrm{M}_{\mathrm{PBH}}$ with M_h. In the second case, we must correct Eq. (2.39) to account for the modified potential. We define

$$\hat{\kappa} \equiv \frac{r_B}{r_h} = 0.22 \left(\frac{1+z}{1000}\right) \left(\frac{\mathrm{M}_h}{\mathrm{M}_\odot}\right)^{2/3} \left(\frac{v_{\mathrm{eff}}}{\mathrm{km/\,s}}\right)^{-2} \tag{2.48}$$

when $\hat{\kappa} < 2$, we consider the following quantities

$$\begin{aligned}
\hat{\iota}^h \quad &\equiv \quad \hat{\kappa}^{p/(1-p)} \iota\,, && (2.49)\\
\lambda^h \quad &\equiv \quad \overline{\Upsilon}^{p/(1-p)} \lambda(\hat{\iota}^h)\,, && (2.50)\\
r^h_{\mathrm{cr.}} \quad &\equiv \quad \left(\frac{\hat{\kappa}}{2}\right)^{p/(1-p)} r_{\mathrm{cr.}} && (2.51)\\
\Upsilon \quad &\equiv \quad \left(1 + 10\hat{\iota}^h\right)^{1/10} \exp\{2-\hat{\kappa}\} \left(\frac{\hat{\kappa}}{2}\right)^2 && (2.52)
\end{aligned}$$

where $p = 2 - \alpha$.

2.3 Friedmann Equations with Primordial Black Holes

The existence of Primordial Black Holes can alter the evolution of the early Universe. This Section examines the effects of Primordial Black Holes evolution accounting for their evaporation.

Primordial Black Holes and radiation energy densities evolve according to the following Friedmann equations [268, 270, 427, 428]

$$\begin{aligned}
\frac{\mathrm{d}\rho_{\mathrm{rad}}}{\mathrm{d}t} + 4H\rho_{\mathrm{rad}} &= -f_{\mathrm{SM}}\frac{\mathrm{dM_{PBH}}}{\mathrm{d}t}\frac{1}{\mathrm{M_{PBH}}}\rho_{\mathrm{PBH}}\,, &(2.53)\\
\frac{\mathrm{d}\rho_{\mathrm{PBH}}}{\mathrm{d}t} + 3H\rho_{\mathrm{PBH}} &= \frac{\mathrm{dM_{PBH}}}{\mathrm{d}t}\frac{1}{\mathrm{M_{PBH}}}\rho_{\mathrm{PBH}}\,, &(2.54)\\
H^2 = \left(\frac{\mathrm{d}a}{\mathrm{d}t}\frac{1}{a}\right)^2 &= \frac{8\pi}{3\mathrm{M}_{\mathrm{Pl}}^2}\left(\rho_{\mathrm{rad}} + \rho_{\mathrm{PBH}}\right)\,. &(2.55)
\end{aligned}$$

where H is the Hubble parameter, a is the cosmological scale factor, and t is the cosmic time. f_{SM} is the fraction of Hawking radiation composed of SM particles.

For simplicity, we recast the equations in terms of $\alpha = \log_{10} a$ and the comoving energy densities ($\varrho_{\mathrm{PBH}} = a^3\rho_{\mathrm{PBH}}$ and $\varrho_{\mathrm{rad}} = a^4\rho_{\mathrm{rad}}$). With this formalism, the Friedmann equations are

$$\begin{aligned}
\frac{\mathrm{d}\varrho_{\mathrm{rad}}}{\mathrm{d}\alpha} &= -f_{\mathrm{SM}}\frac{\mathrm{d}\ln \mathrm{M_{PBH}}}{\mathrm{d}\alpha}10^{\alpha}\varrho_{\mathrm{PBH}}\,, &(2.56)\\
\frac{\mathrm{d}\varrho_{\mathrm{PBH}}}{\mathrm{d}\alpha} &= \frac{\mathrm{d}\ln \mathrm{M_{PBH}}}{\mathrm{d}\alpha}\varrho_{\mathrm{PBH}}\,, &(2.57)\\
H^2 &= \frac{8\pi}{3\mathrm{M}_{\mathrm{Pl}}^2}\left(\frac{\varrho_{\mathrm{PBH}}}{a^3} + \frac{\varrho_{\mathrm{rad}}}{a^4}\right)\,, &(2.58)
\end{aligned}$$

Eq. (2.56) shows that Primordial Black Holes affect the radiation energy density, meaning that the Universe entropy is no longer conserved. The equations describing the Universe's comoving energy density ($\mathcal{S}$) is [428–430]

$$\frac{\mathrm{d}\mathcal{S}}{\mathrm{d}\alpha} = -\frac{f_{\mathrm{SM}}}{T_U}\frac{\mathrm{d}\ln \mathrm{M_{PBH}}}{\mathrm{d}\alpha}\varrho_{\mathrm{PBH}}\,. \tag{2.59}$$

which leads to the following evolution equation for the Universe temperature (T_U)

$$\frac{\mathrm{d}T_U}{\mathrm{d}\alpha} \simeq -\frac{T_U}{\Delta}\left\{\ln(10) - \epsilon_{\mathrm{SM}}\frac{\mathrm{d}\ln \mathrm{M_{PBH}}}{\mathrm{d}\alpha}\frac{a\varrho_{\mathrm{PBH}}}{4\varrho_{\mathrm{rad}}}\right\}\,. \tag{2.60}$$

Δ shows how the entropic relativistic degrees of freedom (g_{*s}) on the Universe temperature [428–430],

$$\Delta = 1 + \frac{T_U}{3g_{*s}(T_U)}\frac{\mathrm{d}g_{*s}}{\mathrm{d}T_U}\,. \tag{2.61}$$

The left panel of Fig. 2.4 shows $\rho_{\mathrm{PBH}}/\rho_{\mathrm{tot}}$ (Red), $\rho_{\mathrm{rad}}/\rho_{\mathrm{tot}}$ (Blue), and $\mathcal{S}_{\beta'}/\mathcal{S}_{\beta'=0}$ (Green) as a function of α assuming $\mathrm{M_{PBH}} = 10^8\,g$, $\beta' = 10^{-9}$. For the mass considered, $\mathrm{M_{PBH}}$ evolution depends only on the evaporation,

$$\frac{\mathrm{d}\ln \mathrm{M_{PBH}}}{\mathrm{d}\alpha} = -\frac{\kappa\ln(10)}{H\mathrm{M}_{\mathrm{PBH}}^3}\,. \tag{2.62}$$

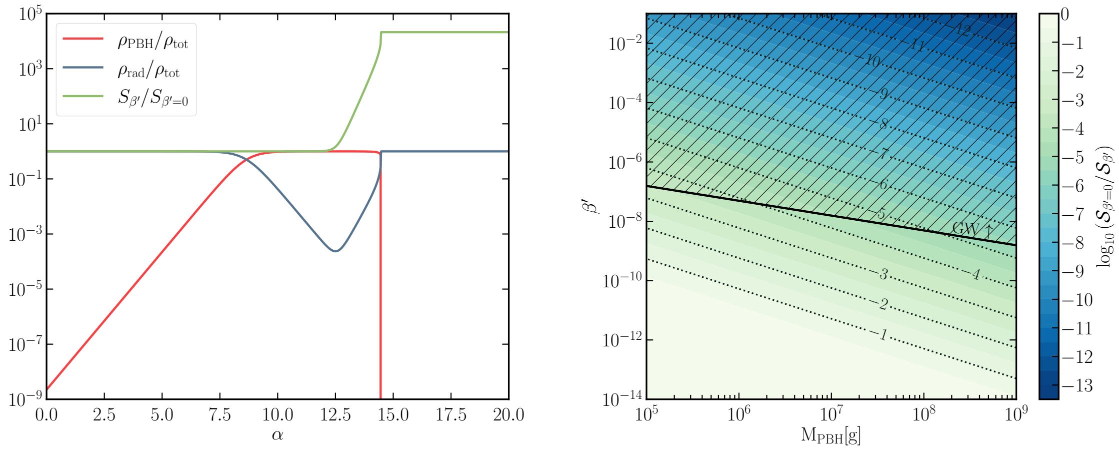

Figure 2.4: **Effect of Primordial Black Holes on Standard Cosmology.** The left panel shows $\rho_{\rm PBH}/\rho_{\rm tot}$ (Red), $\rho_{\rm rad}/\rho_{\rm tot}$ (Blue), and $\mathcal{S}_{\beta'}/\mathcal{S}_{\beta'=0}$ (Green) as a function of α for the benchmark provided by $\mathrm{M_{PBH}} = 10^8\,$g and $\beta' = 10^{-9}$. The right panel illustrates in color the entropy injection ($\log_{10}\mathcal{S}_{\beta'=0}/\mathcal{S}_{\beta'}$) in the plane $\mathrm{M_{PBH}} - \beta'$ for $\mathrm{M_{PBH}} \in [10^5 - 10^9]\,g$. The hatched region portrays the constraints on the gravitational waves' energy density from Big Bang Nucleosynthesis [431].

Solving this equation, we see that $\mathrm{M_{PBH}}$ is almost constant until $\alpha \simeq \alpha_{\rm ev}$. At this point, $\mathrm{M_{PBH}}$ goes to zero rapidly. From the left panel of Fig. 2.4, we see that the Universe is radiation dominated until $\alpha \simeq -\log_{10}\beta$. Primordial Black Hole energy density dominates until they evaporate. Near complete evaporation, radiation and entropy densities grow because of the relativistic particles emitted from Primordial Black Holes evaporation.

The right panel of Fig. 2.4 shows in color the entropy injection in the plane $\mathrm{M_{PBH}} - \beta'$. We consider the range $\mathrm{M_{PBH}} \in [10^5 - 10^9]\,$g. In this range, the mass evolves as shown in Eq. (2.62). We illustrate the limit on the energy density of gravitation waves at the time of Big Bang Nucleosynthesis [431, 432] as the hatched area.

2.4 Constraints

This Section provides an overview of the existing constraints on Primordial Black Holes abundance and categorizes them depending on the mass ranges. The bounds discussed therein derive from several studies and analyses. This Section aims to present the most conservative limits obtained assuming a monochromatic mass distribution and that do not form clusters. Ref. [3] provides a more detailed discussion. In Fig. 2.5, we report the constraints discussed in this Section.

We divide the constraints into six categories: (i) Primordial Black Holes evaporated completely before the present time ($\mathrm{M_{PBH}} \lesssim 5\times10^{14}\,$g); (ii) evaporation ($\mathrm{M_{PBH}} \in [10^{15} - 10^{18}]\,$g);

(*iii*) microlensing ($\mathrm{M_{PBH}} \in [10^{22} - 10^{36}]$ g); (*iv*) gravitational waves ($\mathrm{M_{PBH}} \in [10^{30} - 10^{37}]$ g); (*v*) dynamical effects ($\mathrm{M_{PBH}} \in [10^{34} - 10^{37}]$ g); and accretion ($\mathrm{M_{PBH}} \in [10^{32} - 10^{37}]$ g).

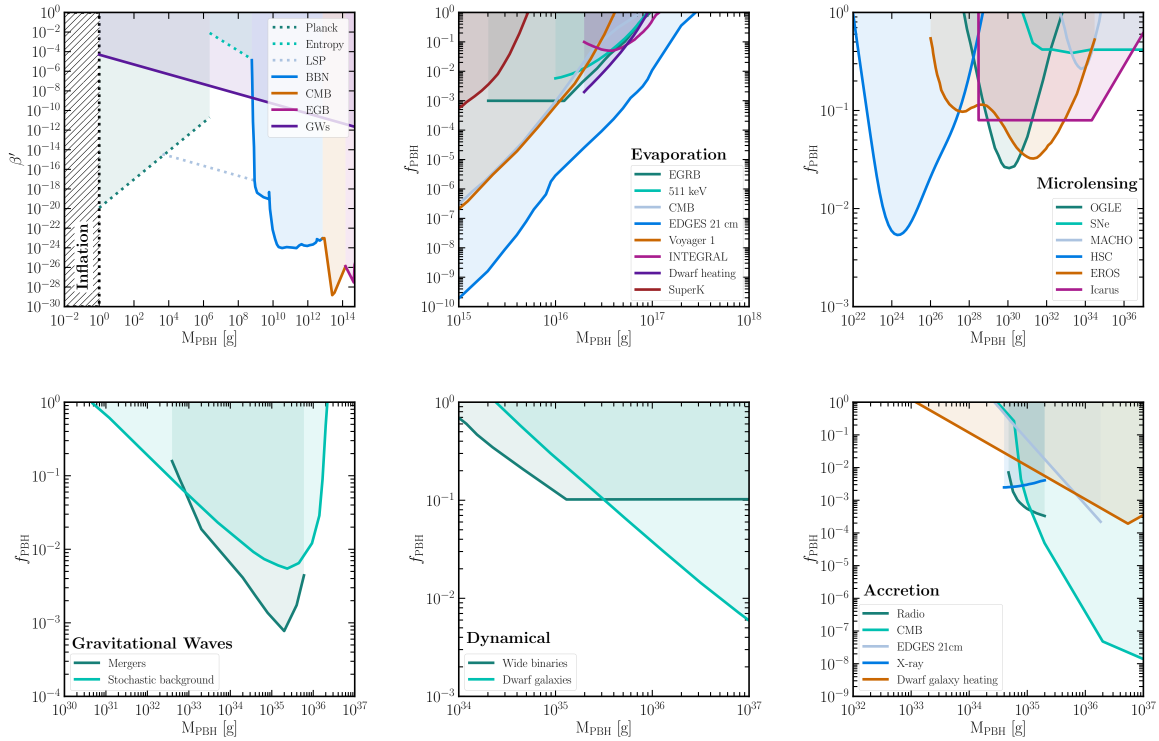

Figure 2.5: **Constraints**: The shaded regions illustrate the excluded areas. Dotted lines refer to constraints that rely on additional assumptions. *Top Left*: Constraints on Primordial Black Holes with lifetime shorter than the Universe's age. We report the bounds in terms of β' assuming Primordial Black Holes leave stable Planck mass relic [304], entropy injection constraints [3], Light Supersymmetric Particle (LSP) relic [324], Big Bang Nucleosynthesis [319], Cosmic Microwave Background spectral distortion and anisotropies [433, 434], Extra-Galactic γ-ray background (EGB) [319], and gravitational waves energy density from Big Bang Nucleosynthesis (GWs) [431]. *Top Middle*: Constraints from evaporation. We portray the constraints from Extra-Galactic γ-ray background (EGRB) [319], 511 keV gamma-ray line (511 keV) [435], Cosmic Microwave Background observations (CMB) [436, 437], EDGES 21cm [438, 439], Voyager $e^{\pm}$ [440], MeV Galactic diffuse flux (INTEGRAL) [441], dwarf Galaxy heating [442], and Super-Kamiokande (SuperK) [434, 443]. *Top Right*: Constraints from Gravitational lensing. We report the constraints from stellar microlensing from OGLE [294], MACHO [444], HSC [445], EROS [446]. Furthermore, we report the constraints from supernovae magnification distribution (SNe) [447] and Icarus lensing events (Icarus) [448]. *Bottom Left*: Constraints from gravitational waves. We depict the constraints from individual mergers [449, 450] and the stochastic background of mergers [451]. *Bottom Middle*: Dynamical constraints. We display the bounds from wide binaries [452] and dwarf Galaxies [453]. *Bottom Right*: Constraints from accretion. We show the from Radio [454], Cosmic Microwave Background (CMB) [426], EDGES 21cm [455], X-ray [454] observations and dwarf Galaxy heating [456]. We obtained the plot combining Ref. [3] and the code `PBHbounds` [457].

2.4.1 Constraints on evaporated Primordial Black Holes

Here, we present the constraints on Primordial Black Holes with a lifetime shorter than the Universe's age. It is worth noting that most of the limits placed on Primordial Black Holes evaporated completely before the Big Bang Nucleosynthesis ($\mathrm{M}_{\mathrm{PBH}} \lesssim 10^9\,\mathrm{g}$) rely on additional assumptions. However, we present three examples of such bounds. For larger masses, the constraints originate from Big Bang Nucleosynthesis, Cosmic Microwave Background, and γ-ray observations.

Planck Mass relic

If Primordial Black Holes leave stable relics behind as they completely evaporate, these relics can account for a fraction of the Dark Matter abundance. Assuming the relics have a mass $\mathrm{M}_{\mathrm{relic}} = \kappa \mathrm{M}_{\mathrm{Pl}}$, we can obtain an upper limit on β' assuming $\Omega^o_{\mathrm{relic}} \leq \Omega^o_{DM}$ [304]

$$\beta' < 8 \times 10^{-28} \kappa^{-1} \left(\frac{\mathrm{M}_{\mathrm{PBH}}}{\mathrm{M}_{\mathrm{Pl}}} \right)^{3/2} , \tag{2.63}$$

where

$$\left(\frac{T_{\mathrm{pl}}}{T_{RH}} \right)^2 < \frac{\mathrm{M}_{\mathrm{PBH}}}{\mathrm{M}_{\mathrm{Pl}}} < 10^{11} \kappa^{2/5} .$$

T_{pl} is the Plank temperature and T_{RH} is the reheating temperature. The mass lower limit arises from the observation that inflation would dilute Primordial Black Holes produced before reheating. The upper limit originates because Primordial Black Holes with larger masses would dominate before evaporating.

Lightest Supersymmetric Particle

Primordial Black Hole evaporation can also emit particles beyond the Standard Model, provided that their mass is smaller than $\mathcal{T}_{\mathrm{PBH}}$. The abundance of stable particles [323] and the decay of long-lived particles [266] strongly constrain Primordial Black Hole abundance. For example, in the Supersymmetry framework, the lightest supersymmetric particle (LSP) is stable and is a suitable Dark Matter candidate. By requiring that it does not exceed the observed Dark Matter density Ω^o_{DM}, Ref. [324] obtains

$$\beta' \lesssim 10^{-18} \left(\frac{\mathrm{M}_{\mathrm{PBH}}}{10^{11}} \right)^{-1/2} \left(\frac{m_{\mathrm{LSP}}}{100\,\mathrm{GeV}} \right)^{-1} \qquad \text{if } \mathrm{M}_{\mathrm{PBH}} < 10^{11} \left(\frac{m_{\mathrm{LSP}}}{100\,\mathrm{GeV}} \right)^{-1} \mathrm{g} \tag{2.64}$$

where m_{mLPS} is the lightest supersymmetric particle mass. It is worth noting that the constraint assumes the validity of SuperSummetry. Thus, different scenarios may lead to different limits.

Big Bang Nucleosynthesis

The interplay between Primordial Black Holes and Big Bang Nucleosynthesis drew significant attention, in particular Primordial Black Holes in the range $[10^9 - 10^{13}]\,\mathrm{g}$. Neutrino and anti-neutrino injection from Primordial Black Holes can alter the freeze-out of weak interaction and lead to modification in the neutron-to-photon ratio at the onset of Big Bang Nucleosynthesis, subsequently affecting the prediction for ^4He and D [458].

Refs. [459–461] discuss the limits associated with these effects. Additionally, Refs.[319, 462] investigate the fragmentation into hadrons of quark and gluon jets from Primordial Black Holes during Big Bang Nucleosynthesis.

Recently, Ref. [431] examines the impact of Primordial Black Holes $5 \times 10^8\,\mathrm{g}$ on the predictions of Big Bang Nucleosynthesis. Specifically, when the Universe transitions back to a radiation-dominated phase, the generation of gravitational waves can potentially alter Big Bang Nucleosynthesis unless

$$\beta \lesssim 1.1 \times 10^{-6} \left(\frac{\gamma_{\mathrm{PBH}}}{0.2}\right)^{-1/2} \left(\frac{\mathrm{M_{PBH}}}{10^4\,\mathrm{g}}\right)^{-17/24} . \tag{2.65}$$

This limit ensures that the gravitational waves produced do not alter significantly Big Bang Nucleosynthesis predictions.

Cosmic Microwave Background

Photons from Primordial Black Holes in the range $[10^{11} - 10^{13}]\,\mathrm{g}$ can noticeably distort the Cosmic Microwave Spectrum [459].

Ref. [459] analyses the effects of Primordial Black Hole evaporation on the Cosmic Microwave Background. The authors notice that photons evaporated from Primordial Black Holes with $\mathrm{M_{PBH}} < 10^9\,\mathrm{g}$ thermalize and only contribute to the photon-to-Baryon ratio. From the request that these photons do not exceed the observed photon-to-Baryon ratio, we get the following limit

$$\beta' < 10^9 \left(\frac{\mathrm{M_{PBH}}}{\mathrm{M_{Pl}}}\right)^{-1} . \tag{2.66}$$

More detailed calculations account for several effects. For instance, μ-distortion caused by the production of a large number of photons after the double-Compton scattering freezes out ($\mathrm{M_{PBH}} > 10^{11}\,\mathrm{g}$) [463, 464]. Moreover, considering the secondary emission of electromagnetic particles leads to stronger constraints [433, 465].

We can associate the damping of small-scale Cosmic Microwave Background anisotropies to Primordial Black Hole evaporating after the recombination. Ref. [319] report the following approximated limit

$$\beta'(\mathrm{M_{PBH}}) < 3\times 10^{-30}\left(\frac{f_H}{0.1}\right)^{-1}\left(\frac{\mathrm{M_{PBH}}}{10^{13}g}\right)^{3.1} \qquad 2.5\times 10^{13}\,\mathrm{g} \lesssim \mathrm{M_{PBH}} \lesssim 10^{14}\,\mathrm{g}\,, \tag{2.67}$$

where we define $f_H \approx 0.1$ as the fraction of emission in $e^{\pm}$. These bounds are valid for Primordial Black Holes evaporating after or at the recombination but before $z = 6$.

2.4.2 Constraints on evaporating Primordial Black Holes

Primordial Black Holes in the range $[5\times 10^{14} - 10^{18}]\,\mathrm{g}$ are sufficiently close to the complete evaporation to infer constraints on their abundance from the non-observation of the expected signal [257]. From the Extra-Galactic γ-ray background data, we obtain [319, 407]

$$f_{\mathrm{PBH}} \lesssim 2\times 10^{-8}\left(\frac{\mathrm{M_{PBH}}}{5\times 10^{14}\,\mathrm{g}}\right)^{3+\epsilon}\,, \tag{2.68}$$

where $\epsilon \sim 0.1 - 0.4$ describes the observed γ-ray intensity as a function of the energy [319]. Ref. [466] points out that accounting for the contribution of known astrophysical sources can improve by a factor $\mathcal{O}(10)$ these bounds. Ref. [438] uses EDGES measurement of 21 cm absorption line to limit f_{PBH}. Similarly, Ref. [442] bounds Primordial Black Hole abundance by looking at the heating of the interstellar medium in dwarf Galaxies. Voyager 1 limits the fraction of Primordial Black Holes composing the local Dark Matter density by looking at the $e^{\pm}$ flux [440]. Subtracting the supernova remnants and pulsar nebulae background improves the constraints of two orders of magnitude [440].

SPI/INTEGRAL limits Primordial Black Holes abundance by looking at the flux of the 511 keV line [467]. Indeed, Primordial Black Holes emit positrons that can annihilate and contribute to the 511 keV line. Ref. [441] further constrain f_{PBH} by using INTEGRAL measurement of the Galactic diffuse flux in the MeV range. Lastly, Super-Kamiokande uses the observation of the diffuse neutrino background to limit Primordial Black Holes parameter space [434].

2.4.3 Microlensing constraints

Stellar Microlensing

We define stellar microlensing as the temporary amplification of the flux of a star caused by the passage of a massive compact object with mass in the range $\mathrm{M_{CO}} \in [5\times 10^{-10} - 10]\mathrm{M_\odot}$ in the line of sight of the star [468]. Since the duration of this effect is proportional to $\mathrm{M_{CO}^{1/2}}$, the frequency of the survey determines the mass range constrainable. For instance, the EROS-2 survey of the Magellanic Clouds places limits on the abundance of compact objects in the range $[10^{-6} - 1]\mathrm{M_\odot}$ [446], whereas MACHO collaboration search for long duration events constrains the range $[1 - 30]\mathrm{M_\odot}$ [444].

Ref. [294] seizes tighter constraints in the range using OGLE microlensing survey of the Galactic bulge [469]. Furthermore, the data set contains six ultrashort events attributable to free-floating planets or Primordial Black Holes[448].

Subaru HSC optical observations of M31 allow limiting the mass range $[5\times10^{-12}-10^{-6}]\mathrm{M}_\odot$. Wave optical effects weaken the expected constraints. Kepler searches of low amplification lensing lead to noticeably weaker constraints [470].

Assuming compact objects compose a sizeable fraction of Dark Matter leads to a dampened magnification of stars [471]. The first microlensing event observed is Icarus/MACS J1149LS1 and is compatible with microlensing by an intracluster star of a source star at a redshift of 1.5 [472, 473]. Ref. [448] constrains f_{CO} by requiring that compact objects in the range $[10^{-5} - 10]\mathrm{M}_\odot$ do not weaken the magnification.

Type 1a supernovae

Compact objects may cause gravitational lensing effects on the magnification of type 1a supernovae. These effects depend on the distribution of the Dark Matter [474]. The data from JLA and Union 2.1 SNe samples constrain compact objects with $\mathrm{M}_{\mathrm{CO}} \gtrsim 10^{-2}\mathrm{M}_\odot$ to have $f_{\mathrm{CO}} \lesssim 0.4$ [447]. We mention that Ref. [475] affirms that such constraints apply if $\mathrm{M}_{\mathrm{CO}} \lesssim 3\mathrm{M}_\odot$.

Strong lensing of Fast Radio Bursts

The non-observation of the strong gravitational of Fast Radio Bursts by compact objects with masses in the range $[10 - 100]\mathrm{M}_\odot$ limits the fraction of Dark Matter comprised of compact objects [476].

2.4.4 Gravitational waves constraints

Refs. [348, 477] study the formation of solar mass Primordial Black Holes binaries. Their coalescence at present generates gravitational waves detectable by LIGO. The expected rate is orders of magnitude larger than the current LIGO-Virgo [291] data. Thus, Refs.[351, 449, 478, 479] place tight constraints on the fraction of Dark Matter composed of Primordial Black Holes in the range $\mathrm{M}_{\mathrm{PBH}} \in [10 - 300]\mathrm{M}_\odot$. Ref. [450] extend the constraints down to $\sim 0.2\mathrm{M}_\odot$ considering a dedicated LIGO-Virgo search for sub-Solar mergers. The stochastic gravitational wave background [451, 480–482] of the mergers and searches for Primordial Black Holes binaries with large mass ratios searches [483] further constrain the parameter space. Assuming that Primordial Black Holes only partially constitute ρ_{DM}, Primordial Black Holes of stellar mass would accrete Dark Matter halos with a sharp density profile during the matter-dominated era [280, 339]. The presence of these halos modifies the evolution of Primordial Black Hole binaries [351, 479] slightly altering the constraints [449].

A long-standing problem is the simulation of the evolution and survival of Primordial Black Hole binaries. For instance, a higher abundance of Primordial Black Holes leads to the formation of clusters close to the matter-radiation equality [288, 484–486]. Refs. [479, 487–491] investigate three-body interactions effect on Primordial Black Holes binaries. Furthermore, scenarios forming Primordial Black Holes with a sizable initial clustering determine a higher merger rate leading to stringent constraints [492, 493]. Conversely, Refs. [494] obtains the weaker limits.

2.4.5 Constraints from dynamical effects

Dwarf Galaxies

The kinetic energies of a system composed of objects with different masses tend to become equal thanks to two-body interactions. In Ultra-faint dwarf Galaxies, the presence of compact objects would lead to noticeable effects on the energy and distribution of the stars. For instance, Ref. [453] places constraints on the abundance of compact objects from the dimensions of the Ultra-faint dwarf Galaxies.

Wide binaries

The encounter with several compact objects increases the energy of wide binary stars. It can potentially lead to its disruption [495]. We can use the distribution of wide binaries to limit the abundance of compact objects [496]. Ref. [452] constrain the abundance of compact objects by considering 25 wide binaries that spend the least time in the Galactic disk [497]

2.4.6 Constraints from accretion

The gas accreting onto Primordial Black Holes emits radiation. It can modify the recombination of the Universe, altering the anisotropies and spectrum of the Cosmic Microwave Background [263, 498]. As shown in Refs. [423, 499], both the accretion rate and the ionizing effects of the radiation present compelling theoretical uncertainties.

The constraints are sensible to the shape of the accretion region. For instance, bounds obtained assuming an accretion disk are more stringent than the ones obtained considering a spherical accretion [425]. Furthermore, assuming the formation of Dark Matter halos around Primordial Black Holes tightens the limits for $\mathrm{M_{PBH}} \geq 10\mathrm{M}_\odot$ [426]. EDGES measurement of the 21-cm spectrum further constrains Primordial Black Holes with $\mathrm{M_{PBH}} \gtrsim 10\mathrm{M}_\odot$ [455].

Observable X-ray and radio emissions originate from the accretion of Primordial Black Holes with $\mathrm{M_{PBH}} > \mathrm{M}_\odot$ in the Milky Way [500]. Limits on f_{PBH} originate from the comparison of numerical simulation of the expected emission with known X-ray and radio sources in the Chandra and VLA Galactic center surveys [454, 501]. Lastly, gas heating in dwarf Galaxies can place constraints on f_{PBH} [456].

2.4.7 Primordial Black Holes as Dark Matter

As discussed above, several observables significantly constrain the current abundance of Primordial Black Holes. In Fig. 2.6, we summarise these bounds using different colors to indicate the specific observables that contributed to their derivation. Notably, a narrow window, highlighted in grey, remains consistent with the scenario where Primordial Black Holes could entirely constitute the Dark Matter abundance. Future experiments may have the potential to delve into uncharted territories of this parameter space to either provide positive observation or expand the existing bounds.

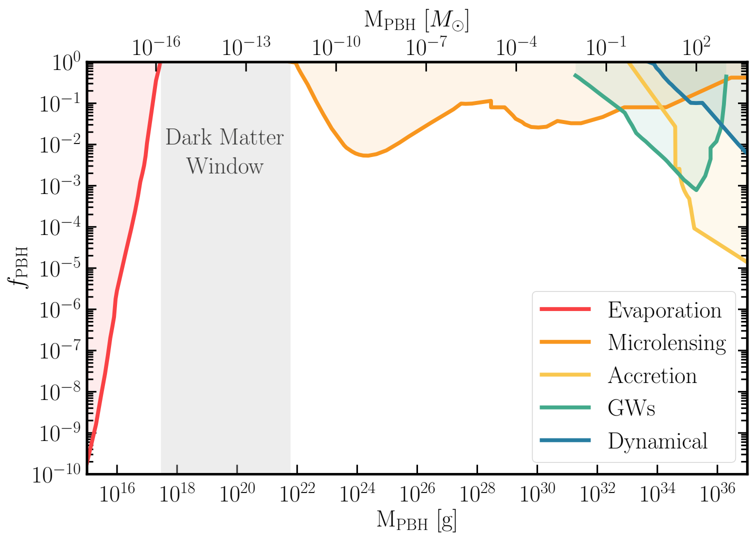

Figure 2.6: This plot encapsulates the constraints placed on existing Primordial Black Holes discussed above: Evaporation (in red), Microlensing (in orange), Accretion (in yellow), Gravitational Waves (in green), and Dynamical effects (in blue). The grey band highlights the region where Primordial Black Holes may constitute the entire Dark Matter abundance. We generate this Figure using `PBHbounds` [457].

2.4.8 Generalization of constraints to different mass functions

Here, we present the prescription bestowed in Ref. [502] to generalize the constraints obtained for a monochromatic mass distribution to a more general one, $\psi(\mathrm{M_{PBH}})$. We define

$$f_{\rm PBH} = \int \mathrm{dM_{PBH}} \psi(\mathrm{M_{PBH}}) \,, \tag{2.69}$$

We can expand astrophysical observable $A[\phi(\mathrm{M_{PBH}})]$ as

$$
\begin{aligned}
A[\phi(\mathrm{M_{PBH}})] = A_0 + \int \mathrm{dM_{PBH}}\phi(\mathrm{M_{PBH}})K_1\left(\mathrm{M_{PBH}}\right) + \\
+ \int \mathrm{dM^{(1)}_{PBH}dM^{(2)}_{PBH}}\psi(\mathrm{M_{PBH}})K_2\left(\mathrm{M^{(1)}_{PBH}}, \mathrm{M^{(2)}_{PBH}}\right) + \ldots ,
\end{aligned}
\tag{2.70}
$$

where A_0 is the background contribution, K_j describe how the observable depends on $\mathrm{M_{PBH}}$ and its distribution. In many scenarios, we obtain constraints by requiring

$$
A[\phi(\mathrm{M_{PBH}})] < A_{\mathrm{exp.}} .
$$

For most of the constraints, Primordial Black Holes of different masses contribute separately to the bound. In such a case $K_j = 0$ for $j \geq 2$ and the constraints translate as

$$
\int \mathrm{dM_{PBH}} \frac{\psi(\mathrm{M_{PBH}})}{f_{\mathrm{PBH}}(\mathrm{M_{PBH}})} \leq 1 . \tag{2.71}
$$

Examples of observables where different masses do not contribute separately are the Gravitational Waves from mergers.

Part II

CHAPTER 3

Primordial black hole dark matter evaporating on the neutrino floor

This Chapter focuses on constraining Primordial Black Holes' abundance today by looking at the evaporated neutrinos. Specifically, we consider Primordial Black Holes with masses in the range $[5 \times 10^{14} - 5 \times 10^{15}]\,\mathrm{g}$, so that the emitted neutrinos have energies below $\sim 100\,\mathrm{MeV}$ allowing for their detection via Coherent Elastic neutrino-Nucleus Scattering in multi-ton Dark Matter direct detection facilities. The high exposure foreseen for the next-generation detectors will enable the establishment of bounds on the fraction of Dark Matter composed of Primordial Black Holes. The projected limits derived in this analysis extend and improve Super-Kamiokande's. In the last Section, we quantify the impact of neutrinos from Primordial Black Holes, a new astrophysical neutrino source, on the neutrino floor.

3.1 Neutrino flux

In this study, we consider a monochromatic mass distribution of neutral and non-rotating Primordial Black Holes in the range $[5 \times 10^{14} - 5 \times 10^{15}]\,\mathrm{g}$.

While Coherent Elastic neutrino-Nucleus Scattering refers only to active neutrinos, it is worth noting that the nature of neutrinos can impact the emission rate from Primordial Black Holes [503]. As shown in Refs. [270, 271, 428], Dirac neutrinos would affect Primordial Black Holes evaporation. Since Dirac neutrinos have twice as many degrees of freedom as Majorana neutrinos, they would accelerate Primordial Black Hole evaporation. Ref. [428] demonstrated that the modification is $\simeq 10\%$ in the mass range considered. To be conservative, we assume Majorana neutrinos throughout our analysis. As Coherent Elastic neutrino-Nucleus Scattering is flavor blind, we can neglect neutrino oscillations in our calculations. We compute the total neutrino flux by following the prescription described in Section,2.2, considering only the

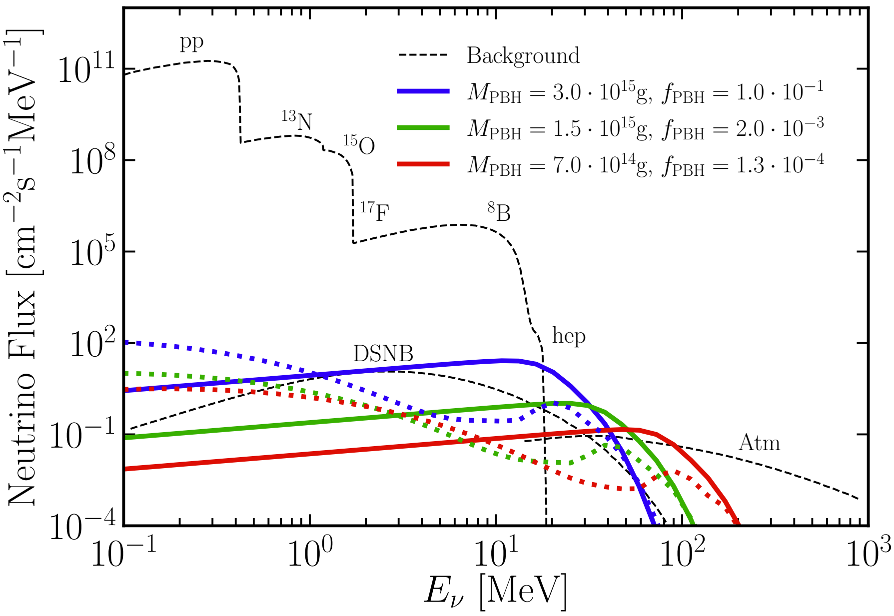

Figure 3.1: **Neutrino fluxes from Primordial Black Holes.** The black dashed lines illustrate the solar, Diffuse supernovae neutrino Background (DSNB), and atmospheric (atm) neutrinos. The colored solid and dotted lines represent the primary and secondary neutrino flux from Primordial Black Holes with parameters shown in the legend. We took the figure from Ref. [5].

primary emission of neutrinos from Primordial Black Holes, with the caveat of considering only the primary emission. In Fig. 3.1, we show the total neutrino flux as a function of the neutrino energy. The dashed black line represents the background constituted by solar [504], Diffuse Supernovae neutrino Background (DSNB) [505], and low-energy atmospheric neutrinos [506, 507]. The solid (dotted) curves depict the primary (secondary) neutrino flux from Primordial Black Holes. The primary flux dominates over the secondary one for higher energies. Furthermore, Primordial Black Holes neutrinos prevail over the background for $E_\nu \gtrsim 20\,\mathrm{MeV}$, where the solar hep neutrinos fall off. Hence, we only consider the primary neutrino flux from Primordial Black Holes.

3.2 Event Rate

The differential event rate for Coherent Elastic neutrino-Nucleus Scattering is given by

$$\frac{\mathrm{d}R_{\nu\mathcal{N}}}{\mathrm{d}E_r} = N_T \epsilon(E_r) \times \int \mathrm{d}E_\nu \frac{\mathrm{d}\sigma_{\nu\mathcal{N}}}{\mathrm{d}E_r} \frac{\mathrm{d}\phi_\nu}{\mathrm{d}E_\nu} \Theta(E_r^{\max} - E_r)\,, \tag{3.1}$$

where $\epsilon(E_r)$ is the detector efficiency which we approximate to one. In Fig. 3.2, we present the event rate in a xenon-based experiment with a 200-tonne yr exposure as a function of the recoil

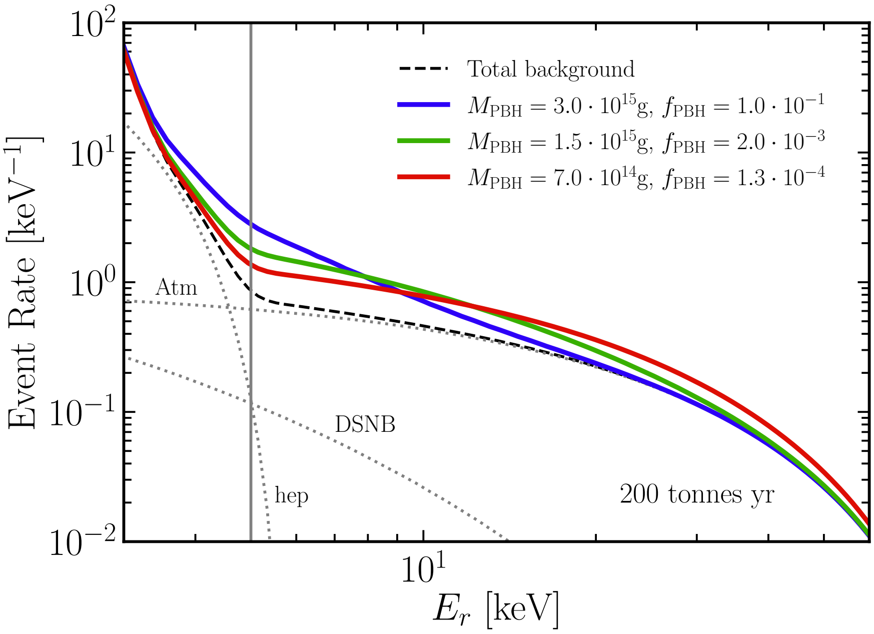

Figure 3.2: **Differential events rate for exposure of 200-tonne yr xenon detector.** The black dashed line shows the total background event rate. We report atmospheric, Diffuse supernovae neutrino, and solar hep events rate components in dotted grey lines. The colored curves represent the event rate assuming the presence of neutrinos from Primordial Black Holes with parameters shown in the legend. The vertical line indicates the threshold energy considered in our analysis. We took the figure from Ref. [5].

energy. We report the standard background as a dashed black line and hep, Diffuse Supernovae neutrino background, and atmospheric neutrinos as dotted grey lines. We picture as colored solid lines the event rate for three Primordial Black Holes benchmarks. We highlight that the spectrum shape depends on $[\mathrm{M}_{\rm PBH},\ f_{\rm PBH}]$. In particular, for greater $\mathrm{M}_{\rm PBH}$, the spectrum shape differs from the background. To extract information on the event rate profile, we employ a binned analysis. In particular, we consider ten bins in the range $E_r \in [5-50]\,\mathrm{keV}$. We choose a threshold recoil energy of $E_r^{\rm tr} = 5\,\mathrm{keV}$ because of the position of the sharp cutoff of the solar hep neutrinos. This approach allows us to efficiently analyze the event rate and derive significant constraints in the plane $[\mathrm{M}_{\rm PBH} - f_{\rm PBH}]$.

3.3 Primordial Black Holes at next-generation detectors

To derive upper limits on the fraction of Dark Matter composed of Primordial Black Holes, we consider a χ^2 test statistic, defined as

$$\chi^2(\theta) = \min_{\alpha} \left[\chi^2(\theta,\alpha) + (1-\alpha)^T \Sigma_\alpha^{-1} (1-\alpha)\right] \,. \tag{3.2}$$

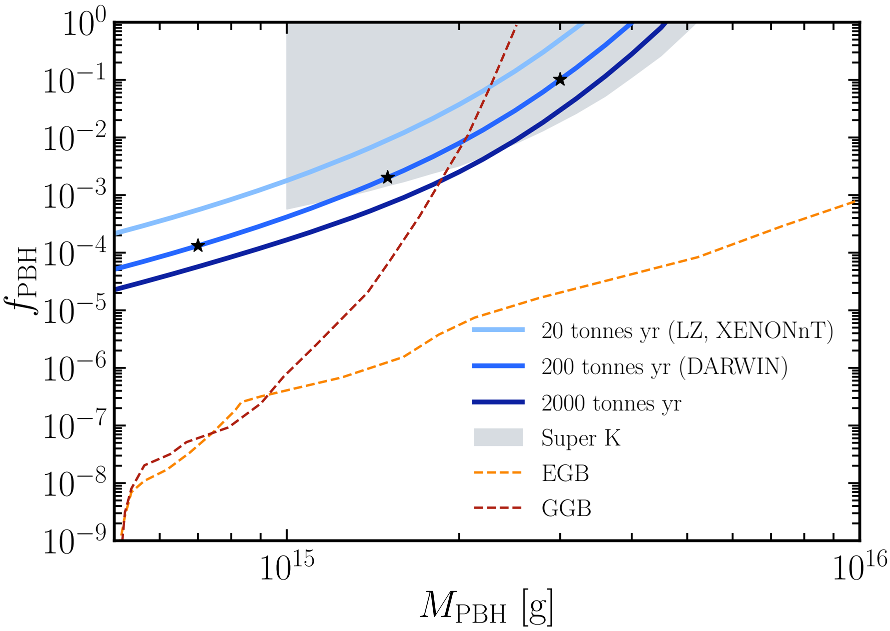

Figure 3.3: **Prospective upper bounds on Primordial Black Holes.** The blue curves illustrate the exclusion contours at 90% C.L. for 1 degree of freedom. The boundaries refer to xenon-based experiments with exposures reported in the legend. We obtain two of them for planned experiments, and the last corresponds to an ideal setup. We indicate with black stars the three benchmark cases used in Figs. (3.1, 3.2, 3.4). We depict the limits from DSNB searches of Super-Kamiokande1 [434, 443] as a shaded grey region. The dashed curves, shown in red and orange, represent the upper limits obtained from Galactic (GGB) and Extra-Galactic (EGB) [3] γ-ray observations, respectively. We took the figure from Ref. [5].

Here, $\theta^T = [\mathrm{M_{PBH}}, f_{\rm PBH}]$ is the vector of the model parameter, and $\alpha^T = [\alpha_1, \alpha_2, \alpha_3]$ is the vector of the nuisance parameters on the normalization of the background components (solar hep, Diffuse supernovae neutrino background, and atmospheric) concerning the theoretical estimations. The covariance matrix $\Sigma_\alpha = \mathrm{diag}(\sigma^2_{\alpha_1} = 0.09,\ \sigma^2_{\alpha_2} = 0.25,\ \sigma^2_{\alpha_3} = 0.04)$ [504–507] embeds the uncertainties on the background. The matrix is diagonal because the three fluxes have independent origins. We define

$$\chi^2(\theta, \alpha) = -2 \ln \frac{L_0}{L_1}\,, \tag{3.3}$$

where the Likelihoods are

$$L_0 = \prod_i P\left(x = \overline{N_{\rm Bck}}^i; \lambda = N^i_{\rm PBH}(\theta) + N^i_{\rm Bck}(\alpha)\right)\,, \tag{3.4}$$

$$L_1 = \prod_i P\left(x = \overline{N_{\rm Bck}}^i; \lambda = N^i_{\rm Bck}\right)\,. \tag{3.5}$$

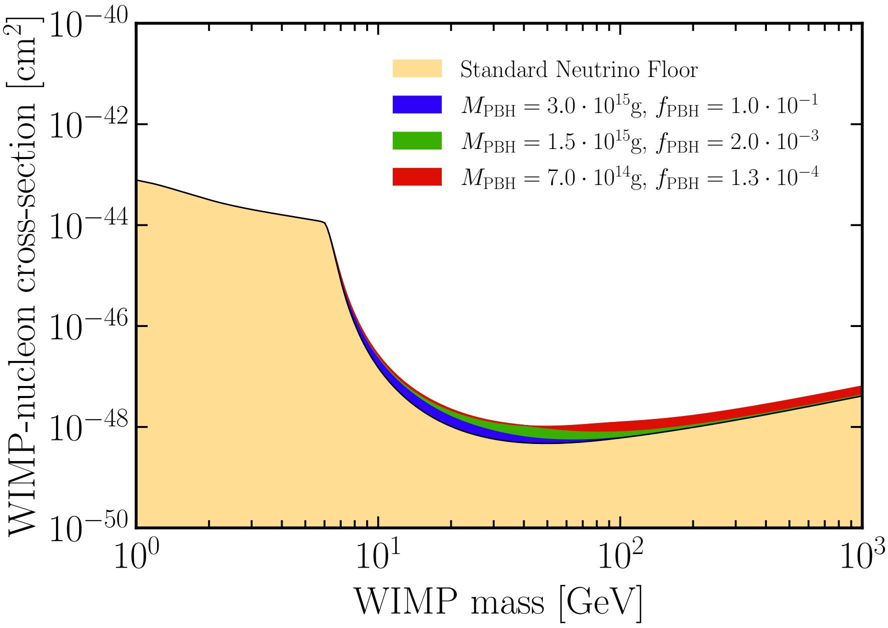

Figure 3.4: **Impact of Primordial Black Holes on the Neutrino Floor.** The black contour indicates the ordinary neutrino floor. The upper border of the colored bands illustrates the modification of the Neutrino floor induced by neutrino evaporated from Primordial Black Holes with parameters reported in the legend. We took the figure from Ref. [5].

$P(x, \lambda)$ is the Poisson distribution, i is the bin index. $\overline{N_{\rm Bck}}^i$ and $N^i_{\rm PBH}(\theta)$ are the nominal number of background events and the number of events from Primordial Black Hole neutrino in the i-th bin respectively. $N^i_{\rm Bck}(\alpha) = \sum_j \alpha_j \overline{N_{\rm Bck}}^i$ is the background event in the i-th bin that varies with the nuisance parameters. In Refs [508–510], the authors point out that Diffuse Supernovae neutrino Background flux can be larger than the nominal value [504]. We verify that our results remain almost unchanged even when considering twice the flux compared to that suggested in Ref [504]. In Fig. 3.3, we show the 90% C.L. bounds in the plane $[\rm M_{PBH}, \mathit{f}_{PBH}]$. The colored curves display the upper limit on $f_{\rm PBH}$ obtained for a xenon-based detector with 20, 200, and 2000 tonne yr exposures. The first two exposures correspond to planned experiments, and the third one to an ideal setup. More precisely, LZ and XENONnT should attain 20-tonne yr exposure, while DARWIN should accomplish an exposure of 200-tonne yr. We report as a grey region the constraints from Super-Kamiokande [443] Diffuse Supernovae neutrino Background searches [434]. We underline that our forecast bounds extend to lower masses and improve those obtained in Super-Kamiokande. Conversely, they are weaker than the ones obtained from the Galactic and Extra-Galactic γ-ray background [3]. We depict them in red and orange, respectively.

3.4 Impact of Primordial Black Holes on the neutrino floor

Lastly, we quantify how neutrinos from Primordial Black Holes can affect the neutrino floor following Section 1.3.2 for $\rho_{\odot} = 0.4\,\mathrm{GeV\,cm^{-3}}$, in agreement with the Navarro-Frenk-White distribution considered in Section 2.2. In particular, we select the exposure leading to 1 Coherent Elastic neutrino-Nucleus Scattering event. In this framework, we obtain the WIMP-nucleon cross-section excluded at 90% C.L.. In Fig. 3.4, we report the standard neutrino floor as the solid black line delimiting the yellow region. The upper border of the colored sectors corresponds to the modification of the neutrino floor associated with the neutrinos emitted from Primordial Black Holes with parameters shown in the legend. In Refs. [279, 280, 511–517], the authors show that Primordial Black Holes with $\mathrm{M_{PBH}} \gtrsim 10^{21}\,\mathrm{g}$ are incompatible with the existence of WIMPs as (sub-)dominant Dark Matter component. Since we are considering Primordial Black Holes with lower masses, this mutual exclusion does not apply to our scenario.

Discussion

In this Chapter, we examine neutrino emission from Primordial Black Hole evaporation. In particular, we focus on neutrino detection via Coherent Elastic neutrino-Nucleus Scattering in multi-ton Dark Matter direct detection experiments. Soon, these experiments will have enough sensitivity to constrain Primordial Black Holes abundance. Our limits will extend and improve Super-Kamiokande's. Lastly, we quantified the effect of Primordial Black Holes neutrino on the neutrino floor. For simplicity, we focused on liquid-xenon-based experiments, like DARWIN [138], LZ [518], and XENONnT [145]. We underline that other targets such as liquid argon employed in DarkSide-20k [126] and ARGO [126], or archeological lead in RES-NOVA [519], should offer a similar opportunity provided that they reach very high exposures. As a final note, it is worth highlighting that in the context of Primordial Black Holes, Dark Matter direct detection experiments operate as indirect detection facilities.

CHAPTER 4

Direct detection of sub-GeV Dark Matter from evaporating Primordial Black Holes

In this Chapter, we present a study on the production of light Dark Matter from Primordial Black Holes evaporating at present. We emphasize that Primordial Black Holes emit Dark Matter of mass $m_\chi < \mathcal{T}_{\mathrm{PBH}}$ with (semi-)relativistic momenta. We highlight that even a modest fraction of Primordial Black Holes could generate a sizeable amount of Dark Matter, resulting in measurable signals in existing detectors. The non-observation of the expected signature can provide valuable constraints on the mixed parameter space.

The first Section of this Chapter focuses on Dark Matter-nucleon scattering. Here, we evaluate the depletion effects on the Dark Matter flux caused by interaction with Earth's and the atmosphere's atoms. Subsequently, we estimate the expected signal in the XENON1T experiment. Finally, we employ the data from XENON1T to constrain the Dark Matter parameter space, assuming the existence of Primordial Black Holes and vice-versa.

The second Section addresses the Dark Matter-electron interactions. This interaction allows us to consider XENON1T and Super-Kamiokande to probe our scenario. However, the complication of Dark Matter-electron interaction is that electrons are not free particles, necessitating the inclusion of ionization effects. We then estimate the signal in XENON1T and Super-Kamiokande. Ultimately, we limit the mixed parameter space considering the data from these detectors.

In both Sections, we consider spinless and neutral Primordial Black Holes with a monochromatic mass distribution. The mass range considered varies depending on the experiment and interaction analyzed. We examine a Dirac fermion ($g_\chi = 4$) Dark Matter candidate χ.

4.1 Dark Matter-nucleon interaction

In this Section, our focus lies on Dark Matter-nucleon interaction, proving that our scenario can yield detectable signals in the XENON1T experiment. To this end, we consider Primordial Black Holes in the range $[5 \cdot 10^{14} - 1 \cdot 10^{16}]$ g. Therefore, we have to examine $m_\chi \lesssim 100\,\mathrm{MeV}$ (see Eq. 2.28). In particular, Primordial Black Holes evaporate Dark Matter particles lighter than $\sim 1\,\mathrm{MeV}$ with ultra-relativistic velocities, revealing that Primordial Black Holes are a new mechanism to have boosted Dark Matter.

To proceed, we calculate χ flux on Earth following the procedure outlined in Section 2.2. In Fig. 2.2.1, we show the Galactic (solid line) and Extra-Galactic (dashed line) χ flux on Earth for $m_\chi = 1\,\mathrm{MeV}$ as a function of the kinetic energy T_χ. The different colors indicate three $[\mathrm{M_{PBH}}, f_{\mathrm{PBH}}]$ combinations. For more detail, see the figure's caption.

4.1.1 Propagation through Earth and atmosphere

In the context of Dark Matter nucleon interactions, the propagation in Earth and atmosphere attenuates χ flux at the detector [520–523]. In this analysis, we adopt the analytical approach described in Ref. [159], where the authors consider a ballistic Dark Matter propagation. However, as shown in Ref. [161], the ballistic approximation may not hold for light Dark Matter collisions with heavy nuclei. Instead, they consider a diffusive propagation that may lead to a larger energy loss, a possible reflection of Dark Matter, and a lower flux. To better understand the impact of the ballistic approximation, we also estimate χ flux under the most conservative assumption that any interaction depletes the particles completely. Even under this assumption, the expected event rate in XENON1T is still detectable. Hence, we do not expect that a more precise modelization of the propagation of a light Dark Matter candidate would substantially alter our scenario. Furthermore, we limit our analysis to Dark Matter-nucleon cross-sections smaller than 10^{-35} cm^2 so that the propagation effects remain negligible.

Since $T_\chi \lesssim 100\,\mathrm{MeV}$, we can neglect quasi-elastic and inelastic scattering as well as the nuclear form-factors. Within this approximation, the interaction length for propagation through Earth ($\ell^{\oplus}_{\mathrm{int}}$) and the atmosphere ($\ell^{\mathrm{atm}}_{\mathrm{int}}$) are

$$\ell^i_{\mathrm{int}} = \left[\sum_{\mathcal{N}} n^i_{\mathcal{N}} \sigma_{\chi\mathcal{N}} \frac{2 m_{\mathcal{N}} m_\chi}{(m_{\mathcal{N}} + m_\chi)^2}\right]^{-1} , \tag{4.1}$$

where the sum is taken over the most abundant elements in the Earth (from iron to aluminum) and in the atmosphere (nitrogen and oxygen) with number density n^i_{N}. Assuming χ couples equally to protons and neutrons, the cross-section is

$$\sigma_{\chi\mathcal{N}} = \sigma^{\mathrm{SI}}_\chi \mathrm{A}^2 \left(\frac{m_{\mathcal{N}}(m_\chi + m_{\mathrm{p}})}{m_{\mathrm{p}}(m_\chi + m_{\mathcal{N}})}\right)^2 . \tag{4.2}$$

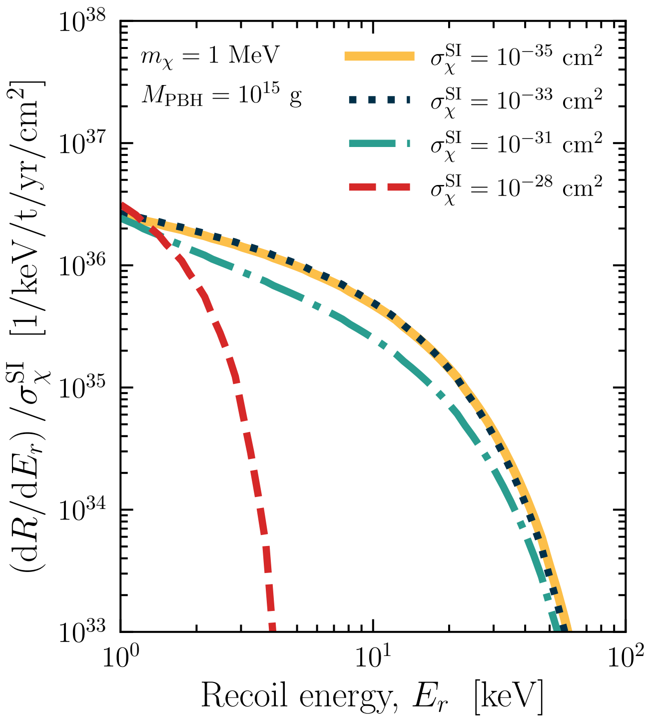

Figure 4.1: **Ratio of XENON1T event rate over Dark Matter-nucleon cross-section.** The figure shows the ratio between the event rate in Eq. (4.5) over the Dark Matter-nucleon cross-section. We fix $M_{\rm PBH} = 10^{15}$ g, $f_{\rm PBH} = 3.9 \times 10^{-7}$, and $m_\chi = 1$ MeV. The curves correspond to different Dark Matter-nucleon cross-sections shown in the legend. We took the figure from Ref. [6].

where $\sigma_\chi^{\rm SI}$ denotes the spin-independent cross-section, the focus of our analysis. We highlight that spin-independent scattering is subject to a coherent enhancement. We indicate with T_0 and T_d χ initial kinetic energy and the kinetic energy after traveling a total geometrical distance $d = d_{\rm atm} + d_\oplus$ respectively. We account for the XENON1T detector located at the Gran Sasso National Laboratory at a depth of about 1.4 km [524]. Therefore, χ flux in XENON1T is

$$\frac{{\rm d}\phi_\chi^d}{{\rm d}T_d {\rm d}\Omega} \approx \frac{4 m_\chi^2 e^\tau}{(2m_\chi + T_d - T_d e^\tau)^2} \left(\left.\frac{{\rm d}\phi_\chi}{{\rm d}T_\chi {\rm d}\Omega}\right|_{T_0} \right), \tag{4.3}$$

where $\tau = d_{\rm atm}/\ell_{\rm int}^{\rm atm} + d_\oplus/\ell_{\rm int}^\oplus$, and the incoming Dark Matter flux is evaluated at

$$T_0\,(T_d) = \frac{2 m_\chi T_d\, e^\tau}{2m_\chi + T_d - T_d e^\tau}\,. \tag{4.4}$$

The distance d depends on the time-dependent longitude of the experiment. Thus, in the following, we consider the average of Eq. (4.3) over a day.

4.1.2 XENON1T event rate

This paragraph discusses the event rate expected in XENON1T, a detector based on liquid Xenon. Assuming a flat recoil energy E_r distribution, the differential event rate per ton year is

$$\frac{\mathrm{d}R}{\mathrm{d}E_r} = \sigma_{\chi\mathrm{Xe}}\, N_{\mathrm{Xe}} \int \mathrm{d}T_d \mathrm{d}\Omega\, \frac{\mathrm{d}\phi_\chi^d}{\mathrm{d}T_d \mathrm{d}\Omega} \frac{\Theta(E_r^{\max} - E_r)}{E_r^{\max}}\,, \tag{4.5}$$

where N_{Xe} is the total number of Xenon targets, and

$$E_r^{\max} = \frac{(T_d)^2 + 2m_\chi T_d}{T_d + (m_\chi + m_{\mathrm{Xe}})^2/(2m_{\mathrm{Xe}})} \tag{4.6}$$

is the recoil energy maximum value. We consider the nuclear form factor provided in Ref.s [74, 76] (see also Chapter 3). In Fig. 4.1, we show the event rate in XENON1T over the Dark Matter-nucleon interaction $\sigma_\chi^{\mathrm{SI}}$ as a function of the recoil energy for an exposure of one tonne year. We highlight that the ratio is independent of the cross-section as long as the propagation effects are negligible (solid yellow and the dotted blue curves). Propagation effects are no longer unimportant for higher $\sigma_\chi^{\mathrm{SI}}$ (green dot-dashed and red dashed lines), leading to lower recoil energies and a weaker signal in the detector.

4.1.3 Discussion

In this analysis, we compare the event rate in Eq. (4.5) with XENON1T data in the recoil energy range $[4.9 - 40.9]\,\mathrm{keV}$, where the experiment does not observe an excess [140]. Following the prescription of Ref. [159], we obtain the upper limit for the total event rate as

$$\int_{E_{r,1}}^{E_{r,2}} \mathrm{d}E_r \frac{\mathrm{d}R}{\mathrm{d}E_r} \lesssim \kappa\, \overline{v}_{\mathrm{DM}}\, \rho_{\mathrm{DM}}^{\odot}\, N_{\mathrm{Xe}} \left(\frac{\sigma_{\chi\mathrm{Xe}}}{m_\chi}\right)_{m_\chi \gtrsim 100\,\mathrm{GeV}}\,, \tag{4.7}$$

where $\kappa \simeq 0.23$, $\overline{v}_{\mathrm{DM}} \simeq 235$ km/s is the mean Dark Matter velocity in the standard scenario, and $\rho_{\mathrm{DM}}^{\odot} = 0.3$ GeV/cm^3 is the local Dark Matter density assumed by XENON1T Collaboration. The term in parentheses is $2.5 \times 10^{-40}\mathrm{cm}^2/\mathrm{GeV}$ based on the current XENON1T limit for large Dark Matter masses [140]. We show our results in Fig. 4.2. The left plot displays the excluded region in the Dark Matter parameter space for three $[\mathrm{M_{PBH}}, f_{\mathrm{PBH}}]$ combinations. Specifically, we assume f_{PBH} equal to the maximum allowed by current limits [3]. The grey region is excluded by cosmic-ray upscatterings [159, 161], CRESST experiment [142, 144], and cosmology [173–176]. We proved that our constraints are unchanged for complex scalar Dark Matter, while they deplete by $\sim 80\%$ for vector Dark Matter.

The right plot illustrates the upper bounds on Primordial Black Holes abundance for four benchmarks $\sigma_\chi^{\mathrm{SI}}$. The limits are valid as long as $m_\chi \lesssim 1\,\mathrm{MeV}$. The figure shows that the constraints are almost inversely proportional on the cross-section of the attenuation effects are

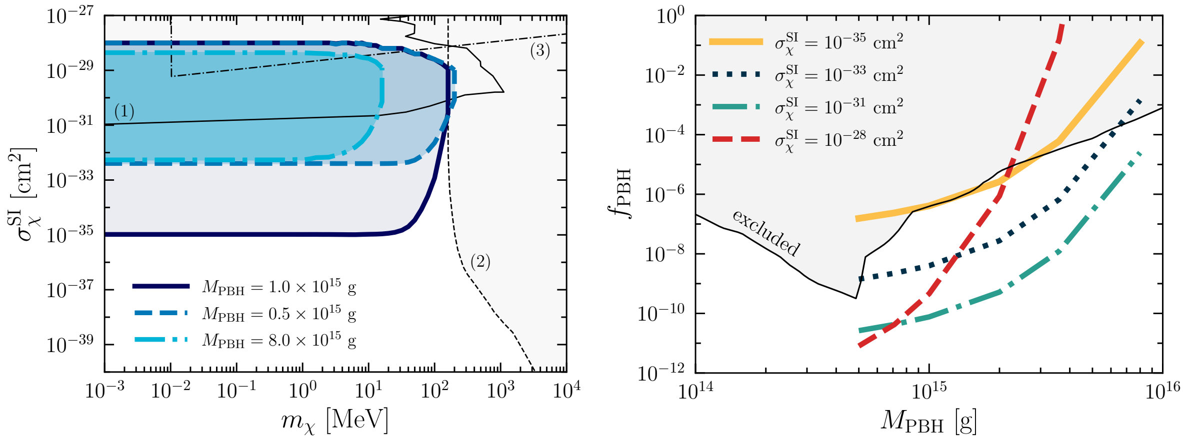

Figure 4.2: **Constraints.** In the left panel, we show the excluded region in the plane m_χ–σ_χ^{SI} for different M_{PBH}. Here, we set f_{PBH} to the maximum value allowed by present constraints [3]. For comparison, we report constraints from cosmic-ray boosted Dark Matter particles [159, 161] (1), from CRESST experiment [142, 144] (2), and cosmology [173–176] (3). The right plot illustrates in colored lines the upper bounds on f_{PBH} as a function of M_{PBH} for different Dark Matter-nucleon cross-sections. We consider m_χ smaller than 1 MeV. The grey region represents the constraints reported in Ref. [3]. We took the figure from Ref. [6]

negligible. For $\sigma_\chi^{SI} = 10^{-28}\,\mathrm{cm}^{-2}$, attenuation effects modify the behavior of the bounds.

In conclusion, our scenario leads to signatures within reach of direct detection experiments. The bounds in Fig.4.2 apply to any model predicting the existence of Primordial Black Holes and Dark Matter coupling to nucleons. The caveat is that more suitable approaches to account for propagation effects may modify the constraints for higher cross-sections. However, it does not sway the possibility of constraining our scenario.

According to existing constraints, Primordial Black Holes in our range can account for a small fraction of Dark Matter. Therefore, χ emission should not change the Dark Matter budget of the Universe. Besides, the expected flux is not particularly large.

As a last remark, we point out that the signal is proportional to $f_{PBH} \cdot \sigma_\chi^{SI}$ for a low cross-section, making f_{PBH} and σ_χ^{SI} degenerate. Observation of evaporating Primordial Black Holes (see Refs [525–532] for detection examples) may remove the degeneracy.

4.2 Dark Matter-electron interaction

In this Section, we investigate Dark Matter-electrons interactions. We consider two classes of experiments to search for χ: (i) double phase dark matter direct detection experiments based on noble liquid technology [126–134, 136]. (ii) Neutrino experiments based on water Cherenkov [533–537]. In the following analysis, we employ XENON1T's and Super-Kamiokande's data to limit our scenario. For the two experiments, we investigate different Primordial Black

Holes mass ranges. XENON1T allows for $\mathrm{M_{PBH}} \in [1 \cdot 10^{15} - 1 \cdot 10^{18}]\,\mathrm{g}$ and Super-Kamiokande for $\mathrm{M_{PBH}} \in [5 \cdot 10^{14} - 3 \cdot 10^{15}]\,\mathrm{g}$. For definiteness, we reckon the following effective Lagrangian

$$\mathcal{L}_\chi = \frac{1}{\Lambda^2}\overline{\chi}\chi\,\overline{\ell}\ell\,. \tag{4.8}$$

where ℓ refers to the Standard Model Leptons and Λ is the energy scale. When the energies involved are smaller than the mediator mass, we can integrate the mediator out, leaving a four-fermion interaction.

χ hits the detector's atom and interacts with the electron through the effective interaction of Eq. (4.8). This interaction can lead to atom ionization freeing a non-relativistic electron. We describe the process as

$$\chi + A \to \chi + A^* + e^-, \tag{4.9}$$

where A denotes the atom, and A^* is the ionized atom. The energy conservation of this process leads to the following equality

$$E_\chi - |E_b^{n,\,l}| = E'_\chi + E_r \tag{4.10}$$

where $E_\chi = T_\chi + m_\chi$ and E'_χ are the initial and final energy of χ particle. $E_b^{n,\,l}$ is the electron binding energy of the atomic orbital (n, l) and E_r is the free electron kinetic energy.

The differential event rate of the process in Eq.(4.9) is

$$\frac{\mathrm{d}R_\chi}{\mathrm{d}E_r} = N_T\,\eta(E_r)\,F(E_r)\int \mathrm{d}T\,\frac{\mathrm{d}\phi_\chi}{\mathrm{d}T_\chi}\sum_{n,\,l}\frac{\mathrm{d}\sigma^{n,\,l}}{\mathrm{d}E_r}(E_r, m_\chi, T_\chi)\,, \tag{4.11}$$

where N_T is the detector exposure and η is the detector's efficiency. $\mathrm{d}\sigma^{n,l}/\mathrm{d}E_r$ denotes the differential cross-section for scattering of a χ particle on a bound electron with principal quantum number n, orbital quantum number l, and recoil energy E_r. We account for the distortion of the scattered electron wave function by the presence of the atom in $F(E_r)$. In the non-relativistic limit, we have

$$F(E_r) = \frac{2\pi\nu}{1 - e^{-2\pi\nu}}, \tag{4.12}$$

where $\nu = Z_{\rm eff}(\alpha m_e/\sqrt{2\,m_e\,E_r})$ and $Z_{\rm eff}$ is the effective charge felt by the scattered electron. Generally, $Z_{\rm eff} \gtrsim 1$ because the shielding of the escaping electron by the remaining electron is imperfect. Ref. [538] shows that $Z_{\rm eff} = 1$ is a good approximation for outer-shell electrons. Moreover, considering $Z_{\rm eff} > 1$ would enhance the event rate. Conservatively, we approximate $Z_{\rm eff} = 1$.

We express $\chi - e$ interaction strength in terms of the cross-section on a free electron at a fixed momentum transfer αm_e

$$\overline{\sigma}_{\chi e} = \frac{\mu_{\chi e}^2}{\pi\,\Lambda^4}\left(1 + \frac{\alpha^2\,m_e^2}{4\,m_\chi^2}\right) \tag{4.13}$$

where α is the fine-structure constant.

It is worth noting that the χ-e interaction would cause an attenuation effect of the χ flux due to the propagation in the atmosphere and the Earth [520–523]. However, Refs. [160, 161] show that the attenuation is negligible for $\overline{\sigma}_{\chi e} \lesssim 10^{-31}\,\mathrm{cm}^2$. To simplify our analysis, we limit our-self to smaller cross-sections.

4.2.1 XENON1T event rate

In this paragraph, we specialize our analysis for a detector based on Liquid Xenon. In particular, we employ the measurements from XENON1T [146] of the event rate for recoil energies E_r in the range $[1-30]$ keV to constrain the χ-e cross-section in Eq. (4.13). The number of the detector's Xe nuclei is $N_T = 4.59 \cdot 10^{27}\,\mathrm{ton}^{-1}$. We consider the efficiency in Ref. [146].

In the following, we consider the outgoing electron non-relativistic and show that the differential cross-section is[1]

$$\frac{\mathrm{d}\sigma^{n,l}}{\mathrm{d}E_r} = \frac{1}{8\pi\,\Lambda^4\,\tilde{p}^2\,m_e}\int_{\tilde{q}_-}^{\tilde{q}_+}\mathrm{d}\tilde{q}\,\tilde{q}\frac{1}{2\,\tilde{k}'^2}\left|f_{\mathrm{ion}}^{n,l}(\tilde{k}',\tilde{q})\right|^2\left[(p\cdot(p-q)+m_\chi^2)\,(k'\cdot(k'-q)+m_e^2)\right]\,. \quad (4.14)$$

where p is χ incoming four-momentum, k' is the four-momentum of the outgoing electron, and q is the momentum transfer. $f_{\mathrm{ion}}^{n,l}$ are the ionization functions defined in Appendix A. We perform the integration between the minimum and maximum momentum transfer allowed, which are

$$\tilde{q}_\pm = \sqrt{(T_\chi + m_\chi)^2 - m_\chi^2} \pm \sqrt{(T_\chi + m_\chi - \varepsilon_{n,l})^2 - m_\chi^2}\,, \quad (4.15)$$

where $\varepsilon_{n,l} = E_r + |E_b^{n,l}|$.

In Appendix A, we show that the differential cross-section is

$$\frac{\mathrm{d}\sigma^{n,l}}{\mathrm{d}E_r}(E_r, m_\chi, T_\chi) = \frac{\overline{\sigma}_{\chi e}\,m_e}{8\,\mu_{\chi e}^2\tilde{k}'^2\,\tilde{p}^2\,\left(1+\frac{\alpha^2\,m_e^2}{4\,m_\chi^2}\right)}\int_{\tilde{q}_-}^{\tilde{q}_+}\mathrm{d}\tilde{q}\,\tilde{q}\left|f_{ion}^{n,l}(\tilde{q},\tilde{k}')\right|^2\left(2m_\chi^2 + \frac{\tilde{q}^2-\varepsilon_{n,l}^2}{2}\right)\,, \quad (4.16)$$

According to the procedure shown in Ref. [539], we define the χ^2 variable as

$$\chi^2\left(\mathrm{M_{PBH}},\,m_\chi,\,\overline{\sigma}_{\chi e},\,f_{\mathrm{PBH}}\right) := \sum_i \frac{\left[\frac{\mathrm{d}R_{\mathrm{obs}}}{\mathrm{d}E_r} - \left(\frac{\mathrm{d}R_{\mathrm{BCK}}}{\mathrm{d}E_r} + \frac{\mathrm{d}R_\chi}{\mathrm{d}E_r}\right)\right]^2_{E_r=E_r^i}}{\sigma_i^2}\,, \quad (4.17)$$

where $\mathrm{d}R_{\mathrm{obs}}/\mathrm{d}E_r$ are the observed and the estimated background event rates taken from Ref. [146], and σ_i are the uncertainties on $\mathrm{d}R_{\mathrm{obs}}/\mathrm{d}E_r|_{E_r^i}$. We perform the sum over all the energy bins. We

[1]In this Section, given a four-momentum k we denote $\tilde{k} = |\boldsymbol{k}|$.

define the test statistic as

$$\lambda = \begin{cases} \chi^2\left(\mathrm{M_{PBH}},\, m_\chi,\, \overline{\sigma}_{\chi e},\, f_{\mathrm{PBH}}\right) - \chi^2\left(\mathrm{M_{PBH}},\, m_\chi,\, \hat{\overline{\sigma}}_{\chi e},\, f_{\mathrm{PBH}}\right), & \overline{\sigma}_{\chi e} > \hat{\overline{\sigma}}_{\chi e} \\ 0, \quad \overline{\sigma}_{\chi e} < \hat{\overline{\sigma}}_{\chi e}\,, & \end{cases} \tag{4.18}$$

where $\hat{\overline{\sigma}}_{\chi e}$ is the cross-section minimizing the χ^2. We then exclude at 90% confidence level the region of the parameter space in which $\lambda > 2.71$, following the prescription in Ref. [539].

4.2.2 Super-Kamiokande event rate

Super-Kamiokande is a Cherenkov detector where the photo-multipliers record the Cherenkov radiation produced by the charged particles in the water tank. The passage of χ in the water tank may produce Cherenkov radiations since it interacts with the electrons. Following the approach of Refs. [160, 540–542], we assume free electrons ($F(E_r) = 1$) at rest in the observer frame. We consider the data provided in Ref. [143] that reports $N_{\mathrm{SK}} = 4042$ events in the recoil energy range $[0.1 - 1.33]$ GeV with $N_T = 3.34 \times 10^{28}$ ton^{-1} and $\eta = 0.93$.

In this case, the differential cross-section is

$$\frac{\mathrm{d}\sigma}{\mathrm{d}E_r} = \frac{\overline{\sigma}_{\chi e}\,\Theta(E_{\max} - E_r)}{8\,\mu_{\chi e}^2\,\tilde{p}^2\left(1 + \frac{\alpha^2\, m_e^2}{4\, m_\chi^2}\right)}(2m_e + E_r)(2m_\chi^2 + m_e E_r) \tag{4.19}$$

where

$$E_{\max} = \frac{2\,m_e\,T_\chi\,(T_\chi + 2\,m_\chi)}{\left((m_e + m_\chi)^2 + 2\,m_e\,T_\chi\right)}\,. \tag{4.20}$$

According to the analysis of Ref. [160], we place limit our scenario requiring

$$\mathcal{E}_{\mathrm{SK}} \times \int_{0.1\,\mathrm{GeV}}^{1.33\,\mathrm{GeV}} \mathrm{d}E_r\, \frac{\mathrm{d}R_\chi}{\mathrm{d}E_r} < N_{\mathrm{SK}}\,, \tag{4.21}$$

where $\mathcal{E}_{\mathrm{SK}} = 161.9\,\mathrm{kton\ yr}$ is the Super-Kamiokande exposure [143].

4.2.3 Discussion

By considering the data from XENON1T [146] and Super-Kamiokande [143], we constrain the combined parameter space of the model. We show the projection of our result in a two-dimensional plane for clarity. The left (right) panel of Fig. 4.3 displays the constrain from XENON1T (Super-Kamiokande) in the plane $m_\chi - \overline{\sigma}_{\chi e}$ as colored regions for some Primordial Black Holes benchmarks. We draw the limits assuming the highest Primordial Black Holes abundance possible. In particular, we consider f_{PBH} upper limits from Extra-Galactic gamma-ray data [3] and isotropic X-ray observations [544]. For comparison, we also report existing bounds (dashed thin lines) that would apply if χ is the dominant Dark Matter component. If χ

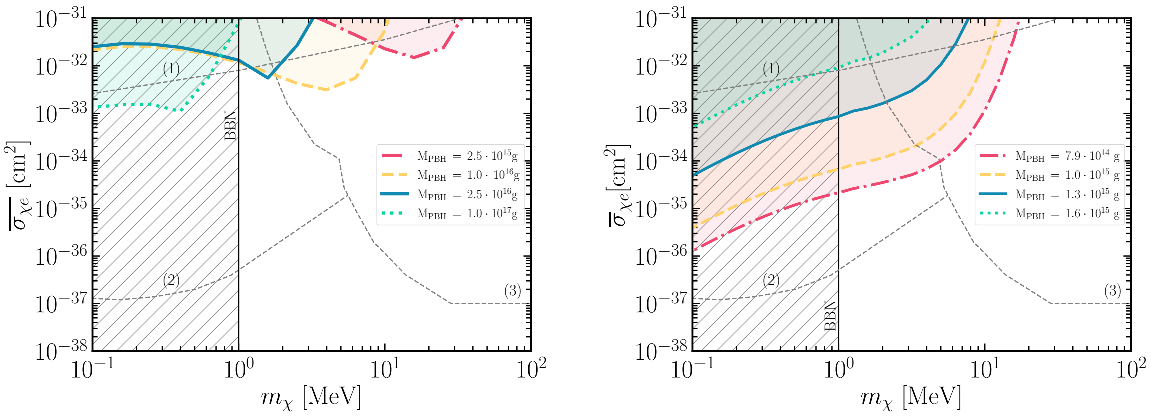

Figure 4.3: **Constraints.** We report our results in the plane m_χ-$\overline{\sigma}_{\chi e}$ for XENON1T (left panel) and Super-Kamiokande (right panel). The colored shaded regions illustrate our bounds for four $[\mathrm{M_{PBH}}, f_{\mathrm{PBH}}]$ benchmarks. In particular, we report $\mathrm{M_{PBH}}$ in the legend, and f_{PBH} is the maximum allowed according to current constraints. Big Bang Nucleosynthesis data exclude the hatched sector. The thin dashed lines illustrate (1) boosted dark matter from cosmic-ray up-scatterings [161]; (2) Solar reflection with XENON1T [543]; (3) combined constraints from dark matter direct detection experiments (see Ref. [161]).

is not the dominant Dark Matter component, the dashed constraints in Fig 4.3 do not apply. If $m_\chi \lesssim 1$ MeV, light species sufficiently strongly interacting are in tension with Big Bang Nucleosynthesis. Hence, we consider the hatched region completely excluded. However, it is worth noting that specific scenarios can overcome this constraints [545].

The different recoil energy ranges considered for the two experiments probe different Primordial Black Holes mass ranges. Interestingly, XENON1T can probe heavier Primordial Black Holes associated with smaller Hawking temperatures.

Collider constraints, not shown in the figure for aesthetic reasons, exclude the region $\overline{\sigma}_{\chi e} \gtrsim 10^{-44}$ cm^2. However, these bounds are strongly sensitive to the mediator mass. For instance, Ref. [546] focuses on the vector mediator. The constraints weaken for light mediators and are limited from above when the cross-section becomes sufficiently large for the χ particle to interact in the calorimeter.

Lastly, astrophysical environments may emit light Dark Matter coupling to electrons. For instance, the emission of light particles from Supernovae would lead to an additional cooling mechanism and modify the neutrino burst. It can noticeably affect SN1987A, as discussed in Ref. [547] with vector mediator. The result is that $\overline{\sigma}_{\chi e} \gtrsim 10^{-39}$ cm^2 does not lead to significant constraints because χ would be trapped inside the Supernova and yield no observable signal. These results do not apply directly to our scenario since we focus on a scalar mediator. However, the authors of Ref. [547] advise that the constraints do not apply to large cross-sections.

Ref.[548] investigate the same scenario. The constraints they obtain for Super-Kamiokande

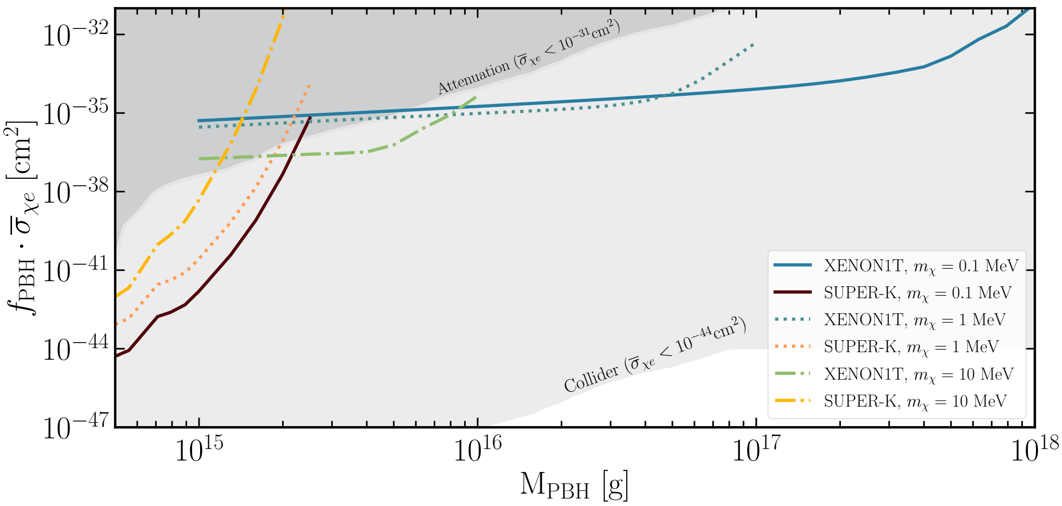

Figure 4.4: Constraints shown in the plane $(f_{\mathrm{PBH}} \cdot \overline{\sigma}_{\chi e}) - \mathrm{M}_{\mathrm{PBH}}$ for different masses m_χ. We show the constraints from Super-Kamiokande in warm tones, while cold tones refer to the constraints obtained using XENON1T. The dark grey band shows the region that cannot be probed in our analysis due to existing constraints on f_{PBH} and assuming $\overline{\sigma}_{\chi e} \lesssim 10^{-31}\,\mathrm{cm}^2$ to neglect attenuation effects. The light grey band is excluded by requiring $\overline{\sigma}_{\chi e} \lesssim 10^{-44}\,\mathrm{cm}^2$ according to collider constraints [546].

are two orders of magnitude stronger than ours because they simply assume a flat recoil energy distribution instead of a more concrete particle model for the χ-electron interaction. We find constraints that are three orders of magnitude weaker for XENON1T because we correctly account for the ionization of the Xenon atoms in the detector instead of assuming them free as in Ref. [548].

Our signal is proportional to $f_{\mathrm{PBH}} \cdot \overline{\sigma}_{\chi e}$ making the parameter effectively determining the constraints (m_χ, $\mathrm{M}_{\mathrm{PBH}}$, $f_{\mathrm{PBH}} \cdot \overline{\sigma}_{\chi e}$). Fig. 4.4 shows the results in the plane $(f_{\mathrm{PBH}} \cdot \overline{\sigma}_{\chi e}) - \mathrm{M}_{\mathrm{PBH}}$ for XENON1T (cool tones) and for Super-Kamiokande (warm tones) for fixed m_χ in different line styles.

In conclusion, this Section investigates the detection of a light Dark Matter candidate evaporated from Primordial Black Holes, assuming it interacts with electrons. We consider XENON1T, a Dark Matter direct detection experiment, and Super-Kamiokande, a neutrino detector. We use the non-observation of the predicted signal to limit the combined parameter space. We perform a binned likelihood analysis comparing the observed event rate with the one expected in our scenario for XENON1T. Here, we accurately treated the ionization process of Xe atoms due to χ-e scattering. For Super-Kamiokande, we consider a more conservative analysis based on the total number of events detected. XENON1T (Super-Kamiokande) can constrain the cross-section down to $10^{-32}\,\mathrm{cm}^2$ ($10^{-35}\,\mathrm{cm}^2$). Our limits complement cosmological and collider constraints and do not require the χ particles to be dark matter.

CHAPTER 5

Towards baryogenesis via absorption from Primordial Black Holes

In this Chapter, we undertake a phenomenological investigation of the scenario proposed in Refs. [549, 550], a baryogenesis mechanism that does not rely on Baryon number violation at the Lagrangian level. The authors suggest a novel approach involving the differential absorption of a new species, denoted with X and $\overline{X}$, with non-zero Baryon number onto Primordial Black Holes. The differential absorption arises due to CP-violating scattering processes.

However, this scenario presents two fundamental challenges. On one side, the intense absorption in Primordial Black Holes initially generates a Baryon asymmetry. Nonetheless, the asymmetry is completely absorbed if it continues indefinitely. Primordial Black Hole evaporation naturally interrupts the absorption. To address this issue, we systematically study the parameter space to identify the regions leading to the production of the observed Baryon asymmetry.

On the other hand, the realization of CP-violating scattering in practice is difficult. Considering a more realistic framework, we find the theoretical Baryon asymmetry smaller than the observed value. It suggests the need for further investigation and the consideration of additional factors to forecast the correct asymmetry.

5.1 The mechanism

X and $\overline{X}$ evolution depends on the interplay of several processes: (i) absorption in Primordial Black Holes, (ii) interaction with the relativistic plasma, (iii) decay processes $X \to b + \mathrm{SM}$, where b is a Standard Model (SM) particle with a Baryon number. We detail the processes in the next Sections.

5.1.1 Absorption rate

The absorption rate of X into Primordial Black Holes is [549]

$$\frac{\mathrm{d}N_X}{\mathrm{d}t} = \frac{4\pi \mathrm{M}_{\mathrm{PBH}} m_X n_X}{n_0 g \sigma_X T_U \mathrm{M}_{\mathrm{Pl}}^2}, \tag{5.1}$$

where $g \sim 100$ represents the plasma's relativistic degrees of freedom. $\sigma_X = f^4/m_X^2$ denotes the scattering cross-section between X and the Standard Model, where f is the interaction coupling and m_X represents the mass of the specie X. We indicate with n_0 and n_X the plasma and X number densities, respectively

We can derive an analogous expression $\overline{X}$, where the main difference resides in the expressions of σ_X and $\sigma_{\overline{X}}$ due to CP violation. We define the CP-violation efficiency parametrizing the difference in the scattering cross-sections as

$$\sigma_X - \sigma_{\overline{X}} \simeq \varepsilon \left(\frac{m_X}{T_U}\right) f^2 \sigma_X \,, \tag{5.2}$$

where $\varepsilon(T_U)$ depends on the processes contributing to the asymmetry. Refs. [549, 550] assume $\varepsilon\left(\frac{m_X}{T_U}\right) = 1$, although in Section 5.2, we consider a specific filed theory model and derive a different form for $\varepsilon\left(\frac{m_X}{T_U}\right)$. However, this theoretically motivated choice spoils the feasibility of the mechanism.

From Eq. (5.1), we derive the absorption rate in terms of the number density as

$$\left(\frac{\mathrm{d}n_X}{\mathrm{d}t}\right)_{\mathrm{abs}} = -\frac{4\pi m_X^3 \beta T_{\mathrm{in}}}{g f^4 T_U \mathrm{M}_{\mathrm{Pl}}^2} n_X \tag{5.3}$$

While the specie is relativistic, its interactions with the plasma and creation processes ($\overline{X} \rightleftharpoons$ SM) are in thermal equilibrium. Because of the crossing symmetry, we assume the coupling for the creation process to have coupling f. However, once X specie becomes non-relativistic, X freezes out, and the interaction rate rapidly decreases. The rate of interaction with the plasma is

$$\left(\frac{\mathrm{d}n_X}{\mathrm{d}t}\right)_{\mathrm{int}} = -\frac{f^4}{m_X^2}(n_X n_{\overline{X}} - n_{\mathrm{eq}}^2), \tag{5.4}$$

where n_{eq} is the number density at thermal equilibrium.

For simplicity, we assume X to decay into much lighter particles with decay width $\Gamma = h^2 m_X$ where h is the coupling of the process. Considering that the absorption becomes relevant when X is non-relativistic, we assume them at rest, and the decay rate is

$$\left(\frac{\mathrm{d}n_X}{\mathrm{d}t}\right)_{\mathrm{dec}} = -h^2 m_X n_X. \tag{5.5}$$

Boltzmann equations

We estimate the Baryon asymmetry generated in this scenario by solving the following set of Boltzmann equations

$$\frac{\mathrm{d}N}{\mathrm{d}z} = -\frac{\lambda}{z^2}(N^2 - \mathrm{Y}_{\mathrm{eq}}^2) - \alpha z^2 N - \mu z N, \tag{5.6}$$

$$\frac{\mathrm{d}A}{\mathrm{d}z} = \alpha z^2 \Big(\varepsilon(z) f^2 N - A\Big) - \mu z A, \tag{5.7}$$

$$\frac{\mathrm{d}\mathrm{Y}_{\mathrm{B}}^{\mathrm{th}}}{\mathrm{d}z} = \mu z A\,, \tag{5.8}$$

where $N \equiv (n_X + n_{\overline{X}})/2s$, $A \equiv (n_X - n_{\overline{X}})/s$, $z \equiv m_X/T$, and Y_{eq} is the equilibrium yield for the species X. The dimensionless parameters in Eq. (5.6), (5.7) are defined as

$$\lambda = \sqrt{\frac{\pi}{45}}\frac{f^4\sqrt{g_*}\mathrm{M}_{\mathrm{Pl}}}{m_X}\,, \tag{5.9}$$

$$\alpha = \frac{\pi^{7/2}}{\sqrt{5}\zeta(3)}\frac{\beta T_{\mathrm{in}}}{g f^4\sqrt{g_*}\mathrm{M}_{\mathrm{Pl}}}\,, \tag{5.10}$$

$$\mu = \sqrt{\frac{45}{4\pi^3}}\frac{h^2\mathrm{M}_{\mathrm{Pl}}}{\sqrt{g_*}m_X}\,. \tag{5.11}$$

5.1.2 Constraints

Five parameters fully describe this mechanism, with two characterizing Primordial Black Holes physics ($\mathrm{M}_{\mathrm{PBH}}$, β) and three the new specie (m_X, f, h).

While solving Eqs. (5.6), (5.7), (5.8), we take into account several constraints: (i) The value of β must be smaller than the existing limits set by previous studies (see Ref. [3]). (ii) The entropy generated by X decay must be negligible. (iii) X decay should happen before the Big Bang Nucleosynthesis. (iv) X should decay after Primordial black holes have evaporated. (v) The annihilation process $X\overline{X}$ $\to$SM induced by the coupling h is negligible compared with the annihilation induced by the coupling f. (vi) Primordial Black Holes should never dominate the energy budget of the Universe, expressed by the condition $\rho_{\mathrm{PBH}}/\rho_{\mathrm{rad}} \simeq \beta T_{\mathrm{in}}/T_{\mathrm{ev.}}$. (vii) The accretion rate should be negligible to the evaporation rate, quantified by the condition

$$R_{\mathrm{ae}} = \left(\frac{\mathrm{dM}_{\mathrm{PBH}}}{\mathrm{d}t}\right)_{\mathrm{acc}} \Big/ \left(\frac{\mathrm{dM}_{\mathrm{PBH}}}{\mathrm{d}t}\right)_{\mathrm{ev}} < 0.1\,, \tag{5.12}$$

where $\left(\frac{\mathrm{dM}_{\mathrm{PBH}}}{\mathrm{d}t}\right)_{\mathrm{acc}} = m_X\frac{\mathrm{d}N_X}{\mathrm{d}t}$. The last request guarantees that evaporation is not delayed or prohibited.

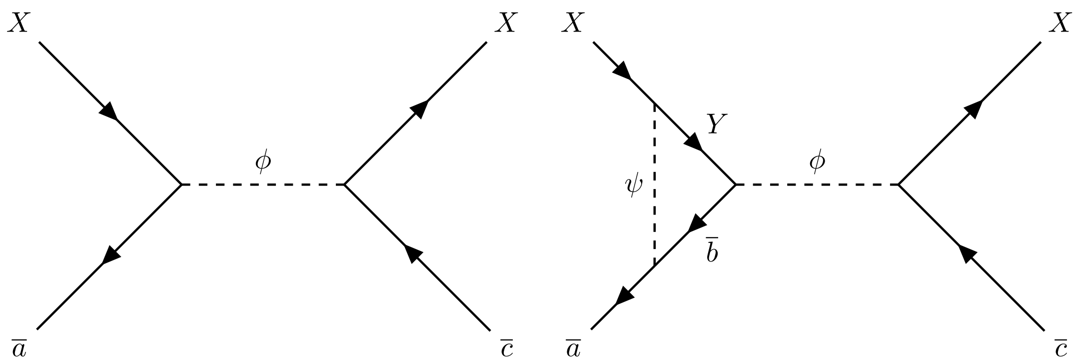

Figure 5.1: Feynman diagrams contributing to the scattering $X\bar{a} \to X\bar{c}$ to one-loop level.

5.2 CP violation realization

In this Section, we provide a detailed calculation of the CP violation efficiency $\varepsilon(z)$ within a realistic scenario. We consider all relevant diagrams contributing to the CP violation in a specific model. We note that Refs. [549, 550] consider it equal to 1.

To achieve CP violatin scatterings, we consider additional heavy fermion particles (X, Y, and b), as well as heavy scalar mediators (ϕ and ψ). We assume them to couple with Standard Model species a and c. The following Lagrangian describes the interactions among these particles

$$\mathcal{L}_{\text{int}} = -g_{\overline{a}X}\overline{\phi}\overline{a}X - g_{\overline{c}X}\overline{\phi}\overline{c}X - g_{\overline{b}Y}\overline{\phi}\overline{b}Y - g_{\overline{Y}X}\psi\overline{Y}X - g_{\overline{b}a}\psi\bar{b}a + \text{h.c.} \tag{5.13}$$

In our analysis, we consider all the coupling to be complex numbers. By assuming the particles charged under an additional (but non-necessarily gauged) $\mathrm{U}(1)$, we can justify the Lagrangian structure. For instance, if X and Y have charge $+1$, ϕ has charge -1, and ψ is neutral. It is worth noting that the same symmetry generates other Lagrangian terms that are not essential for this mechanism, such as $\mathcal{L}'_{\text{int}} = -g_{\overline{b}c}\psi\bar{b}c$. However, we will see that renormalization of the CP-violating efficiency can absorb it.

In this context, the cross-sections of $X\bar{a} \to X\bar{c}$ and $\bar{X}a \to \bar{X}c$ differ at the loop level due to the interference between the diagrams shown in Fig. 5.1. The coupling $g_{\overline{b}c}$ generates a third diagram with a triangle loop in the final state. This term would renormalize the CP violation. Under the assumption that $c = a$ CPT and Lorentz invariance impose that the cross-sections for $X\bar{a} \to X\bar{a}$ and $\bar{X}a \to \bar{X}a$ are necessarily equal. Thus, the contribution from these two diagrams would not add up [550], but rather it would cancel.

The interference between the two diagrams in Fig. 5.1 leads to

$$\delta\sigma = -4\int \frac{\mathrm{d}^3\mathbf{p}'}{(2\pi)^3 2E_{p'}} \frac{\mathrm{d}^3\mathbf{q}'}{(2\pi)^3 2E_{q'}} \frac{1}{4E_pE_q}(2\pi)^4\delta^4(p'+q'-p-q)\mathrm{Im}\left(g^*_{\overline{a}X}g_{\overline{Y}X}g_{\overline{b}Y}g^*_{\overline{b}a}\right)\frac{|g_{\overline{c}X}|^2}{(s-m_\phi^2)^2}\mathrm{Re}\left[\ell\right], \tag{5.14}$$

where s is the first Mandelstam invariant, p, q, p', and q' are respectively the four-momenta of the incoming X and $\bar{a}$ particles and of the outgoing X and $\bar{c}$ particles. For each of these four momenta, we denote in bold the spatial 3-momentum and by E_p, E_q, $E_{p'}$, and $E_{q'}$ their energies in the laboratory frame. Finally, ℓ is the loop integral defined by

$$\ell = \int \frac{\mathrm{d}^4 k}{2(2\pi)^4} \mathrm{Tr}\left[(\not{p}' + m_X)(\not{q}' - m_c)\right] \frac{\mathrm{Tr}\left[(\not{k} - m_b)(\not{p} + \not{q} + \not{k} + m_Y)(\not{p} + m_X)(\not{q} - m_a)\right]}{(k^2 - m_b^2)\left[(p+q+k)^2 - m_Y^2\right]\left[(q+k)^2 - m_\psi^2\right]}, \tag{5.15}$$

where by m_i is the mass of the i-th particle. We can rearrange

$$\mathrm{Tr}\left[(\not{p}' + m_X)(\not{q}' + m_c)\right] = 4\left(m_a m_c + p \cdot q + \frac{m_a^2 - m_c^2}{2}\right), \tag{5.16}$$

so it also does not depend on the final-state properties. In doing so, ℓ does not depend on the final four-momenta p' and q', so it can be taken outside of the integral. Therefore, we can express the cross-section to the lowest order in the couplings as

$$\frac{\delta\sigma}{\sigma_{X\bar{a}\to X\bar{c}}} = -4 \frac{\mathrm{Im}\left(g^*_{\bar{a}X} g_{\overline{Y}X} g_{\bar{b}Y} g^*_{\bar{b}a}\right)}{|g_{\bar{a}X}|^2} \frac{2\mathrm{Re}[\ell]}{\mathrm{Tr}\left[(\not{p}' + m_X)(\not{q}' - m_c)\right] \mathrm{Tr}\left[(\not{p} + m_X)(\not{q} - m_a)\right]}. \tag{5.17}$$

We can determine the real part of the loop using the Cutkosky rules, assuming $m_\psi > m_X, m_a$. Furthermore, we assume m_a to be negligible. This assumption is justified since the center-of-mass energies of the collisions happen at temperatures much higher than the quark masses. The final result is

$$\begin{aligned} \frac{\delta\sigma}{\sigma_{X\bar{a}\to X\bar{c}}} = \frac{\mathrm{Im}\left(g^*_{\bar{a}X} g_{\overline{Y}X} g_{\bar{b}Y} g^*_{\bar{b}a}\right)}{|g_{\bar{a}X}|^2} &(s - (m_b - m_Y) m_X)(s - (m_b + m_Y)^2) \cdot \\ &\cdot \frac{\sqrt{[s - (m_b + m_Y)^2]\,[s - (m_b - m_Y)^2]}}{4\pi s^2 m_\psi^2}, \end{aligned} \tag{5.18}$$

where s is the Mandelstam invariant of the collision.

For $T_U \ll m_X$ the absorption of particles onto Primordial Black Holes becomes relevant, $s = m_X^2 + 2\frac{m_X T}{\sqrt{1-v^2}}(1 - v\cos\theta)$, where v is the velocity of X and θ is the angle between the directions of X and $\bar{a}$. We expect $s \simeq m_X^2 + 2 m_X T$ under the assumption that $v \ll 1$. Additionally, we consider $m_Y + m_b \simeq m_X$. If $m_b + m_Y < m_X$, $X\bar{a} \to Y\bar{b}$ would maintain chemical equilibrium for X even after it becomes non-relativistic. X would rapidly disappear from the plasma because of the inhibition of inverse annihilation. Finally, we choose $|m_b - m_Y| \ll T$ and $m_\psi \simeq m_X$. These choices maximize the asymmetry in the cross-section, which becomes the order

$$\frac{\delta\sigma}{\sigma_{X\bar{a}\to X\bar{c}}} \simeq \frac{\mathrm{Im}\left(g^*_{\bar{a}X} g_{\overline{Y}X} g_{\bar{b}Y} g^*_{\bar{b}a}\right)}{|g_{\bar{a}X}|^2} \frac{1}{\sqrt{2}\pi} \left(\frac{T_U}{m_X}\right)^{3/2}. \tag{5.19}$$

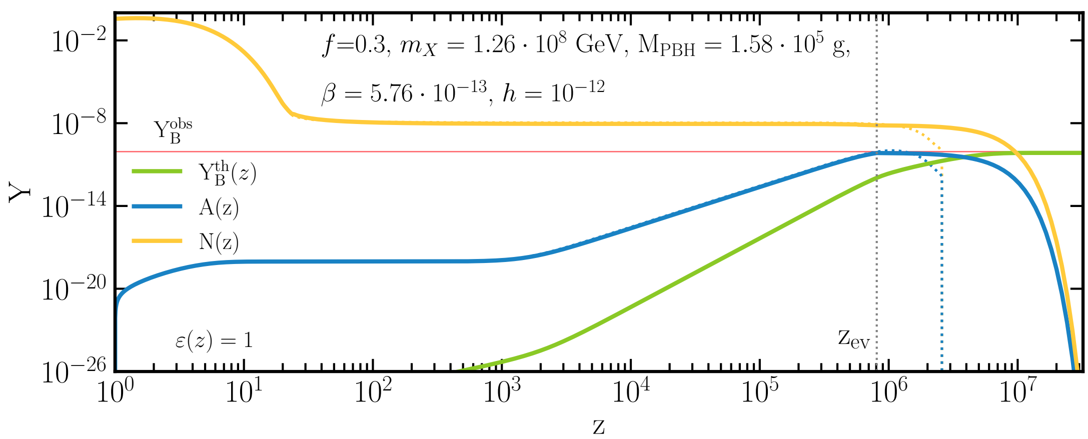

Figure 5.2: **Phenomenological scenario benchmark.** Evolution of X concentration (yellow), X asymmetry (blue), and Baryon asymmetry (green) as a function of x for a benchmark choice of parameters. z_{ev} is the moment at which Primordial black holes evaporate. The dotted curves represent the solution if Primordial black hole evaporation is not taken into account. We assume $\varepsilon(z) = 1$ as in the phenomenological scenario.

The temperature dependence of the CP violation is

$$\varepsilon(z) = \frac{1}{\sqrt{2\pi} z^{3/2}}. \tag{5.20}$$

Compared with $\varepsilon = 1$ of Refs. [549, 550], we find that CP-violations are depleted at a lower temperature. This effect stems from the Cutkosky rules. We link it to the violation at loop level with the amplitude for scattering onto the intermediate state $X\bar{a} \to Y\bar{b}$: the latter vanishes as $T_U \to 0$. In the next Section, we will show the results obtaineda using both choices for $\varepsilon(z)$.

Discussion

In this Section, we summarize the main results of the Chapter. In Ref. [549, 550], the authors present a mechanism that does not require the Baryonic number violation at the Lagrangian level. The Baryon asymmetry originates from the interplay of X freeze-out, different absorption of X and $\overline{X}$ into Primordial Black Holes due to CP violations, and X decays. The last process prevents the overproduction of non-relativistic X that otherwise could dominate over radiation.

To better understand the production of the Baryon asymmetry in both scenario, we exhibiting a benchmark solution to Eq. (5.6), (5.7), (5.8) for a specific parameter choice. Fig. 5.2 shows the solution for the phenomenological scenario, $\varepsilon(z) = 1$. The average yield for X and $\overline{X}$ (yellow curve) undergoes freeze-out at z close to 10, where it reaches a constant value. Before the

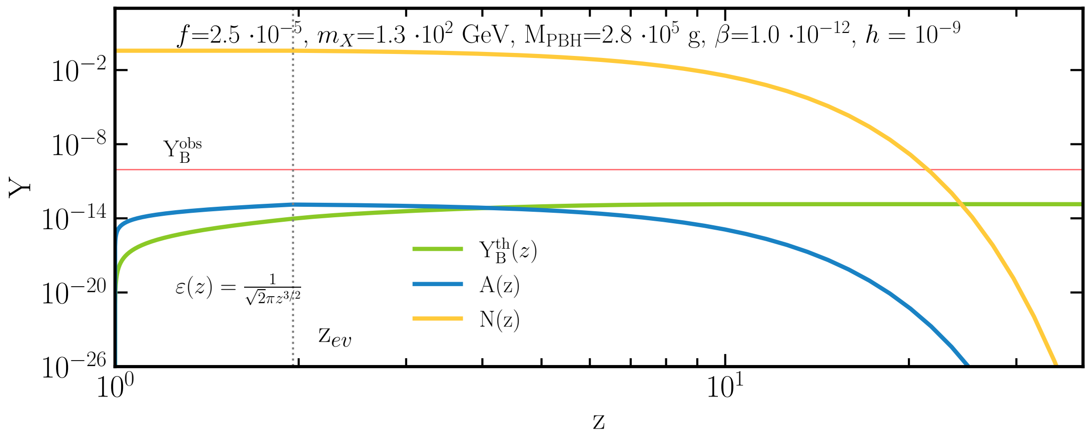

Figure 5.3: **Explicit model realization.** Evolution of X concentration (yellow), X asymmetry (blue), and Baryon asymmetry (green) as a function of z for a benchmark choice of parameters. x_e is the moment at which Primordial black holes evaporate. We assume $\varepsilon(z) = \frac{1}{\sqrt{2\pi}z^{3/2}}$ as in the explicit model realization.

freeze-out, the rapid decrease in N leads the asymmetry to a plateau. It is the first residual component of the asymmetry. After the freeze-out, N is approximately constant while undergoing a slow absorption by Primordial Black Holes, generating continuously the asymmetry (steadily increasing blue curve). This is the second component of asymmetry. The continuous production of the asymmetry dominates only later, for $z \sim 10^3$. Here, we can parametrize $A(z) \propto z^3$. For greater z, absorption becomes stronger to the point that it would eventually deplete all the species X and the asymmetry produced (dashed lines). The complete evaporation of Primordial Black Holes stops the absorption. Soon after the evaporation, N and A remain constants. The dominant process now is X decay which will transfer the asymmetry into the Baryon sector (green curve). At this point, X and $\overline{X}$ number densities vanish without significantly heating the plasma.

We highlight that in Ref [549], the authors need a small coupling to realize a working mechanism. Here, we obtain that small couplings lead to considerable absorption to the point of suppressing the asymmetry before Primordial Black Holes evaporation. Indeed, the benchmark in Fig. 5.3 requires $f \sim 0.1$.

As shown in Section 5.2, the CP violation efficiency decrease with z. It causes the asymmetry to grow much slower than in the phenomenological scenario. Fig. 5.3 illustrates a benchmark for the theoretically motivated scenario. In particular, we show the parameters maximizing the final asymmetry. For $z < z_{\rm ev}$, the asymmetry increases as $A(z) \propto z^{3/2}$, while for the phenomenological case, it grows as $A(z) \propto z^3$. It causes the asymmetry to be significantly smaller than the one obtained in the phenomenological scenario. The greater asymmetry achievable with the constraints shown in Section 5.1 is $\simeq 10^{-13}$, that is orders of magnitude smaller than the experimental value (Eq.(1.70)). Nonetheless, we prove that this model can produce a non-vanishing Baryon asymmetry.

We stress that the additional requirement that Primordial Black Holes evaporate is necessary to halt the absorption before it completely consumes X. This modification allows the mechanism proposed in Refs. [549, 550] to work at the phenomenological level. Moreover, the scenario requires that the CP violation efficiency is constant. However, the minimal model presented in Section 5.2 leads to a CP violation efficiency progressively decreasing in time. The theoretically motivated expression for the CO violation efficiency leads to asymmetry orders of magnitude smaller than the experimental value.

CHAPTER 6

Limits on light Primordial Black Holes from High-scale Leptogenesis

In this Chapter, we explore the influence of Primordial Black Holes on High-scale Leptogenesis (outlined in Section 1.4.3). We identify three competing effects in this scenario: (i) Primordial Black Hole evaporation acts as an additional source of right-handed neutrino source if $M_i \leq \mathcal{T}_{\rm PBH}$, contributing to Eq. (1.128). (ii) The significant production of photons via Primordial Black Hole evaporation leads to an entropy injection, depleting the final asymmetry. (iii) Primordial Black Holes can eventually dominate the Universe for a brief period (as discussed in Section 2.3), altering the expression of the Hubble parameter in Eqs. (1.127) and (1.128).

Refs.[237, 551, 552] investigate the interplay of Primordial Black Holes and different Leptogenesis mechanisms. In contrast with Ref. [237], we focus on Primordial Black Holes in the range $\rm M_{PBH} \in [10^6 - 10^9]\,GeV$, so that they evaporate between the sphaleron transitions freeze out and the Big Bang Nucleosynthesis. Furthermore, Primordial Black Holes in this mass range emit right-handed neutrinos in $M_1 \in [10^{10} - 10^{16}]\,\rm g$ only when sphaleron transitions are negligible. Consequently, the additional source of right-handed neutrinos can not alter the final Baryon yield. Thus, the key effect in our scenario is the entropy injection, which depletes the Baryon asymmetry. If the entropy injection is sufficiently large, it can diminish the asymmetry below the observed value, thereby ruling out regions within the mixed parameter space.

To investigate this, we undertake a systematic study of the Leptogenesis parameter space in search of the absolute maximum Baryon asymmetry achievable. Additionally, we quantify the amount of entropy injection in the Primordial Black Hole parameter space. Consequently, we constrain the combined parameter space and project them in the plane $\beta' - \rm M_{PBH}$ as a function of the active neutrino mass.

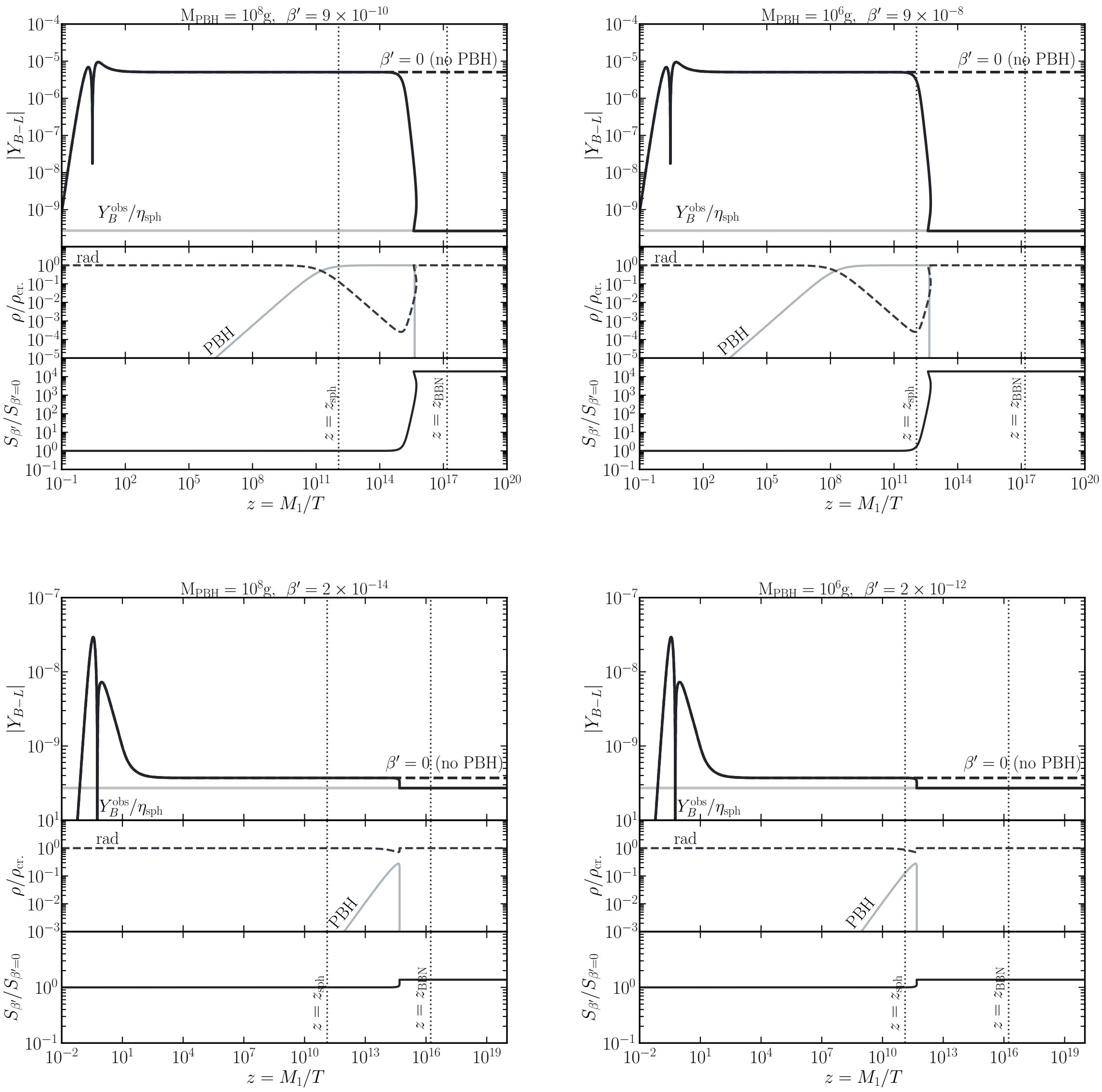

Figure 6.1: The plot shows $Y_{\mathrm{B-L}}$ as a function of $z = M_1/T$ (top plots) with (continuous lines) and without (dashed lines) the presence of Primordial Black Hole. We specify the Primordial Black Holes parameters in the plots' title. In each cases, we chose β' to obtain the observed Baryon asymmetry (solid grey horizontal line) after the complete evaporation of Primordial Black Holes. We fix the neutrino parameters according to the benchmark case 1 of Fig. 1.8 for the top panel and to the benchmark case 4 for the lower panel. The middle and lower plots illustrate the evolution of energy densities divided by the critical energy density and the entropy ratio $\mathcal{S}_{\beta'=0}/\mathcal{S}_{\beta'}$ respectively. We took the Figure from Ref. [9].

6.1 Results

We can fully describe our model with six free parameters: four describing High-scale Leptogenesis x, y, m_h, M_1 and two describing Primordial Black Hole physics $\mathrm{M_{PBH}}$, β'.

By solving Eqs.,(2.56), (2.57), and (2.59), we derive the entropy injection from Primordial Black Holes. In Fig.,6.1, we present the impact of Primordial Black Holes on the evolution of the $\mathrm{B-L}$ asymmetry (top plots), radiation, and Primordial Black Hole energy density (middle plots), and entropy injection (lower plots) as a function of $z \equiv M_1/T_U$ for benchmark "1" (upper panel) and "4" (lower panel) from Fig.,1.8. The left panel corresponds to $\mathrm{M_{PBH}} = 10^6\,\mathrm{g}$, while the right panel corresponds to $\mathrm{M_{PBH}} = 10^8\,\mathrm{g}$, and in both cases, we choose the value of β' such that the final asymmetry matches the observed value.

In the case of benchmark "1", Primordial Black Hole dominate the Universe until they evaporate, resulting in a significant entropy injection. Whereas in the case of benchmark "4", Primordial Black Holes never dominate. However, their evaporation still contributes to the dilution of the final asymmetry. In both cases, Primordial Black Holes in the mass range examined evaporate after the sphaleron transitions freeze out (see the vertical dotted lines) and before BBN ($T_U \simeq 1\,\mathrm{MeV}$). As a result, Primordial Black Holes affect the cosmological evolution after Baryon asymmetry has already been settled. If β' exceeds the values depicted in Figs. 6.1, the final asymmetry would be diluted to the extent that $\overline{\mathrm{Y}}_\mathrm{B} < \mathrm{Y}_\mathrm{B}^{\mathrm{obs.}}$.

In this scenario, sphaleron processes go out of equilibrium in a period dominated by Primordial Black Holes, altering the freeze-out temperature (defined in Eq. (1.89)). The presence of Primordial Black Holes results in a higher freeze-out temperature. However, when considering the maximum allowed value of β', we demonstrate that the freeze-out temperature is still below the temperature at which the electroweak phase transition occurs.

In Fig. 6.2, we show $\ln(\Gamma_{\mathrm{sph.}}/T_U^4)$ as a function of the temperature. The red line corresponds to the standard scenario, whereas the green and blue lines represent scenarios assuming the existence of Primordial Black Holes with masses $10^6\,\mathrm{g}$ and $10^9\,\mathrm{g}$, respectively. Both scenarios, assume the maximum abundance allowed according to existing constraints.

We present the main result of our analysis in Fig. 6.3, where we illustrate the mutual exclusion limit projected in the Primordial Black Holes parameter space. To determine these bounds, we fix the Leptogenesis parameters for each m_h so that they maximize the Baryon asymmetry, allowing us to obtain an upper bound on the Primordial Black Hole parameter space. These values correspond to the black line in Fig. 1.8, whereas the four numbered dashed lines correspond with the four dots in the same figure. The maximum allowed asymmetry is a monotonically decreasing function of m_h. As a result, the most conservative constraints correspond to $m_h = \sqrt{\Delta m^2_{\mathrm{atm}}}$ (darkest red line). Conversely, the most stringent constraint corresponds to the highest m_h for which we achieve the Baryon asymmetry. Our constraints are competitive with the limit on the energy density of gravitation waves [431](hatched area in the plot). We

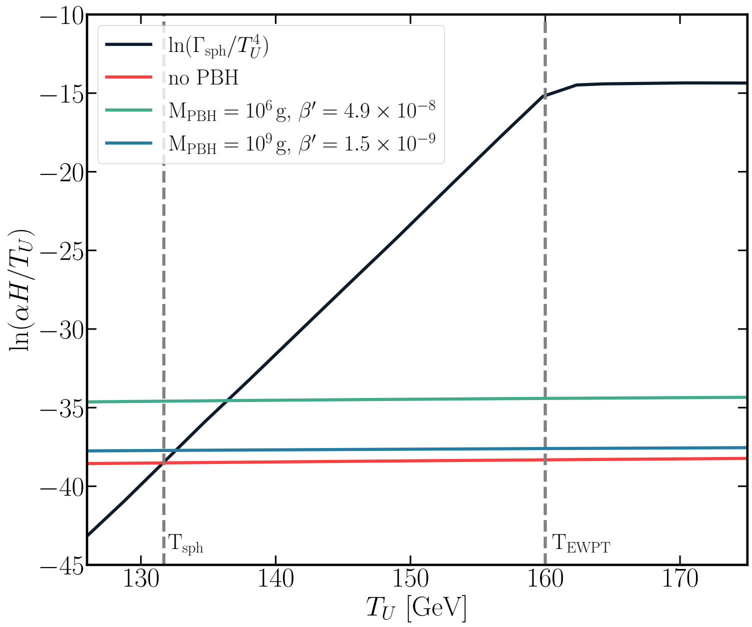

Figure 6.2: The figure illustrates the sphaleron process rate (black line) as a function of the Universe's temperature. The red line shows the behavior of $\ln(\tilde{\alpha}H/T)$ in standard cosmology, whereas the blue and green lines correspond to two scenarios involving Primordial Black Holes. Primordial Black Hole. The crossing point between the colored lines (red, blue, or green) and the black line indicates the freeze-out temperature. We took the Figure from Ref. [9].

also include a shaded grey region to indicate Primordial Black Holes that completely evaporate during Big Bang Nucleosynthesis. Overall, Fig. 6.3 provides a comprehensive overview the regions excluded by our analysis.

Discussion

We investigate the impact of non-standard cosmology determined by the existence of Primordial Black Holes on the production of the Baryon asymmetry via High-scale Leptogenesis. We focus on Primordial Black Holes evaporating between the sphaleron transition and the Big Bang Nucleosynthesis. The crucial effect in this scenario is the entropy injection associated with the complete evaporation. In the first step of our analysis, we demonstrate the existence of a finite maximum Baryon asymmetry achievable in High-scale Leptogenesis, denoted with $\mathrm{Y_B^{max}}$. We highlight that Primordial Black Holes may inject sufficient entropy into the Universe to dilute $\mathrm{Y_B^{max}}$ below the observed asymmetry, thus ruling out the Leptogenesis as the baryogenesis mechanism. Consequently, we delineate regions of the mixed parameter space where Primordial Black Holes and High-scale Leptogenesis are mutually incompatible. We obtain a relation between the heaviest active neutrino and the conservative bounds in the Primordial

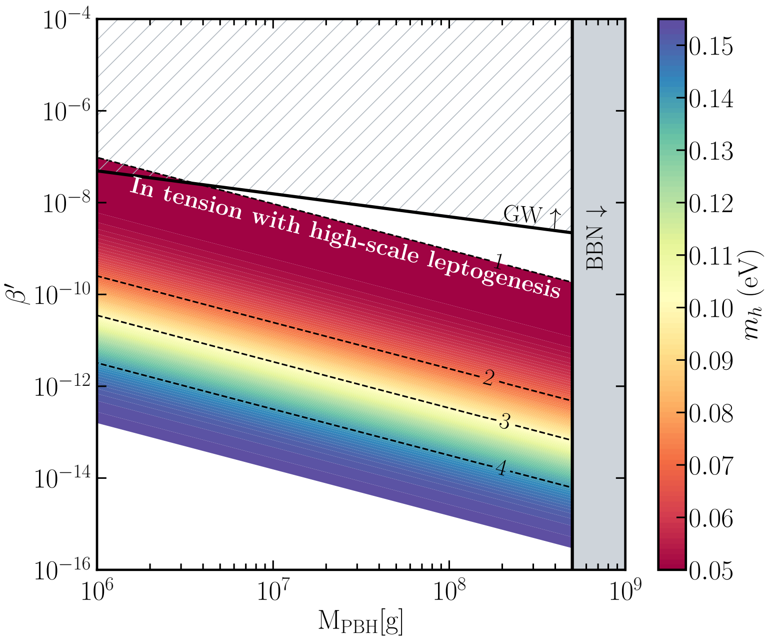

Figure 6.3: **Mutual exclusion limits between Primordial Black Holes and the minimal High-scale Leptogenesis.** We project these limits in the plane M_{PBH}-$\beta\prime$. We illustrate in different colors the upper limit obtained considering different m_h while we fix the other neutrino parameters to maximize the Baryon asymmetry. The dashed lines correspond to the benchmark cases highlighted in Fig. 1.8. The hatched region corresponds to the Gravitational Waves energy density constraints from Big Bang Nucleosynthesis observations [431]. The shaded region corresponds to Primordial Black Holes evaporating completely during Big Bang Nucleosynthesis. We took the Figure from Ref. [9].

Black Hole parameter space, which are more stringent than existing constraints.

Conclusions

Conclusions and outlook

In conclusion, the unending search for a profound understanding of particle physics and cosmology while trying to piece together the pieces of the complex enigmas permeating our Universe leads our journey. To truly untangle the cryptic nature of what surrounds us, we must continue to refine our understanding of the fundamental aspects of the sophisticated tapestry composed by particle physics and cosmology. In this grand adventure, Primordial Black Holes stand out as an appealing needle to sew together micro and macro worlds, allowing us to advance in an ever-expanding frontier of cosmic exploration.

This thesis explores the convoluted relationship between physics Beyond the Standard Model and the captivating realm of Primordial Black Holes. It delves into three crucial areas: neutrino physics, Dark Matter, and the generation of the Baryon asymmetry. The guiding light of this research line is to uncover new insights and connections on the fundamental patterns governing the Universe.

In Part I of this thesis, we begin our dexterous journey, offering a comprehensive overview of the current panorama of both physics Beyond the Standard Model and Primordial Black Holes. We begin with a description of the Standard Model and the compelling reasons driving the need for its extension. Then, we delve into the implication of the neutrino oscillations observation, discussing the neutrinos' nature and seesaw mechanisms. Moreover, we explore Coherent Elastic Neutrino-Nucleus Scattering, pivotal for the Dark Matter discovery limitations in direct detection observatories.

Our journey continues with a comprehensive immersion in the mystery of Dark Matter. We explore the astonishing concept of the WIMP miracle and the array of detection techniques while acknowledging their intrinsic drawbacks.

Lastly, we delve into the captivating subject of the Baryon asymmetry generation. Here, we focus on the fundamental prerequisites for viable baryogenesis mechanisms and underline the significance of the sphaleron processes in Leptogenesis mechanisms. To firmly establish these concepts, we provide noteworthy examples of baryogenesis scenarios.

Then, we present a dedicated insight into Primordial Black Holes physics, beginning with a brief examination of the formation mechanisms. We then delve into the intricate dynamics governing the mass evolution of Primordial Black Holes, elucidating processes such as evaporation and accretion.

Our wandering through Primordial Black Holes extends further as we analyze the impact of a Primordial Black Hole population on cosmological evolution.

Lastly, we conclude with a comprehensive summary of the constraints placed on the abundance of Primordial Black Holes, enclosing the current state of the art in this fascinating field of study.

In Part II of this thesis, we delve deep into the dynamic coaction between physics Beyond the Standard Model and Primordial Black Holes. In the context of the emission of neutrinos from Primordial Black Hole evaporation, we explore the potential avenues for detective these neutrinos via Coherent Elastic Neutrino-Nucleus Scattering, exploiting the sophisticated technologies provided by existing or foreseen Dark Matter direct detection facilities. Assuming these facilities will not measure an excess above the standard background, we derive forecast constraints on the fraction of Dark Matter composed of Primordial Black Holes. Our findings provide competitive bounds, rivaling those from Super-Kamiokande, although smaller than those from γ-rays observations.

Furthermore, we investigate the potential effect of these findings on the Neutrino Floor. As a final exciting note, we underline the possibility of utilizing direct detection facilities as indirect tools, offering new avenues for scientific endeavor.

We then turn our attention to the fascinating phenomenon involving the emission of sub-GeV Dark Matter particles, denoted as χ, from Primordial Black Holes. This process results in the radiation of Dark Matter particles endowed with substantial kinetic energies, allowing their direct detection in existing facilities. In this context, we inspect two distinct schemes pertaining to different interaction channels.

Our analysis shows the exciting possibility of testing Primordial Black Holes in the ranges $[5 \times 10^{14} - 10^{16}]\,\mathrm{g}$ for χ-nucleon interaction and $[5 \times 10^{14} - 10^{18}]\,\mathrm{g}$ for χ-electron one. We operate under the assumption that both Primordial Black Holes and the light species partially contribute to the overall Dark Matter abundance. The existing constraints on Primordial Black Hole abundance prevent the alteration of Galactic and Extra-Galactic Dark Matter distribution because of the additional emission of χ.

In the context of χ-nucleons interaction, we consider a ballistic approach to account for the propagation effect as these particles travel through Earth and the atmosphere. It is worth noting that variation in this modelization could yield slightly different results.

Intriguingly, assuming χ-nucleus interactions and using the data provided by the XENON1T collaboration, our analysis shows that cross-section in the range $[10^{-35} - 10^{-31}]\,\mathrm{cm}^2$, allowed by present constraints, are inconsistent with the existence of a small population of Primordial Black Holes.

When exploring χ-electron interactions, we assume an effective coupling mediated by a heavy scalar. Our investigation employs the detection capabilities of both XENON1T and the neutrino detector Super-Kamiokande. We limit the combined parameter space because of the non-observation of the expected signal in such observatories. For XENON1T, we account for the ionization process of Xenon atoms and employ a meticulous binned likelihood analysis. This rigorous approach leads to stringent bounds down to $10^{-32}\,\mathrm{cm}^2$ for $m_\chi = 1\,\mathrm{MeV}$.

For Super-Kamiokande, we consider a straightforward approach based on the total number of events detected. Here, we obtain an upper limit on the cross-section down to $10^{-35}\,\mathrm{cm}^2$ for $m_\chi = 1\,\mathrm{MeV}$. It is worth mentioning that our bounds complement those arising from cosmological and collider experiments.

The stringent bounds derived in this context using XENON1T and Super-Kamiokande data challenge the possibility of having a small population of Primordial Black Holes at present, setting the stage for deeper studies. Furthermore, we are currently reproducing the same analysis using the data from DarkSide-50 with a more complex analysis.

Our trajectory now shifts to a unique baryogenesis mechanism that hinges on the differential absorption of a heavy species X and $\overline{X}$, both possessing Baryon numbers, by Primordial Black Holes. An appealing feature of this scenario is that it does not need Baryon number violation at the Lagrangian level, standing out from conventional baryogenesis processes.

The scenario evolves via the interplay of several factors: X freeze out, the CP-violating scatterings of X into the plasma that lead to an asymmetric absorption into Primordial Black Holes, the decay of X that transfers the asymmetry to the Baryonic sector and prevents a period dominated by the X.

Moreover, we establish that the viability of the mechanisms relies on the complete evaporation of Primordial Black Holes. This requirement prevents the total absorption of X particles.

Under the assumption that the CP-violation is independent of the Universe temperature (phenomenological scenario), we reproduce the observed Baryon asymmetry. However, while searching for a realistic realization of CP-violation scatterings, we discovered that the efficiency of these interactions diminishes with the Universe temperature. Unfortunately, under this realistic assumption, we find that the scenario is not viable.

This baryogenesis mechanism requires additional investigations with the aim of identifying interactions that can achieve the required CP-violation or proving a no-go theorem demonstrating the impossibility of attaining such an asymmetry.

In a similar fashion, we explore the impact of Primordial Black Holes on the cosmological evolution and the Baryon asymmetry production via high-scale Leptogenesis. Our focus centers on the catastrophic moment when Primordial Black Holes completely evaporate, associated with a sudden injection of entropy and reheating of the Universe.

The critical insight of this study is the following: if the complete evaporation occurs after the sphaleron freeze-out, this scenario only dilutes the pre-existing Baryon asymmetry. Our analysis of the high-scale Leptogenesis parameter space reveals a finite, absolute maximum achievable.

Crucially, we underline that when the entropy injection from Primordial Black Holes is sufficiently substantial, it has the effect of depleting the Baryon asymmetry below the observed one. This observation points out an inherent incompatibility between Primordial Black Holes and Leptogenesis, highlighting fundamental limitations to their coexistence.

Consequently, we derive mutual exclusion limits in the mixed parameter space, delineating a relationship between the heaviest active neutrino mass m_h and the conservative bounds projected in the Primordial Black Hole parameter space. Notably, our limits prevail over the stringency of the existing ones, offering a new perspective to study the intricate dynamics of the very early Universe. Accordingly, we will perform similar studies considering different baryogenesis mechanisms with the aim of obtaining a deeper understanding of Primordial Black Hole effects in the very early Universe and hopefully model-independent constraints.

In summary, this manuscript investigates the intricate interplay between Primordial Black Holes and Physics Beyond the Standard Model in the context of neutrinos, Dark Matter, and Baryogenesis. Throughout this thesis, we identify promising research strategies that may captivate the scientific interest in the near future.

In conclusion, while the current paradigms of particle physics, encapsulated by the Standard Model, and cosmology, represented by the ΛCDM model, have demonstrated remarkable robustness and alignment with several observations, tenacious tensions hint at the presence of new physics and suggest we enlarge our horizons. Upcoming experiments offer an appealing opportunity to test and investigate extensions of the standard frameworks. Primordial Black Holes, whether they exist or not, are exceptional probes for particle physics and the fundamental epochs of the Universe.

The implication of Primordial Black Holes on critical subjects, such as Dark Matter, neutrino physics, baryogenesis, and inflation, continue to inflame the frontiers of scientific inquiries. Despite the plethora of investigations, Primordial Black Holes physics still presents several open questions. For instance, the formation mechanism remains a subject of ongoing investigation, with numerous proposed scenarios, yet without a definitive understanding.

Other challenges encompass the properties of the mass distribution, along with an accurate estimation of the fraction of Dark Matter that might consist of Primordial Black Holes. A deeper understanding of the interplay between Primordial Black Holes and these cosmic aspects is of preeminent importance.

A compelling new avenue to investigate Primordial Black Holes has emerged with the recent measurements provided by the collaboration of Pulsar Timing Arrays, such as NANOGrav [553], Parkes Pulsar Timing Arrays [554], European Pulsar Timing Arrays [555], and the China Pulsar Timing Arrays [556]. These observations yield fresh evidence supporting the existence of a stochastic gravitational wave background,. Although this effect may predominantly have an astrophysical origin [557, 558], several papers explore the possibility of a cosmological origin for a part of it. Among these interpretations, we find scalar-induced gravitational waves generated by an enhanced spectrum of short-wavelength scalar perturbation produced during inflation, which also leads to the formation of Primordial Black Holes [559–566].

Another possible avenue to advance our understanding of Primordial Black Holes consists of a messenger approach considering observation at different redshifts, several formation mechanisms, and complex mass distribution. In this context, an intriguing research area involves the study of theories Beyond the Standard Model, as Primordial Black Hole evaporation is sensitive to the number of emitted degrees of freedom. Models featuring multiple additional degrees of freedom, such as supersymmetry and large extra dimensions, are the most promising candidates for such studies.

As a final remark, we underscore the absence of a dedicated experiment aimed solely at studying Primordial Black Holes, a notable gap in the landscape of available or foreseen observatories. Instead, our current understanding of the subject derives from a diverse array of experiments with different primary objectives. Nevertheless, these collective efforts yield an astonishingly broad spectrum of constraints that span a wide range of Primordial Black Hole masses, enriching our understanding of these enigmatic cosmic entities. Despite the absence of positive observations, Primordial Black Holes have consistently proven their ability to test the early Universe and physics Beyond the Standard Model. While the existing studies have yielded a wealth of constraints, it is premature to declare a saturation of interest. On the contrary, they represent a powerful tool even if they do not exist because they catalyze inspiring studies that might otherwise remain uncharted. From this point of view, Primordial Black Holes hold the potential to unveil intriguing discoveries in the foreseeable future.

Acknowledgments

When the world shoves you around, you just gotta stand up and shove back. It's not like somebody's gonna save you if you start babbling excuses.

RORONOA ZORO

Completing this Ph.D. thesis has been an incredible journey, and I am profoundly grateful for the numerous personal and professional contributions that made this endeavor possible. The unwavering support, guidance, and inspiration generously bestowed upon me by a select group of individuals have been fundamental in completing this manuscript.

The inception of this thesis traces to the moment I resented "Baryogenesis through baryon capture by black holes" by A. D. Dolgov and N. A. Pozdnyakov during our group's Journal Club. That paper ignited my fascination with Primordial Black Holes, an allure that has continued to grow ever since.

First and foremost, I would like to express my deepest gratitude to my supervisors, Profs. G. Miele and S. Morisi and Dr. M. Chianese, whose unwavering guidance has played a pivotal role in shaping me into an independent researcher. I am grateful for their invaluable advice and guidance throughout this journey.

I wish to acknowledge the members of the theoretical astroparticle group (Profs. F. Iocco, G. Mangano, A. Marinelli, O. Pisanti, Drs. R. Samiran, N. Saviano and D. F. G. Fiorillo) for their stimulating scientific discussions and invaluable insights that have greatly enriched my work.

My sincere appreciation goes to all the researchers with whom I collaborated during these years (Profs. G. Cacciapaglia, G. Ricciardi, A. Palazzo, F. Sannino, and P. Santorelli, and Drs. N. Vignaroli and A. De Iorio). Their guidance and willingness to share their time and knowledge have been crucial to my scientific growth. In particular, I am very grateful to Prof. Alberto Orso Maria Iorio for his expertise and encouragement during these years.

I am indebted to Prof. G. Fiorillo for welcoming me into her group, being an incredible mentor over the last few months, and offering me the invaluable opportunity to deepen my scientific studies. I am also profoundly thankful to her group (Profs. F. Di Capua, Y. Suvorov, N. Canci, Dr. D. Rudik, G. Matteucci, and G. Botogoske) for their warm welcome and support during my time there.

I express my gratitude to the esteemed committee members, Profs. P. Di Bari and D. Montanino, for their valuable feedback and constructive criticisms. Their deep expertise has played a fundamental role in refining the quality and depth of this thesis

I am grateful to Guido Celentano for his unwavering assistance throughout my Ph.D. journey. His dedication and professionalism have been invaluable, and I appreciate his tireless efforts.

To my cherished colleagues and friends in the room "1G10" (Alessandra D'Alise, Vittorio D. Esposito, Giuseppe Fabiano, Domenico Frattulillo, Elisa Gandolfi, and Jaber Adam Musa Ibrahim), I wish to convey my heartfelt gratitude for the camaraderie, intellectual discourse, and unwavering support that rendered this journey unique. The stimulating environment of our shared space played a pivotal role in my academic adventure, fostering a profound sense of community.

I extend my deepest appreciation to my fellow Ph.D. students and friends (Especially Mattia Cielo, Cristina Giordano, Matteo Manzo, Renato Maria Prisco, and Dario Vincenzi) with whom I had the privilege of engaging in rich and enlightening discussions over these years. Their unwavering intellectual curiosity and insightful perspectives were instrumental in broadening and redefining my research approach.

In particular, I reserve a special thank you to Giuseppe Matteucci, whose support, patience, and engaging discussions, especially in these last few months, have been invaluable.

My friends deserve my deepest gratitude for their love and encouragement. Their unwavering belief in my abilities was not only a constant source of motivation but also a comforting anchor during the most challenging moments of this arduous Ph.D. journey.

Finally, and most importantly, I am boundlessly grateful to my parents, siblings, and my Aunt Maria for their undying love and support and for always believing in me. This adventure would not have been possible without them.

I would be remiss if I didn't acknowledge my pocket-size tiger, Pallino, who offered constant companionship during late-night research sessions. He provided constant company, warmth, and occasional distraction during the arduous journey of completing this thesis.

This thesis is a testament to the collective effort of many, and I am humbled and grateful for the opportunity to have undertaken this research.

APPENDIX A

$\chi - e$ cross-section

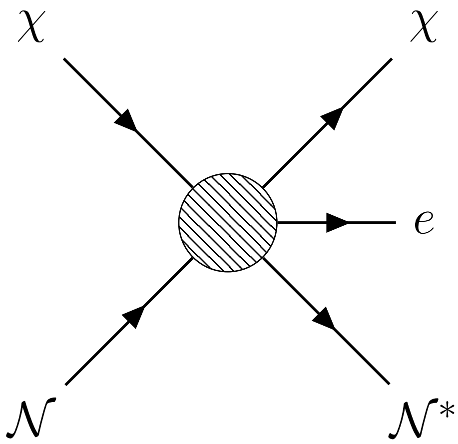

Figure A.1: The diagram depicts χ-e scatterings leading to the ionization of the atom.

Dark Matter direct detection observatories look for Dark Matter-nucleus recoil energies or the electronic transitions induced by the Dark Matter-electron scatterings. We dedicate this appendix to the comprehensive calculation of the cross-section for the Dark Matter-electron scattering when the electron is bound to the nucleus in the initial state (it is described in Eq. (4.9) and depicted Fig. A.1).

We are interested in calculating the transition rate from the initial and final states described as

$$|\psi^{n,l}, \mathbf{p}\rangle = |\psi^{n,l}\rangle \otimes |\mathbf{p}\rangle \ , \tag{A.1}$$

$$|\psi_{\mathbf{k}'}, \mathbf{p}'\rangle = |\psi_{\mathbf{k}'}\rangle \otimes |\mathbf{p}'\rangle \ , \tag{A.2}$$

where $\psi^{n,\,l}$ is the electron bounded eigenstate characterized by the quantum numbers $(n,\,l)$, $|\psi_{\mathbf{k}'}\rangle$ is the electron unbounded final state, and $|\mathbf{p}^{(\prime)}\rangle$ refers to χ initial (final) state. The single particle space state is normalized as $\langle\mathbf{p}|\mathbf{p}\rangle = (2\pi)^3\,\delta^3(0)\,2\,E_p = V\,2\,E_p$, where V is the divergent volume factor. In this case, the first non-trivial term of the Dyson expansion of the S-matrix is

$$S^{n,\,l} = -i\,\langle\mathbf{p}',\,\psi_{\mathbf{k}'}|\int \mathrm{d}^4x\,\mathcal{H}_I(x)|\psi^{n,\,l},\,\mathbf{p}\rangle\ , \tag{A.3}$$

where x is a space-time point and $\mathcal{H}_I$ is the Hamiltonian density in the interaction picture. Defining $\mathcal{H}_I$ in terms of the Hamiltonian density in the Schrodinger picture, $\mathcal{H}_S$, and of the Hamiltonian of the system $\chi - e$ in which $\mathcal{H}_I$ is set to zero, H_0, we get

$$\begin{aligned} S^{n,\,l} &= -i\int \mathrm{d}^4x\,\langle\mathbf{p}',\,\psi_{\mathbf{k}'}|e^{iH_0t}\mathcal{H}_S(x)e^{-iH_0t}|\psi^{n,\,l},\,\mathbf{p}\rangle && \text{(A.4)}\\ &= -i\int \mathrm{d}^3\mathbf{x}\,\langle\mathbf{p}',\,\psi_{\mathbf{k}'}|\mathcal{H}_S(x)|\psi^{n,\,l},\,\mathbf{p}\rangle\int \mathrm{d}t\,e^{i(E'_\chi+E'_e-E_\chi-E_e)t} && \text{(A.5)}\\ &= -i(2\pi)\delta(E'_\chi+E'_e-E_e-E_\chi)\int \mathrm{d}^3x\,\langle\mathbf{p}',\,\psi_{\mathbf{k}'}|\mathcal{H}_S|\psi^{n,\,l},\,\mathbf{p}\rangle\ . && \text{(A.6)} \end{aligned}$$

Our aim is to rearrange $S^{n,\,l}$ in in terms of the S-matrix of the scattering between χ and a free electron, defined as

$$S^{\mathrm{free}} = -i(2\pi)\delta(E'_\chi+E'_e-E_e-E_\chi)\int \mathrm{d}^3\mathbf{x}\,\langle\mathbf{k}',\,\mathbf{p}'|\mathcal{H}_S|\mathbf{p},\,\mathbf{k}\rangle = i(2\pi)^4\delta^4(p+k-p'-k')M^{\mathrm{free}}\,, \tag{A.7}$$

where M^{free} is the transition amplitude of the process. Assuming the effective Lagrangian in Eq. (4.8), it takes the following expression

$$\begin{aligned} \overline{|M^{\mathrm{free}}|^2} &= \frac{g_\ell^2}{4\Lambda^4}J_\chi J_e\,, && \text{(A.8)}\\ J_e &= \sum_{\mathrm{spin}}\left[\overline{u}_e\,(k')\,u_e\,(k)\right]\,\left[\overline{u}_e\,(k)\,u_e\,(k')\right]\,, && \text{(A.9)}\\ J_\chi &= \sum_{\mathrm{spin}}\left[\overline{u}_\chi\,(p')\,u_\chi\,(p)\right]\,\left[\overline{u}_\chi\,(p)\,u_\chi\,(p')\right]\,. && \text{(A.10)}\\ & && \text{(A.11)} \end{aligned}$$

With this in mind, we recast the initial and final states as

$$\begin{aligned} |\psi^{n,\,l},\,\mathbf{p}\rangle &= \int\frac{\mathrm{d}^3\mathbf{k}}{(2\pi)^3}\,\langle\mathbf{k}|\psi^{n,\,l}\rangle\,|\mathbf{k},\,\mathbf{p}\rangle\ , && \text{(A.12)}\\ \langle\mathbf{p}',\,\psi_{\mathbf{k}'}| &= \int\frac{\mathrm{d}^3\mathbf{k}'}{(2\pi)^3}\,\langle\psi_{\mathbf{k}'}|\mathbf{k}'\rangle\,\langle\mathbf{p}',\mathbf{k}'|\ , && \text{(A.13)} \end{aligned}$$

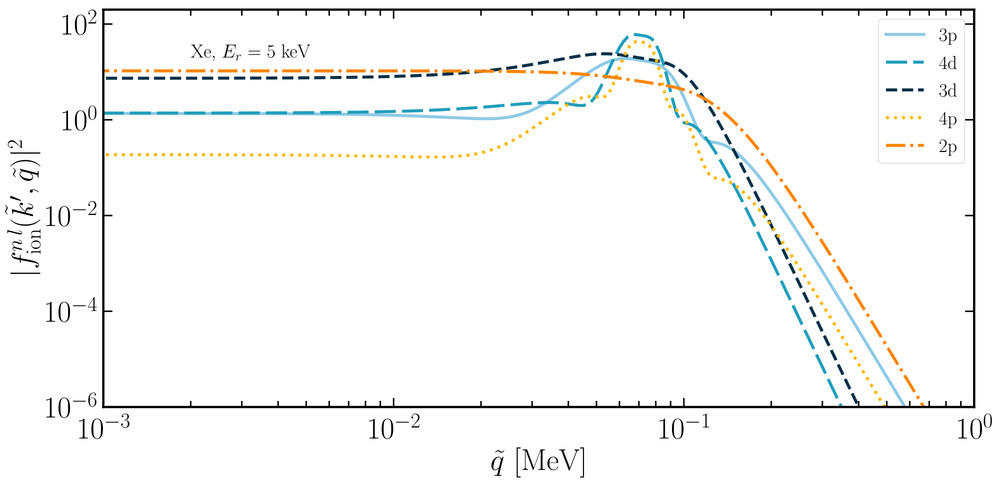

Figure A.2: Xenon ionization function for $E_r = 5$ keV in terms of $\tilde{q}$.

where we introduced a full set of free electron eigenstates satisfying the following identity

$$\int \frac{\mathrm{d}^3\mathbf{k}}{(2\pi)^3} \left|\mathbf{k}\right\rangle \left\langle \mathbf{k}\right| = \mathbb{I}\,. \tag{A.14}$$

These positions allow us to adjust Eq. (A.6) as

$$S^{n,\,l} = -i(2\pi)\delta(E'_\chi + E'_e - E_e - E_\chi) \int \mathrm{d}^3\mathbf{x} \int \frac{\mathrm{d}^3\mathbf{k}'}{(2\pi)^3} \int \frac{\mathrm{d}^3\mathbf{k}}{(2\pi)^3} \left\langle \psi_{\mathbf{k}'} | \mathbf{k}' \right\rangle \left\langle \mathbf{k}',\, \mathbf{p}' | \mathcal{H}_S | \mathbf{p},\, \mathbf{k} \right\rangle \left\langle \mathbf{k} | \psi^{n,\,l} \right\rangle \,. \tag{A.15}$$

Comparing Eqs. (A.7), (A.15), we get

$$\begin{aligned} S^{n,\,l} &= -i(2\pi)^4\delta(E'_\chi + E'_e - E_e - E_\chi)\,\cdot & \text{(A.16)} \\ &\quad \cdot \int \frac{\mathrm{d}^3\mathbf{k}}{(2\pi)^3} \int \frac{\mathrm{d}^3\mathbf{k}'}{(2\pi)^3} \left\langle \psi_{\mathbf{k}'} | \mathbf{k}' \right\rangle \left\langle \mathbf{k} | \psi^{n,\,l} \right\rangle \delta^3(\mathbf{p} + \mathbf{k} - \mathbf{p}' - \mathbf{k}') M^{\rm free} \\ &= -i(2\pi)\delta(E'_\chi + E'_e - E_e - E_\chi) \int \frac{\mathrm{d}^3\mathbf{k}'}{(2\pi)^3} \left\langle \psi_{\mathbf{k}'} | \mathbf{k}' \right\rangle \left\langle \mathbf{k}' - \mathbf{q} | \psi^{n,\,l} \right\rangle M^{\rm free}\Big|_{\mathbf{k}=\mathbf{k}'-\mathbf{q}} & \text{(A.17)} \\ &= -i(2\pi)\delta(E'_\chi + E'_e - E_e - E_\chi) \int \frac{\mathrm{d}^3\mathbf{k}'}{(2\pi)^3} \left\langle \psi_{\mathbf{k}'} | \mathbf{k}' \right\rangle \left\langle \mathbf{k}' | e^{i\mathbf{q}\cdot\hat{\mathbf{x}}} | \psi^{n,\,l} \right\rangle M^{\rm free}\Big|_{\mathbf{k}=\mathbf{k}'-\mathbf{q}} & \text{(A.18)} \\ &= -i(2\pi)\delta(E'_\chi + E'_e - E_e - E_\chi) \left\langle \psi_{\mathbf{k}'} | e^{i\mathbf{q}\cdot\hat{\mathbf{x}}} | \psi^{n,\,l} \right\rangle M^{\rm free}\Big|_{\mathbf{k}=\mathbf{k}'-\mathbf{q}}\,. & \text{(A.19)} \end{aligned}$$

We obtain Eq. (A.17) integrating in $\mathbf{k}$ and considering that $\mathbf{q} = \mathbf{p} - \mathbf{p}'$, Eq. (A.18) using the definition of the momentum boost, and Eq. (A.19) using the identity shown in Eq. (A.14). $\left\langle \psi_{\mathbf{k}'} | e^{i\mathbf{q}\cdot\hat{\mathbf{x}}} | \psi^{n,\,l} \right\rangle$ is the matrix element between the initial bound state of the electron and the final free state.

The cross-section is then defined as

$$d\sigma^{n,l} = \frac{d^3\mathbf{p}'}{(2\pi)^3}\frac{d^3\mathbf{k}'}{(2\pi)^3}\delta(E'_\chi + E'_e - E_e - E_\chi)\frac{1}{v_{\chi e}}\frac{2\pi}{2E_p 2E_e 2E'_\chi 2E'_e}\overline{|M^{\rm free}|^2}_{\mathbf{k}=\mathbf{k}'-\mathbf{q}}\sum_{deg.state}\left|\langle\psi_{\mathbf{k}'}|e^{i\mathbf{q}\cdot\hat{\mathbf{x}}}|\psi^{n,l}\rangle\right|^2, \quad (A.20)$$

where $v_{\chi e}$ is the modulus of the relative velocity between χ and the electron, while $\overline{|M^{\rm free}|^2}$ is the transition amplitude for a free electron mediated over spin. The matrix elements in Eq. (A.20) describe the ionization of bounded electrons and can be written in terms of the ionization functions. Refs. [148, 567, 568] define the ionization functions as

$$\left|f^{n,l}_{ion}(\tilde{k}', \tilde{q})\right|^2 := \frac{2\tilde{k}'^3}{(2\pi)^3}\sum_{deg.state}\left|\langle\psi_{\mathbf{k}'}|e^{i\mathbf{q}\cdot\hat{\mathbf{x}}}|\psi^{n,l}\rangle\right|^2 \quad (A.21)$$

$\tilde{q}$ and $\tilde{k}$ are the module of the momentum transfer and the electron initial momentum respectively. Approximating the final state as a plane wave and spherically symmetric atomic target with full shell, the ionization functions are

$$|f^{n,l}_{\rm ion}(\tilde{k}', \tilde{q})|^2 = \frac{(2l+1)\tilde{k}'^2}{4\pi^3\tilde{q}}\int_{|\tilde{k}'-\tilde{q}|}^{\tilde{k}'+\tilde{q}} d\tilde{k}\;\tilde{k}|\widetilde{\mathcal{R}}_{n,l}(\tilde{k})|^2\,, \quad (A.22)$$

where we perform the integral for all the allowed values for the modulus of the electron initial momentum, k. $\widetilde{\mathcal{R}}_{n,l}(\tilde{k})$ is the Fourier transform of the radial part of the bounded wave function, defined as

$$\begin{aligned}\widetilde{\mathcal{R}}_{n,l}(\tilde{k}) = \; & \textstyle\sum_\theta \frac{C_{n,l\theta}2^{-l+n_{l\theta}}}{\Gamma(3/2+l)}\left(\frac{2\pi a_0}{Z_{l\theta}}\right)^{3/2}\left(\frac{i\tilde{k}a_0}{Z_{l\theta}}\right)^l\frac{(1+n_{l\theta}+l)!}{\sqrt{(2n_{l\theta})!}}\cdot \\ & \cdot {}_2F_1\left[\frac{(2+n_{l\theta}+l)}{2}, \frac{(3+n_{l\theta}+l)}{2}, \frac{3}{2}+l, -\left(\frac{\tilde{k}a_0}{Z_{l\theta}}\right)^2\right]\end{aligned} \quad (A.23)$$

where ${}_2F_1(a,b,c,x)$ is the hyper-geometric function and a_0 is Bohr radius. The coefficients appearing in this expression are tabulated in Ref. [569]. In Fig. A.2 we show some examples of the ionization functions for Xenon orbitals as a function of the momentum transfer $\tilde{q}$ once the electron recoil energy is fixed to 5 keV.

Substituting Eq. (A.21) in Eq. (A.20), and using that $d^3\mathbf{p}' = d^3\mathbf{q}$, we get

$$d\sigma^{n,l} = \frac{d^3\mathbf{q}'}{(2\pi)^3}\frac{d^3\mathbf{k}'}{(2\pi)^3}\frac{1}{v_{\chi e}}\frac{2\pi}{2E_\chi 2E_e 2E'_\chi 2E'_e}\delta(E'_\chi + E'_e - E_e - E_\chi)\overline{|M^{\rm free}|^2}_{\mathbf{k}=\mathbf{k}'-\mathbf{q}}\frac{(2\pi)^3}{2\,\tilde{k}'^3}\left|f^{n,l}_{ion}(\tilde{k}', \tilde{q})\right|^2. \quad (A.24)$$

Hence, we get that the differential cross-section is

$$\frac{d\sigma^{n,l}}{dE_r} = \frac{1}{8\pi\,\Lambda^4\,\tilde{p}^2\,m_e}\int_{\tilde{q}_-}^{\tilde{q}_+} d\tilde{q}\,\tilde{q}\frac{1}{2\,\tilde{k}'^2}\left|f^{n,l}_{\rm ion}(\tilde{k}', \tilde{q})\right|^2\left[(p\cdot(p-q)+m_\chi^2)\,(k'\cdot(k'-q)+m_e^2)\right]. \quad (A.25)$$

Bibliography

[1] Y. Nagashima, *Beyond the standard model of elementary particle physics* (Wiley-VCH, Weinheim, USA, 2014).

[2] Khlopov, Maxim Yu., Res. Astron. Astrophys. **10**, 495 (2010), arXiv:0801.0116 [astro-ph] .

[3] B. Carr, K. Kohri, Y. Sendouda, and J. Yokoyama, Rept. Prog. Phys. **84**, 116902 (2021), arXiv:2002.12778 [astro-ph.CO] .

[4] B. Carr, S. Clesse, J. Garcia-Bellido, M. Hawkins, and F. Kuhnel, (2023), arXiv:2306.03903 [astro-ph.CO] .

[5] Calabrese, Roberta and Fiorillo, Damiano F. G. and Miele, Gennaro and Morisi, Stefano and Palazzo, Antonio, Phys. Lett. B **829**, 137050 (2022), arXiv:2106.02492 [hep-ph] .

[6] Calabrese, Roberta and Chianese, Marco and Fiorillo, Damiano F. G. and Saviano, Ninetta, Phys. Rev. D **105**, L021302 (2022), arXiv:2107.13001 [hep-ph] .

[7] Calabrese, Roberta and Chianese, Marco and Fiorillo, Damiano F. G. and Saviano, Ninetta, Phys. Rev. D **105**, 103024 (2022), arXiv:2203.17093 [hep-ph] .

[8] Ambrosone, Antonio and Calabrese, Roberta and Fiorillo, Damiano F. G. and Miele, Gennaro and Morisi, Stefano, Phys. Rev. D **105**, 045001 (2022), arXiv:2106.11980 [hep-ph] .

[9] R. Calabrese, M. Chianese, J. Gunn, G. Miele, S. Morisi, and N. Saviano, Phys. Rev. D **107**, 123537 (2023), arXiv:2305.13369 [hep-ph] .

[10] Y. Fukuda *et al.* (Super-Kamiokande), Phys. Rev. Lett. **81**, 1562 (1998), arXiv:hep-ex/9807003 .

[11] N. Aghanim *et al.* (Planck), Astron. Astrophys. **641**, A6 (2020), arXiv:1807.06209 [astro-ph.CO] .

[12] G. Bertone and T. Tait, M. P., Nature **562**, 51 (2018), arXiv:1810.01668 [astro-ph.CO] .

[13] V. A. Kuzmin, V. A. Rubakov, and M. E. Shaposhnikov, Phys. Lett. B **155**, 36 (1985).

[14] P. J. E. Peebles and B. Ratra, Rev. Mod. Phys. **75**, 559 (2003), arXiv:astro-ph/0207347 .

[15] A. O. Sushkov, W. J. Kim, D. A. R. Dalvit, and S. K. Lamoreaux, Phys. Rev. Lett. **107**, 171101 (2011), arXiv:1108.2547 [quant-ph] .

[16] F. Englert and R. Brout, Phys. Rev. Lett. **13**, 321 (1964).

[17] P. W. Higgs, Phys. Lett. **12**, 132 (1964).

[18] P. W. Higgs, Phys. Rev. Lett. **13**, 508 (1964).

[19] P. A. Zyla *et al.* (Particle Data Group), PTEP **2020**, 083C01 (2020).

[20] M. Aker *et al.* (KATRIN), Nature Phys. **18**, 160 (2022), arXiv:2105.08533 [hep-ex] .

[21] I. Esteban, M. C. Gonzalez-Garcia, M. Maltoni, T. Schwetz, and A. Zhou, JHEP **09**, 178 (2020), arXiv:2007.14792 [hep-ph] .

[22] F. Capozzi, E. Di Valentino, E. Lisi, A. Marrone, A. Melchiorri, and A. Palazzo, Phys. Rev. D **104**, 083031 (2021), arXiv:2107.00532 [hep-ph] .

[23] S. Weinberg, Phys. Rev. Lett. **43**, 1566 (1979).

[24] C. Giunti and C. W. Kim, *Fundamentals of Neutrino Physics and Astrophysics* (2007).

[25] B. Pontecorvo, Sov. Phys. JETP **6**, 429 (1957).

[26] B. Pontecorvo, Zh. Eksp. Teor. Fiz. **34**, 247 (1957).

[27] M. Gell-Mann and A. Pais, Phys. Rev. **97**, 1387 (1955).

[28] Z. Maki, M. Nakagawa, and S. Sakata, Prog. Theor. Phys. **28**, 870 (1962).

[29] M. Nakagawa, H. Okonogi, S. Sakata, and A. Toyoda, Prog. Theor. Phys. **30**, 727 (1963).

[30] B. Pontecorvo, Zh. Eksp. Teor. Fiz. **53**, 1717 (1967).

[31] V. N. Gribov and B. Pontecorvo, Phys. Lett. B **28**, 493 (1969).

[32] H. Fritzsch and P. Minkowski, Phys. Lett. B **62**, 72 (1976).

[33] S. M. Bilenky, Sov. J. Part. Nucl. **18**, 188 (1987).

[34] L. Wolfenstein, Phys. Rev. D **17**, 2369 (1978).

[35] S. P. Mikheyev and A. Y. Smirnov, Sov. J. Nucl. Phys. **42**, 913 (1985).

[36] S. P. Mikheev and A. Y. Smirnov, Nuovo Cim. C **9**, 17 (1986).

[37] R. Davis, Jr., D. S. Harmer, and K. C. Hoffman, Phys. Rev. Lett. **20**, 1205 (1968).

[38] K. S. Hirata *et al.* (Kamiokande-II), Phys. Rev. Lett. **63**, 16 (1989).

[39] K. S. Hirata *et al.* (Kamiokande-II), Phys. Rev. Lett. **65**, 1297 (1990).

[40] J. N. Bahcall and R. K. Ulrich, Rev. Mod. Phys. **60**, 297 (1988).

[41] K. S. Hirata *et al.* (Kamiokande-II), Phys. Rev. D **44**, 2241 (1991), [Erratum: Phys.Rev.D 45, 2170 (1992)].

[42] J. N. Bahcall and M. H. Pinsonneault, Rev. Mod. Phys. **64**, 885 (1992).

[43] P. Anselmann *et al.* (GALLEX), Phys. Lett. B **327**, 377 (1994).

[44] B. T. Cleveland, T. Daily, R. Davis, Jr., J. Distel, K. Lande, C. K. Lee, P. Wildenhain, and J. Ullman, Nucl. Phys. B Proc. Suppl. **38**, 47 (1995).

[45] B. T. Cleveland, T. Daily, R. Davis, Jr., J. R. Distel, K. Lande, C. K. Lee, P. S. Wildenhain, and J. Ullman, Astrophys. J. **496**, 505 (1998).

[46] W. Hampel *et al.* (GALLEX), Phys. Lett. B **447**, 127 (1999).

[47] J. N. Abdurashitov *et al.* (SAGE), Phys. Rev. C **60**, 055801 (1999), arXiv:astro-ph/9907113 .

[48] J. N. Abdurashitov *et al.* (SAGE), J. Exp. Theor. Phys. **95**, 181 (2002), arXiv:astro-ph/0204245 .

[49] S. Fukuda *et al.* (Super-Kamiokande), Phys. Rev. Lett. **86**, 5651 (2001), arXiv:hep-ex/0103032 .

[50] S. Fukuda *et al.* (Super-Kamiokande), Phys. Rev. Lett. **86**, 5656 (2001), arXiv:hep-ex/0103033 .

[51] S. Fukuda *et al.* (Super-Kamiokande), Phys. Lett. B **539**, 179 (2002), arXiv:hep-ex/0205075 .

[52] Q. R. Ahmad *et al.* (SNO), Phys. Rev. Lett. **87**, 071301 (2001), arXiv:nucl-ex/0106015 .

[53] Q. R. Ahmad *et al.* (SNO), Phys. Rev. Lett. **89**, 011301 (2002), arXiv:nucl-ex/0204008 .

[54] S. N. Ahmed *et al.* (SNO), Phys. Rev. Lett. **92**, 181301 (2004), arXiv:nucl-ex/0309004 .

[55] Y. Ashie *et al.* (Super-Kamiokande), Phys. Rev. Lett. **93**, 101801 (2004), arXiv:hep-ex/0404034 .

[56] Y. Ashie *et al.* (Super-Kamiokande), Phys. Rev. D **71**, 112005 (2005), arXiv:hep-ex/0501064 .

[57] K. Eguchi *et al.* (KamLAND), Phys. Rev. Lett. **90**, 021802 (2003), arXiv:hep-ex/0212021 .

[58] T. Araki *et al.* (KamLAND), Phys. Rev. Lett. **94**, 081801 (2005), arXiv:hep-ex/0406035 .

[59] M. H. Ahn *et al.* (K2K), Phys. Rev. Lett. **90**, 041801 (2003), arXiv:hep-ex/0212007 .

[60] E. Aliu *et al.* (K2K), Phys. Rev. Lett. **94**, 081802 (2005), arXiv:hep-ex/0411038 .

[61] D. G. Michael *et al.* (MINOS), Phys. Rev. Lett. **97**, 191801 (2006), arXiv:hep-ex/0607088 .

[62] S. M. Bilenky, J. Hosek, and S. T. Petcov, Phys. Lett. B **94**, 495 (1980).

[63] P. F. de Salas, D. V. Forero, S. Gariazzo, P. Martínez-Miravé, O. Mena, C. A. Ternes, M. Tórtola, and J. W. F. Valle, JHEP **02**, 071 (2021), arXiv:2006.11237 [hep-ph] .

[64] P. Ramond, in *International Symposium on Fundamentals of Quantum Theory and Quantum Field Theory* (1979) arXiv:hep-ph/9809459 .

[65] S. F. King, A. Merle, S. Morisi, Y. Shimizu, and M. Tanimoto, New J. Phys. **16**, 045018 (2014), arXiv:1402.4271 [hep-ph] .

[66] J. A. Casas and A. Ibarra, Nucl. Phys. B **618**, 171 (2001), arXiv:hep-ph/0103065 .

[67] D. Z. Freedman, Phys. Rev. D **9**, 1389 (1974).

[68] T. Kozynets, S. Fallows, and C. B. Krauss, Astropart. Phys. **105**, 25 (2019), arXiv:1806.01417 [astro-ph.HE] .

[69] C. A. J. O'Hare, Phys. Rev. Lett. **127**, 251802 (2021), arXiv:2109.03116 [hep-ph] .

[70] D. Akimov *et al.* (COHERENT), Science **357**, 1123 (2017), arXiv:1708.01294 [nucl-ex] .

[71] V. De Romeri, O. G. Miranda, D. K. Papoulias, G. Sanchez Garcia, M. Tórtola, and J. W. F. Valle, JHEP **04**, 035 (2023), arXiv:2211.11905 [hep-ph] .

[72] M. Cadeddu, F. Dordei, C. Giunti, Y. F. Li, E. Picciau, and Y. Y. Zhang, Phys. Rev. D **102**, 015030 (2020), arXiv:2005.01645 [hep-ph] .

[73] C. Patrignani *et al.* (Particle Data Group), Chin. Phys. C **40**, 100001 (2016).

[74] R. H. Helm, Phys. Rev. **104**, 1466 (1956).

[75] M. Abdullah *et al.*, (2022), arXiv:2203.07361 [hep-ph] .

[76] J. D. Lewin and P. F. Smith, Astropart. Phys. **6**, 87 (1996).

[77] J. Billard, L. Strigari, and E. Figueroa-Feliciano, Phys. Rev. D **89**, 023524 (2014), arXiv:1307.5458 [hep-ph] .

[78] J. A. Formaggio and G. P. Zeller, Rev. Mod. Phys. **84**, 1307 (2012), arXiv:1305.7513 [hep-ex] .

[79] Bertone, Gianfranco and Hooper, Dan, Rev. Mod. Phys. **90**, 045002 (2018), arXiv:1605.04909 [astro-ph.CO] .

[80] F. Zwicky, Helv. Phys. Acta **6**, 110 (1933).

[81] F. Zwicky, Astrophys. J. **86**, 217 (1937).

[82] V. C. Rubin and W. K. Ford, Jr., Astrophys. J. **159**, 379 (1970).

[83] M. S. Roberts, The Astrophysical Journal **144**, 639 (1966).

[84] Tyson, J. Anthony and Kochanski, Greg P. and Dell'Antonio, Ian P., Astrophys. J. Lett. **498**, L107 (1998), arXiv:astro-ph/9801193 .

[85] A. Refregier, Ann. Rev. Astron. Astrophys. **41**, 645 (2003), arXiv:astro-ph/0307212 .

[86] D. Clowe, M. Bradac, A. H. Gonzalez, M. Markevitch, S. W. Randall, C. Jones, and D. Zaritsky, Astrophys. J. Lett. **648**, L109 (2006), arXiv:astro-ph/0608407 .

[87] A. D. Lewis, D. A. Buote, and J. T. Stocke, Astrophys. J. **586**, 135 (2003), arXiv:astro-ph/0209205 .

[88] S. W. Allen, A. C. Fabian, R. W. Schmidt, and H. Ebeling, Mon. Not. Roy. Astron. Soc. **342**, 287 (2003), arXiv:astro-ph/0208394 .

[89] C. Amsler *et al.* (Particle Data Group), Phys. Lett. B **667**, 1 (2008).

[90] E. Komatsu *et al.* (WMAP), Astrophys. J. Suppl. **192**, 18 (2011), arXiv:1001.4538 [astro-ph.CO] .

[91] A. G. Riess *et al.* (Supernova Search Team), Astron. J. **116**, 1009 (1998), arXiv:astro-ph/9805201 .

[92] S. Perlmutter *et al.* (Supernova Cosmology Project), Astrophys. J. **517**, 565 (1999), arXiv:astro-ph/9812133 .

[93] R. D. Peccei and H. R. Quinn, Phys. Rev. Lett. **38**, 1440 (1977).

[94] E. W. Kolb, D. J. H. Chung, and A. Riotto, AIP Conf. Proc. **484**, 91 (1999), arXiv:hep-ph/9810361 .

[95] S. Dodelson and L. M. Widrow, Phys. Rev. Lett. **72**, 17 (1994), arXiv:hep-ph/9303287 .

[96] W. Hu, R. Barkana, and A. Gruzinov, Phys. Rev. Lett. **85**, 1158 (2000), arXiv:astro-ph/0003365 .

[97] D. E. Kaplan, M. A. Luty, and K. M. Zurek, Phys. Rev. D **79**, 115016 (2009), arXiv:0901.4117 [hep-ph] .

[98] K. Griest, Astrophys. J. **366**, 412 (1991).

[99] Y. Zel'Dovich and A. Starobinsky, Jetp Letters - JETP LETT-ENGL TR **24**, 571 (1976).

[100] G. Steigman and M. S. Turner, Nucl. Phys. B **253**, 375 (1985).

[101] G. Bertone, D. Hooper, and J. Silk, Phys. Rept. **405**, 279 (2005), arXiv:hep-ph/0404175 .

[102] Sanders, Robert H. and McGaugh, Stacy S., Ann. Rev. Astron. Astrophys. **40**, 263 (2002), arXiv:astro-ph/0204521 .

[103] Y. b. Zeldovich, Adv. Astron. Astrophys. **3**, 241 (1965).

[104] H.-Y. Chiu, Phys. Rev. Lett. **17**, 712 (1966).

[105] G. Steigman, Ann. Rev. Nucl. Part. Sci. **29**, 313 (1979).

[106] R. J. Scherrer and M. S. Turner, Phys. Rev. D **33**, 1585 (1986), [Erratum: Phys.Rev.D 34, 3263 (1986)].

[107] J. L. Feng, Ann. Rev. Astron. Astrophys. **48**, 495 (2010), arXiv:1003.0904 [astro-ph.CO] .

[108] V. Khachatryan *et al.* (CMS), Eur. Phys. J. C **75**, 235 (2015), arXiv:1408.3583 [hep-ex] .

[109] M. Aaboud *et al.* (ATLAS), JHEP **01**, 126 (2018), arXiv:1711.03301 [hep-ex] .

[110] E. Guido (BELLE-II), PoS **FPCP2017**, 036 (2017).

[111] F. Aharonian *et al.* (H.E.S.S.), Astron. Astrophys. **425**, L13 (2004), arXiv:astro-ph/0408145 .

[112] J. Holder *et al.* (VERITAS), Astropart. Phys. **25**, 391 (2006), arXiv:astro-ph/0604119 .

[113] E. Aliu *et al.* (MAGIC), Science **320**, 1752 (2008), arXiv:0807.2822 [astro-ph] .

[114] W. B. Atwood *et al.* (Fermi-LAT), Astrophys. J. **697**, 1071 (2009), arXiv:0902.1089 [astro-ph.IM] .

[115] J. Carr *et al.* (CTA), PoS **ICRC2015**, 1203 (2016), arXiv:1508.06128 [astro-ph.HE] .

[116] A. U. Abeysekara *et al.* (HAWC), Science **358**, 911 (2017), arXiv:1711.06223 [astro-ph.HE] .

[117] S. Desai *et al.* (Super-Kamiokande), Phys. Rev. D **70**, 083523 (2004), [Erratum: Phys.Rev.D 70, 109901 (2004)], arXiv:hep-ex/0404025 .

[118] M. G. Aartsen *et al.* (IceCube), Phys. Rev. Lett. **110**, 131302 (2013), arXiv:1212.4097 [astro-ph.HE] .

[119] A. D. Avrorin *et al.*, JETP Lett. **101**, 289 (2015), arXiv:1412.3672 [astro-ph.HE] .

[120] S. Adrian-Martinez *et al.* (ANTARES), Phys. Lett. B **759**, 69 (2016), arXiv:1603.02228 [astro-ph.HE] .

[121] D. Lopez-Coto, S. Navas, and J. D. Zornoza (KM3NeT), PoS **ICRC2019**, 536 (2020).

[122] A. Bruno (PAMELA), Italian Phys. Soc. Proc. **103**, 139 (2011).

[123] F. Palmonari, V. Bindi, A. Contin, N. Masi, and L. Quadrani (AMS 02), J. Phys. Conf. Ser. **335**, 012066 (2011).

[124] P. Abreu *et al.* (Pierre Auger), Phys. Rev. D **107**, 042002 (2023), arXiv:2208.02353 [astro-ph.HE] .

[125] T. Aramaki, S. E. Boggs, P. von Doetinchem, H. Fuke, C. J. Hailey, S. A. I. Mognet, R. A. Ong, K. Perez, and J. Zweerink (GAPS), Astropart. Phys. **59**, 12 (2014), arXiv:1401.8245 [astro-ph.HE] .

[126] C. E. Aalseth *et al.* (DarkSide-20k), Eur. Phys. J. Plus **133**, 131 (2018), arXiv:1707.08145 [physics.ins-det] .

[127] E. Aprile, M. Alfonsi, K. Arisaka, F. Arneodo, C. Balan, L. Baudis, B. Bauermeister, A. Behrens, P. Beltrame, K. Bokeloh, and et al., Physical Review Letters **109** (2012), 10.1103/physrevlett.109.181301.

[128] E. Aprile *et al.* (XENON), Phys. Rev. Lett. **123**, 251801 (2019), arXiv:1907.11485 [hep-ex] .

[129] Meng, Yue and others (PandaX-4T), Phys. Rev. Lett. **127**, 261802 (2021), arXiv:2107.13438 [hep-ex] .

[130] D. S. Akerib *et al.* (LUX-ZEPLIN), Phys. Rev. D **101**, 052002 (2020), arXiv:1802.06039 [astro-ph.IM] .

[131] A. Bueno (ArDM), in *6th International Workshop on the Identification of Dark Matter* (2006) pp. 198–203.

[132] G. Fiorillo *et al.* (WArP), PoS **IDM2008**, 016 (2008).

[133] A. Marchionni *et al.* (ArDM), J. Phys. Conf. Ser. **308**, 012006 (2011), arXiv:1012.5967 [physics.ins-det] .

[134] P. A. Amaudruz *et al.* (DEAP), Astropart. Phys. **85**, 1 (2016), arXiv:0904.2930 [astro-ph.IM] .

[135] G. Angloher, C. Bucci, P. Christ, C. Cozzini, F. von Feilitzsch, D. Hauff, S. Henry, T. Jagemann, J. Jochum, H. Kraus, and et al., Astroparticle Physics **23**, 325339 (2005).

[136] P. Agnes *et al.* (DarkSide), Phys. Lett. B **743**, 456 (2015), arXiv:1410.0653 [astro-ph.CO] .

[137] G. Angloher *et al.*, Eur. Phys. J. C **76**, 441 (2016), arXiv:1603.02214 [physics.ins-det] .

[138] J. Aalbers *et al.* (DARWIN), JCAP **11**, 017 (2016), arXiv:1606.07001 [astro-ph.IM] .

[139] R. Agnese *et al.* (SuperCDMS), Phys. Rev. D **95**, 082002 (2017), arXiv:1610.00006 [physics.ins-det] .

[140] E. Aprile *et al.* (XENON), Phys. Rev. Lett. **121**, 111302 (2018), arXiv:1805.12562 [astro-ph.CO] .

[141] E. Aprile *et al.* (XENON), Phys. Rev. Lett. **123**, 241803 (2019), arXiv:1907.12771 [hep-ex] .

[142] G. Angloher *et al.* (CRESST), Eur. Phys. J. C **77**, 637 (2017), arXiv:1707.06749 [astro-ph.CO] .

[143] C. Kachulis *et al.* (Super-Kamiokande), Phys. Rev. Lett. **120**, 221301 (2018), arXiv:1711.05278 [hep-ex] .

[144] A. H. Abdelhameed *et al.* (CRESST), Phys. Rev. D **100**, 102002 (2019), arXiv:1904.00498 [astro-ph.CO] .

[145] E. Aprile *et al.* (XENON), JCAP **11**, 031 (2020), arXiv:2007.08796 [physics.ins-det] .

[146] E. Aprile *et al.* (XENON), Phys. Rev. D **102**, 072004 (2020), arXiv:2006.09721 [hep-ex] .

[147] G. Adhikari *et al.* (COSINE-100), Sci. Adv. **7**, abk2699 (2021), arXiv:2104.03537 [hep-ex] .

[148] R. Essig, J. Mardon, and T. Volansky, Phys. Rev. D **85**, 076007 (2012), arXiv:1108.5383 [hep-ph] .

[149] R. Essig, A. Manalaysay, J. Mardon, P. Sorensen, and T. Volansky, Phys. Rev. Lett. **109**, 021301 (2012), arXiv:1206.2644 [astro-ph.CO] .

[150] R. Essig, T. Volansky, and T.-T. Yu, Phys. Rev. D **96**, 043017 (2017), arXiv:1703.00910 [hep-ph] .

[151] M. Crisler, R. Essig, J. Estrada, G. Fernandez, J. Tiffenberg, M. Sofo haro, T. Volansky, and T.-T. Yu (SENSEI), Phys. Rev. Lett. **121**, 061803 (2018), arXiv:1804.00088 [hep-ex] .

[152] P. Agnes *et al.* (DarkSide), Phys. Rev. Lett. **121**, 111303 (2018), arXiv:1802.06998 [astro-ph.CO] .

[153] A. Aguilar-Arevalo *et al.* (DAMIC), Phys. Rev. Lett. **123**, 181802 (2019), arXiv:1907.12628 [astro-ph.CO] .

[154] E. Andersson, A. Bökmark, R. Catena, T. Emken, H. K. Moberg, and E. Åstrand, JCAP **05**, 036 (2020), arXiv:2001.08910 [hep-ph] .

[155] K. Agashe, Y. Cui, L. Necib, and J. Thaler, JCAP **10**, 062 (2014), arXiv:1405.7370 [hep-ph] .

[156] G. F. Giudice, D. Kim, J.-C. Park, and S. Shin, Phys. Lett. B **780**, 543 (2018), arXiv:1712.07126 [hep-ph] .

[157] B. Fornal, P. Sandick, J. Shu, M. Su, and Y. Zhao, Phys. Rev. Lett. **125**, 161804 (2020), arXiv:2006.11264 [hep-ph] .

[158] C. V. Cappiello, K. C. Y. Ng, and J. F. Beacom, Phys. Rev. D **99**, 063004 (2019), arXiv:1810.07705 [hep-ph] .

[159] T. Bringmann and M. Pospelov, Phys. Rev. Lett. **122**, 171801 (2019), arXiv:1810.10543 [hep-ph] .

[160] Y. Ema, F. Sala, and R. Sato, Phys. Rev. Lett. **122**, 181802 (2019), arXiv:1811.00520 [hep-ph] .

[161] C. Cappiello and J. F. Beacom, Phys. Rev. D **100**, 103011 (2019), arXiv:1906.11283 [hep-ph] .

[162] Y. Ema, F. Sala, and R. Sato, SciPost Phys. **10**, 072 (2021), arXiv:2011.01939 [hep-ph] .

[163] M. Andriamirado *et al.* (PROSPECT, (PROSPECT Collaboration)*), Phys. Rev. D **104**, 012009 (2021), arXiv:2104.11219 [hep-ex] .

[164] A. Boyarsky, O. Ruchayskiy, and D. Iakubovskyi, JCAP **03**, 005 (2009), arXiv:0808.3902 [hep-ph] .

[165] C. Di Paolo, F. Nesti, and F. L. Villante, Mon. Not. Roy. Astron. Soc. **475**, 5385 (2018), arXiv:1704.06644 [astro-ph.GA] .

[166] S. Tremaine and J. E. Gunn, Phys. Rev. Lett. **42**, 407 (1979).

[167] T. Cohen, M. Lisanti, and H. K. Lou, Phys. Rev. Lett. **115**, 171804 (2015), arXiv:1503.00009 [hep-ph] .

[168] N. Daci, I. De Bruyn, S. Lowette, M. H. G. Tytgat, and B. Zaldivar, JHEP **11**, 108 (2015), arXiv:1503.05505 [hep-ph] .

[169] Y. Ali-Haïmoud, J. Chluba, and M. Kamionkowski, Phys. Rev. Lett. **115**, 071304 (2015), arXiv:1506.04745 [astro-ph.CO] .

[170] M. Baryakhtar, J. Bramante, S. W. Li, T. Linden, and N. Raj, Phys. Rev. Lett. **119**, 131801 (2017), arXiv:1704.01577 [hep-ph] .

[171] K. Bondarenko, A. Boyarsky, T. Bringmann, M. Hufnagel, K. Schmidt-Hoberg, and A. Sokolenko, JHEP **03**, 118 (2020), arXiv:1909.08632 [hep-ph] .

[172] A. Coogan, L. Morrison, and S. Profumo, JCAP **08**, 044 (2021), arXiv:2104.06168 [hep-ph] .

[173] V. Gluscevic and K. K. Boddy, Phys. Rev. Lett. **121**, 081301 (2018), arXiv:1712.07133 [astro-ph.CO] .

[174] W. L. Xu, C. Dvorkin, and A. Chael, Phys. Rev. D **97**, 103530 (2018), arXiv:1802.06788 [astro-ph.CO] .

[175] T. R. Slatyer and C.-L. Wu, Phys. Rev. D **98**, 023013 (2018), arXiv:1803.09734 [astro-ph.CO] .

[176] E. O. Nadler, V. Gluscevic, K. K. Boddy, and R. H. Wechsler, Astrophys. J. Lett. **878**, 32 (2019), [Erratum: Astrophys.J.Lett. 897, L46 (2020), Erratum: Astrophys.J. 897, L46 (2020)], arXiv:1904.10000 [astro-ph.CO] .

[177] Savage, C. and Gelmini, G. and Gondolo, P. and Freese, K., JCAP **04**, 010 (2009), arXiv:0808.3607 [astro-ph] .

[178] Hehn, L. and others (EDELWEISS), Eur. Phys. J. C **76**, 548 (2016), arXiv:1607.03367 [astro-ph.CO] .

[179] Amole, C. and others (PICO), Phys. Rev. D **93**, 061101 (2016), arXiv:1601.03729 [astro-ph.CO] .

[180] Akerib, D. S. and others (LUX), Phys. Rev. Lett. **118**, 021303 (2017), arXiv:1608.07648 [astro-ph.CO] .

[181] Amole, C. and others (PICO), Phys. Rev. Lett. **118**, 251301 (2017), arXiv:1702.07666 [astro-ph.CO] .

[182] Arnaud, Q. and others (NEWS-G), Astropart. Phys. **97**, 54 (2018), arXiv:1706.04934 [astro-ph.IM] .

[183] Cui, Xiangyi and others (PandaX-II), Phys. Rev. Lett. **119**, 181302 (2017), arXiv:1708.06917 [astro-ph.CO] .

[184] Agnese, R. and others (SuperCDMS), Phys. Rev. D **99**, 062001 (2019), arXiv:1808.09098 [astro-ph.CO] .

[185] Adhikari, Govinda and others, Nature **564**, 83 (2018), [Erratum: Nature 566, E2 (2019)], arXiv:1906.01791 [astro-ph.IM] .

[186] Bernabei, R. and others, Nucl. Phys. Atom. Energy **19**, 307 (2018), arXiv:1805.10486 [hep-ex] .

[187] Agnes, P. and others (DarkSide), Phys. Rev. Lett. **121**, 081307 (2018), arXiv:1802.06994 [astro-ph.HE] .

[188] Ajaj, R. and others (DEAP), Phys. Rev. D **100**, 022004 (2019), arXiv:1902.04048 [astro-ph.CO] .

[189] Aprile, E. and others (XENON), Phys. Rev. Lett. **126**, 091301 (2021), arXiv:2012.02846 [hep-ex] .

[190] R. Agnese *et al.* (CDMS), Phys. Rev. Lett. **111**, 251301 (2013), arXiv:1304.4279 [hep-ex] .

[191] E. Aprile *et al.* (XENON100), Phys. Rev. Lett. **109**, 181301 (2012), arXiv:1207.5988 [astro-ph.CO] .

[192] D. Z. Freedman, D. N. Schramm, and D. L. Tubbs, Ann. Rev. Nucl. Part. Sci. **27**, 167 (1977).

[193] A. Drukier and L. Stodolsky, Phys. Rev. D **30**, 2295 (1984).

[194] J. Billard *et al.*, JINST **9**, P01013 (2014), arXiv:1305.2360 [astro-ph.IM] .

[195] Riotto, Antonio, in *ICTP Summer School in High-Energy Physics and Cosmology* (1998) pp. 326–436, arXiv:hep-ph/9807454 .

[196] S. Davidson, E. Nardi, and Y. Nir, Phys. Rept. **466**, 105 (2008), arXiv:0802.2962 [hep-ph] .

[197] A. D. Sakharov, Pisma Zh. Eksp. Teor. Fiz. **5**, 32 (1967).

[198] M. Kobayashi and T. Maskawa, Prog. Theor. Phys. **49**, 652 (1973).

[199] A. Y. Ignatiev, N. V. Krasnikov, V. A. Kuzmin, and A. N. Tavkhelidze, Phys. Lett. B **76**, 436 (1978).

[200] M. Yoshimura, Phys. Rev. Lett. **41**, 281 (1978), [Erratum: Phys.Rev.Lett. 42, 746 (1979)].

[201] D. Toussaint, S. B. Treiman, F. Wilczek, and A. Zee, Phys. Rev. D **19**, 1036 (1979).

[202] S. Dimopoulos and L. Susskind, Phys. Rev. D **18**, 4500 (1978).

[203] J. R. Ellis, M. K. Gaillard, and D. V. Nanopoulos, Phys. Lett. B **80**, 360 (1979), [Erratum: Phys.Lett.B 82, 464 (1979)].

[204] S. Weinberg, Phys. Rev. Lett. **42**, 850 (1979).

[205] M. Yoshimura, Phys. Lett. B **88**, 294 (1979).

[206] S. M. Barr, G. Segre, and H. A. Weldon, Phys. Rev. D **20**, 2494 (1979).

[207] D. V. Nanopoulos and S. Weinberg, Phys. Rev. D **20**, 2484 (1979).

[208] A. Yildiz and P. H. Cox, Phys. Rev. D **21**, 906 (1980).

[209] M. Fukugita and T. Yanagida, Physics Letters B **174**, 45 (1986).

[210] A. Pilaftsis and T. E. J. Underwood, Nucl. Phys. B **692**, 303 (2004), arXiv:hep-ph/0309342 .

[211] Hambye, Thomas and Lin, Yin and Notari, Alessio and Papucci, Michele and Strumia, Alessandro, Nucl. Phys. B **695**, 169 (2004), arXiv:hep-ph/0312203 .

[212] W. Buchmuller, P. Di Bari, and M. Plumacher, Annals Phys. **315**, 305 (2005), arXiv:hep-ph/0401240 .

[213] W. Buchmuller, R. D. Peccei, and T. Yanagida, Ann. Rev. Nucl. Part. Sci. **55**, 311 (2005), arXiv:hep-ph/0502169 .

[214] A. Strumia, in *Les Houches Summer School on Theoretical Physics: Session 84: Particle Physics Beyond the Standard Model* (2006) pp. 655–680, arXiv:hep-ph/0608347 .

[215] A. Riotto, J. Phys. Conf. Ser. **335**, 012008 (2011).

[216] A. Pilaftsis, J. Phys. Conf. Ser. **171**, 012017 (2009), arXiv:0904.1182 [hep-ph] .

[217] P. S. Bhupal Dev, P. Millington, A. Pilaftsis, and D. Teresi, Nucl. Phys. B **891**, 128 (2015), arXiv:1410.6434 [hep-ph] .

[218] P. S. Bhupal Dev, P. Millington, A. Pilaftsis, and D. Teresi, Nucl. Phys. B **886**, 569 (2014), arXiv:1404.1003 [hep-ph] .

[219] R. N. Mohapatra and G. Senjanovic, Phys. Rev. D **23**, 165 (1981).

[220] D. Delepine, J. M. Gerard, R. Gonzalez Felipe, and J. Weyers, Phys. Lett. B **386**, 183 (1996), arXiv:hep-ph/9604440 .

[221] M. Carena, M. Quiros, and C. E. M. Wagner, Phys. Lett. B **380**, 81 (1996), arXiv:hep-ph/9603420 .

[222] M. Losada, Phys. Rev. D **56**, 2893 (1997), arXiv:hep-ph/9605266 .

[223] V. A. Rubakov and M. E. Shaposhnikov, Usp. Fiz. Nauk **166**, 493 (1996), arXiv:hep-ph/9603208 .

[224] A. Riotto and M. Trodden, Ann. Rev. Nucl. Part. Sci. **49**, 35 (1999), arXiv:hep-ph/9901362 .

[225] J. M. Cline, in *Les Houches Summer School - Session 86: Particle Physics and Cosmology: The Fabric of Spacetime* (2006) arXiv:hep-ph/0609145 .

[226] G. 't Hooft, Phys. Rev. Lett. **37**, 8 (1976).

[227] S. L. Adler, Phys. Rev. **177**, 2426 (1969).

[228] J. S. Bell and R. Jackiw, Nuovo Cim. A **60**, 47 (1969).

[229] M. Trodden, Rev. Mod. Phys. **71**, 1463 (1999), arXiv:hep-ph/9803479 .

[230] M. D'Onofrio, K. Rummukainen, and A. Tranberg, Phys. Rev. Lett. **113**, 141602 (2014), arXiv:1404.3565 [hep-ph] .

[231] G. D. Moore, C.-r. Hu, and B. Muller, Phys. Rev. D **58**, 045001 (1998), arXiv:hep-ph/9710436 .

[232] D. Bodeker, G. D. Moore, and K. Rummukainen, Phys. Rev. D **61**, 056003 (2000), arXiv:hep-ph/9907545 .

[233] G. D. Moore, in *4th International Conference on Strong and Electroweak Matter* (2000) pp. 82–94, arXiv:hep-ph/0009161 .

[234] Y. Burnier, M. Laine, and M. Shaposhnikov, JCAP **02**, 007 (2006), arXiv:hep-ph/0511246 .

[235] J. A. Harvey and M. S. Turner, Phys. Rev. D **42**, 3344 (1990).

[236] E. Nardi, J. Racker, and E. Roulet, JHEP **09**, 090 (2007), arXiv:0707.0378 [hep-ph] .

[237] N. Bernal, C. S. Fong, Y. F. Perez-Gonzalez, and J. Turner, Phys. Rev. D **106**, 035019 (2022), arXiv:2203.08823 [hep-ph] .

[238] E. W. Kolb and M. S. Turner, *The Early Universe*, Vol. 69 (1990).

[239] A. G. Cohen, D. B. Kaplan, and A. E. Nelson, Ann. Rev. Nucl. Part. Sci. **43**, 27 (1993), arXiv:hep-ph/9302210 .

[240] Quiros, Mariano, in *ICTP Summer School in High-Energy Physics and Cosmology* (1999) pp. 187–259, arXiv:hep-ph/9901312 .

[241] Coleman, Sidney R. and Weinberg, Erick J., Phys. Rev. D **7**, 1888 (1973).

[242] Anderson, Greg W. and Hall, Lawrence J., Phys. Rev. D **45**, 2685 (1992).

[243] Morrissey, David E. and Ramsey-Musolf, Michael J., New J. Phys. **14**, 125003 (2012), arXiv:1206.2942 [hep-ph] .

[244] Aoki, Y. and Csikor, F. and Fodor, Z. and Ukawa, A., Phys. Rev. D **60**, 013001 (1999), arXiv:hep-lat/9901021 .

[245] Csikor, F. and Fodor, Z. and Heitger, J., Phys. Rev. Lett. **82**, 21 (1999), arXiv:hep-ph/9809291 .

[246] Laine, M. and Rummukainen, K., Nucl. Phys. B Proc. Suppl. **73**, 180 (1999), arXiv:hep-lat/9809045 .

[247] Gurtler, M. and Ilgenfritz, Ernst-Michael and Schiller, A., Phys. Rev. D **56**, 3888 (1997), arXiv:hep-lat/9704013 .

[248] G. Servant, Phil. Trans. Roy. Soc. Lond. A **376**, 20170124 (2018), arXiv:1807.11507 [hep-ph] .

[249] Zel'dovich, Ya. B. and Novikov, I. D., Soviet Astron. AJ (Engl. Transl.), **10**, 602 (1967).

[250] Hawking, Stephen, Mon. Not. Roy. Astron. Soc. **152**, 75 (1971).

[251] Carr, Bernard J. and Hawking, S. W., Mon. Not. Roy. Astron. Soc. **168**, 399 (1974).

[252] Carr, Bernard J., Astrophys. J. **201**, 1 (1975).

[253] Hawking, S. W., Nature **248**, 30 (1974).

[254] Hawking, S. W., Commun. Math. Phys. **43**, 199 (1975), [Erratum: Commun.Math.Phys. 46, 206 (1976)].

[255] Barrau, Aurelien, Astropart. Phys. **12**, 269 (2000), arXiv:astro-ph/9907347 .

[256] Lehoucq, R. and Casse, M. and Casandjian, J. -M. and Grenier, I., Astron. Astrophys. **502**, 37 (2009), arXiv:0906.1648 [astro-ph.HE] .

[257] Page, Don N. and Hawking, S. W., Astrophys. J. **206**, 1 (1976).

[258] Belotsky, K. M. and Kirillov, A. A., JCAP **01**, 041 (2015), arXiv:1409.8601 [astro-ph.CO] .

[259] P. N. Okele and M. J. Rees, Astron. Astrophys. **81**, 263 (1980).

[260] Cline, D. B. and Sanders, D. A. and Hong, W., Astrophys. J. **486**, 169 (1997).

[261] R. Bean and J. Magueijo, Phys. Rev. D **66**, 063505 (2002), arXiv:astro-ph/0204486 .

[262] N. Afshordi, P. McDonald, and D. N. Spergel, Astrophys. J. Lett. **594**, L71 (2003), arXiv:astro-ph/0302035 .

[263] M. Ricotti, J. P. Ostriker, and K. J. Mack, Astrophys. J. **680**, 829 (2008), arXiv:0709.0524 [astro-ph] .

[264] Chapline, George F., Nature **253**, 251 (1975).

[265] Bell, Nicole F. and Volkas, R. R., Phys. Rev. D **59**, 107301 (1999), arXiv:astro-ph/9812301 .

[266] Khlopov, M. Yu. and Barrau, Aurelien and Grain, Julien, Class. Quant. Grav. **23**, 1875 (2006), arXiv:astro-ph/0406621 .

[267] Fujita, Tomohiro and Kawasaki, Masahiro and Harigaya, Keisuke and Matsuda, Ryo, Phys. Rev. D **89**, 103501 (2014), arXiv:1401.1909 [astro-ph.CO] .

[268] Lennon, Olivier and March-Russell, John and Petrossian-Byrne, Rudin and Tillim, Hannah, JCAP **04**, 009 (2018), arXiv:1712.07664 [hep-ph] .

[269] Allahverdi, Rouzbeh and Dent, James and Osinski, Jacek, Phys. Rev. D **97**, 055013 (2018), arXiv:1711.10511 [astro-ph.CO] .

[270] Hooper, Dan and Krnjaic, Gordan and McDermott, Samuel D., JHEP **08**, 001 (2019), arXiv:1905.01301 [hep-ph] .

[271] Masina, Isabella, Eur. Phys. J. Plus **135**, 552 (2020), arXiv:2004.04740 [hep-ph] .

[272] Arbey, Alexandre and Auffinger, Jérémy and Sandick, Pearl and Shams Es Haghi, Barmak and Sinha, Kuver, Phys. Rev. D **103**, 123549 (2021), arXiv:2104.04051 [astro-ph.CO] .

[273] A. Cheek, L. Heurtier, Y. F. Perez-Gonzalez, and J. Turner, Phys. Rev. D **105**, 015023 (2022), arXiv:2107.00016 [hep-ph] .

[274] A. Cheek, L. Heurtier, Y. F. Perez-Gonzalez, and J. Turner, Phys. Rev. D **105**, 015022 (2022), arXiv:2107.00013 [hep-ph] .

[275] Smyth, Nolan and Santos-Olmsted, Lillian and Profumo, Stefano, JCAP **03**, 013 (2022), arXiv:2110.14660 [hep-ph] .

[276] García-Bellido, Juan and Carr, Bernard and Clesse, Sebastien, Universe **8**, 12 (2021), arXiv:1904.11482 [astro-ph.CO] .

[277] McDermott, Samuel D. and Yu, Hai-Bo and Zurek, Kathryn M., Phys. Rev. D **85**, 023519 (2012), arXiv:1103.5472 [hep-ph] .

[278] Morrison, Logan and Profumo, Stefano and Yu, Yan, JCAP **05**, 005 (2019), arXiv:1812.10606 [astro-ph.CO] .

[279] B. Carr, F. Kuhnel, and L. Visinelli, Mon. Not. Roy. Astron. Soc. **506**, 3648 (2021), arXiv:2011.01930 [astro-ph.CO] .

[280] J. Adamek, C. T. Byrnes, M. Gosenca, and S. Hotchkiss, Phys. Rev. D **100**, 023506 (2019), arXiv:1901.08528 [astro-ph.CO] .

[281] B. J. Carr, Astrophys. J. **206**, 8 (1976).

[282] Y. B. Zel'dovich, JETP Lett.(USSR)(Engl. Transl.);(United States) **24** (1976).

[283] M. S. Turner, Phys. Lett. B **89**, 155 (1979).

[284] A. F. Grillo, Phys. Lett. B **94**, 364 (1980).

[285] D. Baumann, P. J. Steinhardt, and N. Turok, (2007), arXiv:hep-th/0703250 .

[286] A. Hook, Phys. Rev. D **90**, 083535 (2014), arXiv:1404.0113 [hep-ph] .

[287] D. Hooper and G. Krnjaic, Phys. Rev. D **103**, 043504 (2021), arXiv:2010.01134 [hep-ph] .

[288] D. Inman and Y. Ali-Haïmoud, Phys. Rev. D **100**, 083528 (2019), arXiv:1907.08129 [astro-ph.CO] .

[289] G. M. Fuller, A. Kusenko, and V. Takhistov, Phys. Rev. Lett. **119**, 061101 (2017), arXiv:1704.01129 [astro-ph.HE] .

[290] D. Bödeker, F. Kühnel, I. M. Oldengott, and D. J. Schwarz, Phys. Rev. D **103**, 063506 (2021), arXiv:2011.07283 [astro-ph.CO] .

[291] B. P. Abbott *et al.* (LIGO Scientific, Virgo), Phys. Rev. Lett. **116**, 061102 (2016), arXiv:1602.03837 [gr-qc] .

[292] B. P. Abbott *et al.* (LIGO Scientific, Virgo), Phys. Rev. X **6**, 041015 (2016), [Erratum: Phys.Rev.X 8, 039903 (2018)], arXiv:1606.04856 [gr-qc] .

[293] R. Abbott *et al.* (LIGO Scientific, VIRGO, KAGRA), (2021), arXiv:2111.03606 [gr-qc] .

[294] H. Niikura, M. Takada, S. Yokoyama, T. Sumi, and S. Masaki, Phys. Rev. D **99**, 083503 (2019), arXiv:1901.07120 [astro-ph.CO] .

[295] E. Mediavilla, J. Jiménez-Vicente, J. A. Muñoz, H. Vives-Arias, and J. Calderón-Infante, Astrophys. J. Lett. **836**, L18 (2017), arXiv:1702.00947 [astro-ph.GA] .

[296] G. E. Brown, C. H. Lee, and H. A. Bethe, (1999), arXiv:astro-ph/9909270 .

[297] L. Wyrzykowski and I. Mandel, Astron. Astrophys. **636**, A20 (2020), arXiv:1904.07789 [astro-ph.SR] .

[298] A. Kashlinsky, R. G. Arendt, J. C. Mather, and S. H. Moseley, Nature **438**, 45 (2005), arXiv:astro-ph/0511105 .

[299] S. Clesse and J. García-Bellido, Phys. Dark Univ. **22**, 137 (2018), arXiv:1711.10458 [astro-ph.CO] .

[300] I. Labbé, P. van Dokkum, E. Nelson, R. Bezanson, K. A. Suess, J. Leja, G. Brammer, K. Whitaker, E. Mathews, M. Stefanon, *et al.*, Nature , 1 (2023).

[301] J. Smirnov, A. Goobar, T. Linden, and E. Mörtsell, (2022), arXiv:2211.00013 [astro-ph.CO] .

[302] Abbott, R. and others (KAGRA, VIRGO, LIGO Scientific), Phys. Rev. X **13**, 011048 (2023), arXiv:2111.03634 [astro-ph.HE] .

[303] B. Carr, S. Clesse, J. García-Bellido, and F. Kühnel, Phys. Dark Univ. **31**, 100755 (2021), arXiv:1906.08217 [astro-ph.CO] .

[304] B. J. Carr, J. H. Gilbert, and J. E. Lidsey, Phys. Rev. D **50**, 4853 (1994), arXiv:astro-ph/9405027 .

[305] D. Blais, C. Kiefer, and D. Polarski, Phys. Lett. B **535**, 11 (2002), arXiv:astro-ph/0203520 .

[306] J. H. MacGibbon, Nature **329**, 308 (1987).

[307] J. D. Barrow, E. J. Copeland, and A. R. Liddle, Phys. Rev. D **46**, 645 (1992).

[308] A. M. Green and A. R. Liddle, Phys. Rev. D **56**, 6166 (1997), arXiv:astro-ph/9704251 .

[309] S. Alexeyev, A. Barrau, G. Boudoul, O. Khovanskaya, and M. Sazhin, Class. Quant. Grav. **19**, 4431 (2002), arXiv:gr-qc/0201069 .

[310] P. Chen and R. J. Adler, Nucl. Phys. B Proc. Suppl. **124**, 103 (2003), arXiv:gr-qc/0205106 .

[311] A. Barrau, D. Blais, G. Boudoul, and D. Polarski, Annalen Phys. **13**, 115 (2004), arXiv:astro-ph/0303330 .

[312] P. Chen, New Astron. Rev. **49**, 233 (2005), arXiv:astro-ph/0406514 .

[313] K. Nozari and S. H. Mehdipour, Mod. Phys. Lett. A **20**, 2937 (2005), arXiv:0809.3144 [gr-qc] .

[314] S. Alexander and P. Meszaros, (2007), arXiv:hep-th/0703070 .

[315] J. D. Barrow, E. J. Copeland, E. W. Kolb, and A. R. Liddle, Phys. Rev. D **43**, 984 (1991).

[316] N. Upadhyay, P. Das Gupta, and R. P. Saxena, Phys. Rev. D **60**, 063513 (1999), arXiv:astro-ph/9903253 .

[317] A. D. Dolgov, P. D. Naselsky, and I. D. Novikov, (2000), arXiv:astro-ph/0009407 .

[318] Bugaev, E. V. and Elbakidze, M. G. and Konishchev, K. V., Phys. Atom. Nucl. **66**, 476 (2003), arXiv:astro-ph/0110660 .

[319] B. J. Carr, K. Kohri, Y. Sendouda, and J. Yokoyama, Phys. Rev. D **81**, 104019 (2010), arXiv:0912.5297 [astro-ph.CO] .

[320] E. Bugaev and P. Klimai, Phys. Rev. D **79**, 103511 (2009), arXiv:0812.4247 [astro-ph] .

[321] E. V. Bugaev and K. V. Konishchev, Phys. Rev. D **66**, 084004 (2002), arXiv:astro-ph/0206082 .

[322] D. Stojkovic, K. Freese, and G. D. Starkman, Phys. Rev. D **72**, 045012 (2005), arXiv:hep-ph/0505026 .

[323] A. M. Green, Phys. Rev. D **60**, 063516 (1999), arXiv:astro-ph/9903484 .

[324] M. Lemoine, Phys. Lett. B **481**, 333 (2000), arXiv:hep-ph/0001238 .

[325] M. Izawa and K. Sato, Prog. Theor. Phys. **72**, 768 (1984).

[326] D. Stojkovic and K. Freese, Phys. Lett. B **606**, 251 (2005), arXiv:hep-ph/0403248 .

[327] P. He and L.-Z. Fang, Astrophys. J. Lett. **568**, L1 (2002), arXiv:astro-ph/0202218 .

[328] K. J. Mack and D. H. Wesley, (2008), arXiv:0805.1531 [astro-ph] .

[329] E. L. Wright, Astrophys. J. **459**, 487 (1996), arXiv:astro-ph/9509074 .

[330] M. S. Turner, Nature **297**, 379 (1982).

[331] P. Kiraly, J. Szabelski, J. Wdowczyk, and A. W. Wolfendale, Nature **293**, 120 (1981).

[332] D. B. Cline and W.-p. Hong, Astrophys. J. Lett. **401**, L57 (1992).

[333] M. J. Rees, Nature **266**, 333 (1977).

[334] F. Halzen, E. Zas, J. H. MacGibbon, and T. C. Weekes, Nature **353**, 807 (1991).

[335] T. Kanazawa, M. Kawasaki, and T. Yanagida, Phys. Lett. B **482**, 174 (2000), arXiv:hep-ph/0002236 .

[336] D. Blais, T. Bringmann, C. Kiefer, and D. Polarski, Phys. Rev. D **67**, 024024 (2003), arXiv:astro-ph/0206262 .

[337] R. Saito, J. Yokoyama, and R. Nagata, JCAP **06**, 024 (2008), arXiv:0804.3470 [astro-ph] .

[338] Frampton, Paul H. and Kawasaki, Masahiro and Takahashi, Fuminobu and Yanagida, Tsutomu T., JCAP **04**, 023 (2010), arXiv:1001.2308 [hep-ph] .

[339] K. J. Mack, J. P. Ostriker, and M. Ricotti, Astrophys. J. **665**, 1277 (2007), arXiv:astro-ph/0608642 .

[340] P. Meszaros, Astron. Astrophys. **38**, 5 (1975).

[341] B. Carr, Astronomy and Astrophysics **56**, 377 (1977).

[342] K. Freese, R. Price, and D. N. Schramm, The Astrophysical Journal **275**, 405 (1983).

[343] B. Carr and J. Silk, Astrophysical Journal, Part 1 (ISSN 0004-637X), vol. 268, May 1, 1983, p. 1-16. **268**, 1 (1983).

[344] B. J. Carr and M. J. Rees, Monthly Notices of the Royal Astronomical Society **206**, 801 (1984).

[345] N. Duechting, Phys. Rev. D **70**, 064015 (2004), arXiv:astro-ph/0406260 .

[346] M. Y. Khlopov, S. G. Rubin, and A. S. Sakharov, Astropart. Phys. **23**, 265 (2005), arXiv:astro-ph/0401532 .

[347] B. Carr, Astronomy and Astrophysics **89**, 6 (1980).

[348] Nakamura, Takashi and Sasaki, Misao and Tanaka, Takahiro and Thorne, Kip S., Astrophys. J. Lett. **487**, L139 (1997), arXiv:astro-ph/9708060 .

[349] K. Ioka, T. Tanaka, and T. Nakamura, Phys. Rev. D **60**, 083512 (1999), arXiv:astro-ph/9809395 .

[350] K. T. Inoue and T. Tanaka, Phys. Rev. Lett. **91**, 021101 (2003), arXiv:gr-qc/0303058 .

[351] K. Hayasaki, K. Takahashi, Y. Sendouda, and S. Nagataki, Publ. Astron. Soc. Jap. **68**, 66 (2016), arXiv:0909.1738 [astro-ph.CO] .

[352] B. J. Carr and J. E. Lidsey, Phys. Rev. D **48**, 543 (1993).

[353] S. M. Leach, I. J. Grivell, and A. R. Liddle, Phys. Rev. D **62**, 043516 (2000), arXiv:astro-ph/0004296 .

[354] K. Kohri, C.-M. Lin, and D. H. Lyth, JCAP **12**, 004 (2007), arXiv:0707.3826 [hep-ph] .

[355] H. M. Hodges and G. R. Blumenthal, Phys. Rev. D **42**, 3329 (1990).

[356] P. Ivanov, P. Naselsky, and I. Novikov, Phys. Rev. D **50**, 7173 (1994).

[357] J. Yokoyama, Astron. Astrophys. **318**, 673 (1997), arXiv:astro-ph/9509027 .

[358] J. Yokoyama, Phys. Rev. D **58**, 083510 (1998), arXiv:astro-ph/9802357 .

[359] J. Yokoyama, Phys. Rept. **307**, 133 (1998).

[360] M. Kawasaki and T. Yanagida, Phys. Rev. D **59**, 043512 (1999), arXiv:hep-ph/9807544 .

[361] J. Yokoyama, Prog. Theor. Phys. Suppl. **136**, 338 (1999).

[362] R. Easther and M. Parry, Phys. Rev. D **62**, 103503 (2000), arXiv:hep-ph/9910441 .

[363] A. Barrau, D. Blais, G. Boudoul, and D. Polarski, Phys. Lett. B **551**, 218 (2003), arXiv:astro-ph/0210149 .

[364] S. Chongchitnan and G. Efstathiou, JCAP **01**, 011 (2007), arXiv:astro-ph/0611818 .

[365] K. Nozari, Astropart. Phys. **27**, 169 (2007), arXiv:hep-th/0701274 .

[366] J. Garcia-Bellido, A. D. Linde, and D. Wands, Phys. Rev. D **54**, 6040 (1996), arXiv:astro-ph/9605094 .

[367] L. Randall, M. Soljacic, and A. H. Guth, Nucl. Phys. B **472**, 377 (1996), arXiv:hep-ph/9512439 .

[368] Lidsey, James E. and Matos, Tonatiuh and Urena-Lopez, L. Arturo, Phys. Rev. D **66**, 023514 (2002), arXiv:astro-ph/0111292 .

[369] Easther, Richard and Khoury, Justin and Schalm, Koenraad, JCAP **06**, 006 (2004), arXiv:hep-th/0402218 .

[370] Lyth, David. H and Malik, Karim A. and Sasaki, Misao and Zaballa, Ignacio, JCAP **01**, 011 (2006), arXiv:astro-ph/0510647 .

[371] Kohri, Kazunori and Lyth, David H. and Melchiorri, Alessandro, JCAP **04**, 038 (2008), arXiv:0711.5006 [hep-ph] .

[372] Bugaev, Edgar and Klimai, Peter, Phys. Rev. D **78**, 063515 (2008), arXiv:0806.4541 [astro-ph] .

[373] Alabidi, Laila and Kohri, Kazunori, Phys. Rev. D **80**, 063511 (2009), arXiv:0906.1398 [astro-ph.CO] .

[374] Taruya, A., Phys. Rev. D **59**, 103505 (1999), arXiv:hep-ph/9812342 .

[375] Bassett, Bruce A. and Tsujikawa, Shinji, Phys. Rev. D **63**, 123503 (2001), arXiv:hep-ph/0008328 .

[376] Green, Anne M. and Malik, Karim A., Phys. Rev. D **64**, 021301 (2001), arXiv:hep-ph/0008113 .

[377] Finelli, F. and Khlebnikov, S., Phys. Lett. B **504**, 309 (2001), arXiv:hep-ph/0009093 .

[378] Kawaguchi, Toshihiro and Kawasaki, Masahiro and Takayama, Tsutomu and Yamaguchi, Masahide and Yokoyama, Jun'ichi, Mon. Not. Roy. Astron. Soc. **388**, 1426 (2008), arXiv:0711.3886 [astro-ph] .

[379] Kawasaki, Masahiro and Takayama, Tsutomu and Yamaguchi, Masahide and Yokoyama, Jun'ichi, Mod. Phys. Lett. A **22**, 1911 (2007).

[380] Jedamzik, Karsten, Phys. Rev. D **55**, 5871 (1997), arXiv:astro-ph/9605152 .

[381] Widerin, Peter and Schmid, Christoph, (1998), arXiv:astro-ph/9808142 .

[382] Jedamzik, K. and Niemeyer, Jens C., Phys. Rev. D **59**, 124014 (1999), arXiv:astro-ph/9901293 .

[383] Khlopov, M. Yu. and Polnarev, A. G., Phys. Lett. B **97**, 383 (1980).

[384] Crawford, Matt and Schramm, David N., Nature **298**, 538 (1982).

[385] Hawking, S. W. and Moss, I. G. and Stewart, J. M., Phys. Rev. D **26**, 2681 (1982).

[386] Kodama, Hideo and Sasaki, Misao and Sato, Katsuhiko, Prog. Theor. Phys. **68**, 1979 (1982).

[387] La, Daile and Steinhardt, Paul J., Phys. Lett. B **220**, 375 (1989).

[388] Moss, I. G., Phys. Rev. D **50**, 676 (1994).

[389] Konoplich, R. V. and Rubin, S. G. and Sakharov, A. S. and Khlopov, M. Yu., Phys. Atom. Nucl. **62**, 1593 (1999).

[390] Hogan, C. J., Phys. Lett. B **143**, 87 (1984).

[391] Hawking, S. W., Phys. Lett. B **231**, 237 (1989).

[392] Polnarev, Alexander and Zembowicz, Robert, Phys. Rev. D **43**, 1106 (1991).

[393] Garriga, Jaume and Sakellariadou, Maria, Phys. Rev. D **48**, 2502 (1993), arXiv:hep-th/9303024 .

[394] Caldwell, R. R. and Casper, Paul, Phys. Rev. D **53**, 3002 (1996), arXiv:gr-qc/9509012 .

[395] Cheng, Hong-Bo and Li, Xin-Zhou, Chin. Phys. Lett. **13**, 317 (1996).

[396] MacGibbon, Jane H. and Brandenberger, Robert H. and Wichoski, U. F., Phys. Rev. D **57**, 2158 (1998), arXiv:astro-ph/9707146 .

[397] Hansen, R. N. and Christensen, M. and Larsen, A. L., Int. J. Mod. Phys. A **15**, 4433 (2000), arXiv:gr-qc/9902048 .

[398] Nagasawa, M., Gen. Rel. Grav. **37**, 1635 (2005).

[399] Matsuda, Tomohiro, JHEP **04**, 017 (2006), arXiv:hep-ph/0509062 .

[400] Lake, Matthew and Thomas, Steven and Ward, John, JHEP **12**, 033 (2009), arXiv:0906.3695 [hep-ph] .

[401] Berezin, V. A. and Kuzmin, V. A. and Tkachev, I. I., Phys. Lett. B **120**, 91 (1983).

[402] Caldwell, R. R. and Chamblin, A. and Gibbons, G. W., Phys. Rev. D **53**, 7103 (1996), arXiv:hep-th/9602126 .

[403] Khlopov, M. Yu. and Konoplich, R. V. and Rubin, S. G. and Sakharov, A. S., Grav. Cosmol. **6**, 153 (2000).

[404] Rubin, S. G. and Khlopov, M. Yu. and Sakharov, A. S., Grav. Cosmol. **6**, 51 (2000), arXiv:hep-ph/0005271 .

[405] Rubin, Sergei G. and Sakharov, Alexander S. and Khlopov, Maxim Yu., J. Exp. Theor. Phys. **91**, 921 (2001), arXiv:hep-ph/0106187 .

[406] Dokuchaev, Vyacheslav and Eroshenko, Yury and Rubin, Sergei, Grav. Cosmol. **11**, 99 (2005), arXiv:astro-ph/0412418 .

[407] B. Carr, F. Kuhnel, and M. Sandstad, Phys. Rev. D **94**, 083504 (2016), arXiv:1607.06077 [astro-ph.CO] .

[408] Musco, Ilia, Phys. Rev. D **100**, 123524 (2019), arXiv:1809.02127 [gr-qc] .

[409] Niemeyer, Jens C. and Jedamzik, K., Phys. Rev. Lett. **80**, 5481 (1998), arXiv:astro-ph/9709072 .

[410] Niemeyer, Jens C. and Jedamzik, K., Phys. Rev. D **59**, 124013 (1999), arXiv:astro-ph/9901292 .

[411] Y. Akrami *et al.* (Planck), Astron. Astrophys. **641**, A10 (2020), arXiv:1807.06211 [astro-ph.CO] .

[412] Press, William H. and Schechter, Paul, Astrophys. J. **187**, 425 (1974).

[413] Sasaki, Misao, Prog. Theor. Phys. **76**, 1036 (1986).

[414] Mukhanov, Viatcheslav F. and Feldman, H. A. and Brandenberger, Robert H., Phys. Rept. **215**, 203 (1992).

[415] Young, Sam and Byrnes, Christian T. and Sasaki, Misao, JCAP **07**, 045 (2014), arXiv:1405.7023 [gr-qc] .

[416] M. Sasaki, T. Suyama, T. Tanaka, and S. Yokoyama, Class. Quant. Grav. **35**, 063001 (2018), arXiv:1801.05235 [astro-ph.CO] .

[417] J. H. MacGibbon, Phys. Rev. D **44**, 376 (1991).

[418] Lehmann, Benjamin V. and Johnson, Christian and Profumo, Stefano and Schwemberger, Thomas, JCAP **10**, 046 (2019), arXiv:1906.06348 [hep-ph] .

[419] J. F. Navarro, C. S. Frenk, and S. D. M. White, Astrophys. J. **490**, 493 (1997), arXiv:astro-ph/9611107 .

[420] Ricotti, Massimo, Astrophys. J. **662**, 53 (2007), arXiv:0706.0864 [astro-ph] .

[421] De Luca, V. and Franciolini, G. and Pani, P. and Riotto, A., JCAP **06**, 044 (2020), arXiv:2005.05641 [astro-ph.CO] .

[422] De Luca, V. and Franciolini, G. and Pani, P. and Riotto, A., JCAP **04**, 052 (2020), arXiv:2003.02778 [astro-ph.CO] .

[423] Y. Ali-Haïmoud and M. Kamionkowski, Phys. Rev. D **95**, 043534 (2017), arXiv:1612.05644 [astro-ph.CO] .

[424] Horowitz, Benjamin, (2016), arXiv:1612.07264 [astro-ph.CO] .

[425] V. Poulin, P. D. Serpico, F. Calore, S. Clesse, and K. Kohri, Phys. Rev. D **96**, 083524 (2017), arXiv:1707.04206 [astro-ph.CO] .

[426] Serpico, Pasquale D. and Poulin, Vivian and Inman, Derek and Kohri, Kazunori, Phys. Rev. Res. **2**, 023204 (2020), arXiv:2002.10771 [astro-ph.CO] .

[427] J. D. Barrow, E. J. Copeland, and A. R. Liddle, Mon. Not. Roy. Astron. Soc. **253**, 675 (1991).

[428] Lunardini, Cecilia and Perez-Gonzalez, Yuber F., JCAP **08**, 014 (2020), arXiv:1910.07864 [hep-ph] .

[429] N. Bernal and F. Hajkarim, Phys. Rev. D **100**, 063502 (2019), arXiv:1905.10410 [astro-ph.CO] .

[430] P. Arias, N. Bernal, A. Herrera, and C. Maldonado, JCAP **10**, 047 (2019), arXiv:1906.04183 [hep-ph] .

[431] Domènech, Guillem and Lin, Chunshan and Sasaki, Misao, JCAP **04**, 062 (2021), [Erratum: JCAP 11, E01 (2021)], arXiv:2012.08151 [gr-qc] .

[432] Papanikolaou, Theodoros and Vennin, Vincent and Langlois, David, JCAP **03**, 053 (2021), arXiv:2010.11573 [astro-ph.CO] .

[433] J. Chluba, A. Ravenni, and S. K. Acharya, Mon. Not. Roy. Astron. Soc. **498**, 959 (2020), arXiv:2005.11325 [astro-ph.CO] .

[434] B. Dasgupta, R. Laha, and A. Ray, Phys. Rev. Lett. **125**, 101101 (2020), arXiv:1912.01014 [hep-ph] .

[435] W. DeRocco and P. W. Graham, Phys. Rev. Lett. **123**, 251102 (2019), arXiv:1906.07740 [astro-ph.CO] .

[436] V. Poulin, J. Lesgourgues, and P. D. Serpico, JCAP **03**, 043 (2017), arXiv:1610.10051 [astro-ph.CO] .

[437] S. Clark, B. Dutta, Y. Gao, L. E. Strigari, and S. Watson, Phys. Rev. D **95**, 083006 (2017), arXiv:1612.07738 [astro-ph.CO] .

[438] S. Clark, B. Dutta, Y. Gao, Y.-Z. Ma, and L. E. Strigari, Phys. Rev. D **98**, 043006 (2018), arXiv:1803.09390 [astro-ph.HE] .

[439] R. Laha, Phys. Rev. Lett. **123**, 251101 (2019), arXiv:1906.09994 [astro-ph.HE] .

[440] M. Boudaud and M. Cirelli, Phys. Rev. Lett. **122**, 041104 (2019), arXiv:1807.03075 [astro-ph.HE] .

[441] R. Laha, J. B. Muñoz, and T. R. Slatyer, Phys. Rev. D **101**, 123514 (2020), arXiv:2004.00627 [astro-ph.CO] .

[442] H. Kim, Mon. Not. Roy. Astron. Soc. **504**, 5475 (2021), arXiv:2007.07739 [hep-ph] .

[443] K. Bays *et al.* (Super-Kamiokande), Phys. Rev. D **85**, 052007 (2012), arXiv:1111.5031 [hep-ex] .

[444] R. A. Allsman *et al.* (Macho), Astrophys. J. Lett. **550**, L169 (2001), arXiv:astro-ph/0011506 .

[445] D. Croon, D. McKeen, N. Raj, and Z. Wang, Phys. Rev. D **102**, 083021 (2020), arXiv:2007.12697 [astro-ph.CO] .

[446] P. Tisserand *et al.* (EROS-2), Astron. Astrophys. **469**, 387 (2007), arXiv:astro-ph/0607207 .

[447] M. Zumalacarregui and U. Seljak, Phys. Rev. Lett. **121**, 141101 (2018), arXiv:1712.02240 [astro-ph.CO] .

[448] M. Oguri, J. M. Diego, N. Kaiser, P. L. Kelly, and T. Broadhurst, Phys. Rev. D **97**, 023518 (2018), arXiv:1710.00148 [astro-ph.CO] .

[449] B. J. Kavanagh, D. Gaggero, and G. Bertone, Phys. Rev. D **98**, 023536 (2018), arXiv:1805.09034 [astro-ph.CO] .

[450] B. P. Abbott *et al.* (LIGO Scientific, Virgo), Phys. Rev. Lett. **123**, 161102 (2019), arXiv:1904.08976 [astro-ph.CO] .

[451] Z.-C. Chen and Q.-G. Huang, JCAP **08**, 039 (2020), arXiv:1904.02396 [astro-ph.CO] .

[452] M. A. Monroy-Rodríguez and C. Allen, Astrophys. J. **790**, 159 (2014), arXiv:1406.5169 [astro-ph.GA] .

[453] T. D. Brandt, Astrophys. J. Lett. **824**, L31 (2016), arXiv:1605.03665 [astro-ph.GA] .

[454] J. Manshanden, D. Gaggero, G. Bertone, R. M. T. Connors, and M. Ricotti, JCAP **06**, 026 (2019), arXiv:1812.07967 [astro-ph.HE] .

[455] A. Hektor, G. Hütsi, L. Marzola, M. Raidal, V. Vaskonen, and H. Veermäe, Phys. Rev. D **98**, 023503 (2018), arXiv:1803.09697 [astro-ph.CO] .

[456] P. Lu, V. Takhistov, G. B. Gelmini, K. Hayashi, Y. Inoue, and A. Kusenko, Astrophys. J. Lett. **908**, L23 (2021), arXiv:2007.02213 [astro-ph.CO] .

[457] A. M. Green and B. J. Kavanagh, J. Phys. G **48**, 043001 (2021), arXiv:2007.10722 [astro-ph.CO] .

[458] S. Miyama and K. Sato, Prog. Theor. Phys. **59**, 1012 (1978).

[459] I. B. Zeldovich, A. Starobinskii, M. I. Khlopov, and V. Chechetkin, Soviet Astronomy Letters, vol. 3, May-June 1977, p. 110-112. Translation. Pisma v Astronomicheskii Zhurnal, vol. 3, May 1977, p. 208-211. **3**, 110 (1977).

[460] D. Lindley, Monthly Notices of the Royal Astronomical Society **193**, 593 (1980), https://academic.oup.com/mnras/article-pdf/193/3/593/18194205/mnras193-0593.pdf .

[461] J. R. Ellis, G. B. Gelmini, J. L. Lopez, D. V. Nanopoulos, and S. Sarkar, Nucl. Phys. B **373**, 399 (1992).

[462] K. Kohri and J. Yokoyama, Phys. Rev. D **61**, 023501 (2000), arXiv:astro-ph/9908160 .

[463] H. Tashiro and N. Sugiyama, Phys. Rev. D **78**, 023004 (2008), arXiv:0801.3172 [astro-ph] .

[464] M. Lucca, N. Schöneberg, D. C. Hooper, J. Lesgourgues, and J. Chluba, JCAP **02**, 026 (2020), arXiv:1910.04619 [astro-ph.CO] .

[465] S. K. Acharya and R. Khatri, JCAP **02**, 010 (2020), arXiv:1912.10995 [astro-ph.CO] .

[466] G. Ballesteros, J. Coronado-Blázquez, and D. Gaggero, Phys. Lett. B **808**, 135624 (2020), arXiv:1906.10113 [astro-ph.CO] .

[467] MacGibbon, Jane H. and Carr, Bernard J., Astrophys. J. **371**, 447 (1991).

[468] B. Paczynski, Astrophys. J. **304**, 1 (1986).

[469] P. Mróz, A. Udalski, J. Skowron, R. Poleski, S. Kozłowski, M. K. Szymański, I. Soszyński, Ł. Wyrzykowski, P. Pietrukowicz, K. Ulaczyk, D. Skowron, and M. Pawlak, Nature **548**, 183 (2017).

[470] K. Griest, A. M. Cieplak, and M. J. Lehner, Astrophys. J. **786**, 158 (2014), arXiv:1307.5798 [astro-ph.CO] .

[471] T. Venumadhav, L. Dai, and J. Miralda-Escudé, Astrophys. J. **850**, 49 (2017), arXiv:1707.00003 [astro-ph.CO] .

[472] P. L. Kelly *et al.*, Nature Astron. **2**, 334 (2018), arXiv:1706.10279 [astro-ph.GA] .

[473] J. M. Diego *et al.*, Astrophys. J. **857**, 25 (2018), arXiv:1706.10281 [astro-ph.CO] .

[474] R. B. Metcalf and J. Silk, Phys. Rev. Lett. **98**, 071302 (2007), arXiv:astro-ph/0612253 .

[475] J. Garcia-Bellido, S. Clesse, and P. Fleury, Phys. Dark Univ. **20**, 95 (2018), arXiv:1712.06574 [astro-ph.CO] .

[476] K. Liao, S. B. Zhang, Z. Li, and H. Gao, Astrophys. J. **896**, L11 (2020), arXiv:2003.13349 [astro-ph.CO] .

[477] K. Ioka, T. Chiba, T. Tanaka, and T. Nakamura, Phys. Rev. D **58**, 063003 (1998), arXiv:astro-ph/9807018 .

[478] M. Sasaki, T. Suyama, T. Tanaka, and S. Yokoyama, Phys. Rev. Lett. **117**, 061101 (2016), [Erratum: Phys.Rev.Lett. 121, 059901 (2018)], arXiv:1603.08338 [astro-ph.CO] .

[479] Y. Ali-Haïmoud, E. D. Kovetz, and M. Kamionkowski, Phys. Rev. D **96**, 123523 (2017), arXiv:1709.06576 [astro-ph.CO] .

[480] S. Wang, Y.-F. Wang, Q.-G. Huang, and T. G. F. Li, Phys. Rev. Lett. **120**, 191102 (2018), arXiv:1610.08725 [astro-ph.CO] .

[481] M. Raidal, V. Vaskonen, and H. Veermäe, JCAP **09**, 037 (2017), arXiv:1707.01480 [astro-ph.CO] .

[482] B. P. Abbott *et al.* (LIGO Scientific, Virgo), Phys. Rev. D **100**, 061101 (2019), arXiv:1903.02886 [gr-qc] .

[483] A. H. Nitz and Y.-F. Wang, Phys. Rev. Lett. **126**, 021103 (2021), arXiv:2007.03583 [astro-ph.HE] .

[484] J. R. Chisholm, Phys. Rev. D **73**, 083504 (2006), arXiv:astro-ph/0509141 .

[485] J. R. Chisholm, Phys. Rev. D **84**, 124031 (2011), arXiv:1110.4402 [astro-ph.CO] .

[486] M. Raidal, C. Spethmann, V. Vaskonen, and H. Veermäe, JCAP **02**, 018 (2019), arXiv:1812.01930 [astro-ph.CO] .

[487] S. Young and A. S. Hamers, JCAP **10**, 036 (2020), arXiv:2006.15023 [astro-ph.CO] .

[488] V. Vaskonen and H. Veermäe, Phys. Rev. D **101**, 043015 (2020), arXiv:1908.09752 [astro-ph.CO] .

[489] K. Jedamzik, JCAP **09**, 022 (2020), arXiv:2006.11172 [astro-ph.CO] .

[490] K. Jedamzik, Phys. Rev. Lett. **126**, 051302 (2021), arXiv:2007.03565 [astro-ph.CO] .

[491] M. Trashorras, J. García-Bellido, and S. Nesseris, Universe **7**, 18 (2021), arXiv:2006.15018 [astro-ph.CO] .

[492] G. Ballesteros, P. D. Serpico, and M. Taoso, JCAP **10**, 043 (2018), arXiv:1807.02084 [astro-ph.CO] .

[493] T. Bringmann, P. F. Depta, V. Domcke, and K. Schmidt-Hoberg, Phys. Rev. D **99**, 063532 (2019), arXiv:1808.05910 [astro-ph.CO] .

[494] V. Atal, A. Sanglas, and N. Triantafyllou, JCAP **11**, 036 (2020), arXiv:2007.07212 [astro-ph.CO] .

[495] J. N. Bahcall, P. Hut, and S. Tremaine, The Astrophysical Journal **290**, 15 (1985).

[496] J. Yoo, J. Chaname, and A. Gould, Astrophys. J. **601**, 311 (2004), arXiv:astro-ph/0307437 .

[497] C. Allen and M. A. Monroy-Rodríguez, Astrophys. J. **790**, 158 (2014), arXiv:1406.5164 [astro-ph.SR] .

[498] Carr, B. J., Monthly Notices of the Royal Astronomical Society **194**, 639 (1981).

[499] V. Bosch-Ramon and N. Bellomo, Astron. Astrophys. **638**, A132 (2020), arXiv:2004.11224 [astro-ph.CO] .

[500] D. Gaggero, G. Bertone, F. Calore, R. M. T. Connors, M. Lovell, S. Markoff, and E. Storm, Phys. Rev. Lett. **118**, 241101 (2017), arXiv:1612.00457 [astro-ph.HE] .

[501] Y. Inoue and A. Kusenko, JCAP **10**, 034 (2017), arXiv:1705.00791 [astro-ph.CO] .

[502] B. Carr, M. Raidal, T. Tenkanen, V. Vaskonen, and H. Veermäe, Phys. Rev. D **96**, 023514 (2017), arXiv:1705.05567 [astro-ph.CO] .

[503] S. Wang, D.-M. Xia, X. Zhang, S. Zhou, and Z. Chang, Phys. Rev. D **103**, 043010 (2021), arXiv:2010.16053 [hep-ph] .

[504] N. Vinyoles, A. M. Serenelli, F. L. Villante, S. Basu, J. Bergström, M. C. Gonzalez-Garcia, M. Maltoni, C. Peña Garay, and N. Song, Astrophys. J. **835**, 202 (2017), arXiv:1611.09867 [astro-ph.SR] .

[505] J. F. Beacom, Ann. Rev. Nucl. Part. Sci. **60**, 439 (2010), arXiv:1004.3311 [astro-ph.HE] .

[506] G. Battistoni, A. Ferrari, T. Montaruli, and P. R. Sala, Astropart. Phys. **23**, 526 (2005).

[507] M. Honda, T. Kajita, K. Kasahara, and S. Midorikawa, Phys. Rev. D **83**, 123001 (2011), arXiv:1102.2688 [astro-ph.HE] .

[508] A. Priya and C. Lunardini, JCAP **11**, 031 (2017), arXiv:1705.02122 [astro-ph.HE] .

[509] S. Horiuchi, K. Sumiyoshi, K. Nakamura, T. Fischer, A. Summa, T. Takiwaki, H.-T. Janka, and K. Kotake, Mon. Not. Roy. Astron. Soc. **475**, 1363 (2018), arXiv:1709.06567 [astro-ph.HE] .

[510] K. Møller, A. M. Suliga, I. Tamborra, and P. B. Denton, JCAP **05**, 066 (2018), arXiv:1804.03157 [astro-ph.HE] .

[511] B. C. Lacki and J. F. Beacom, Astrophys. J. Lett. **720**, L67 (2010), arXiv:1003.3466 [astro-ph.CO] .

[512] S. M. Boucenna, F. Kuhnel, T. Ohlsson, and L. Visinelli, JCAP **07**, 003 (2018), arXiv:1712.06383 [hep-ph] .

[513] G. Bertone, A. M. Coogan, D. Gaggero, B. J. Kavanagh, and C. Weniger, Phys. Rev. D **100**, 123013 (2019), arXiv:1905.01238 [hep-ph] .

[514] R.-G. Cai, Y.-C. Ding, X.-Y. Yang, and Y.-F. Zhou, JCAP **03**, 057 (2021), arXiv:2007.11804 [astro-ph.CO] .

[515] M. P. Hertzberg, S. Nurmi, E. D. Schiappacasse, and T. T. Yanagida, Phys. Rev. D **103**, 063025 (2021), arXiv:2011.05922 [hep-ph] .

[516] K. Kadota and J. Silk, Phys. Rev. D **103**, 043530 (2021), arXiv:2012.03698 [astro-ph.CO] .

[517] H. Tashiro and K. Kadota, Phys. Rev. D **103**, 123532 (2021), arXiv:2104.09738 [astro-ph.CO] .

[518] D. S. Akerib *et al.* (LZ), Phys. Rev. D **101**, 052002 (2020), arXiv:1802.06039 [astro-ph.IM] .

[519] L. Pattavina, N. Ferreiro Iachellini, and I. Tamborra, Phys. Rev. D **102**, 063001 (2020), arXiv:2004.06936 [astro-ph.HE] .

[520] G. D. Starkman, A. Gould, R. Esmailzadeh, and S. Dimopoulos, Phys. Rev. D **41**, 3594 (1990).

[521] G. D. Mack, J. F. Beacom, and G. Bertone, Phys. Rev. D **76**, 043523 (2007), arXiv:0705.4298 [astro-ph] .

[522] B. J. Kavanagh, R. Catena, and C. Kouvaris, JCAP **01**, 012 (2017), arXiv:1611.05453 [hep-ph] .

[523] T. Emken and C. Kouvaris, Phys. Rev. D **97**, 115047 (2018), arXiv:1802.04764 [hep-ph] .

[524] P. Capuano, G. De Luca, F. Di Sena, P. Gasparini, and R. Scarpa, Journal of applied geophysics **39**, 25 (1998).

[525] G. Tesic (VERITAS), J. Phys. Conf. Ser. **375**, 052024 (2012).

[526] J.-F. Glicenstein, A. Barnacka, M. Vivier, and T. Herr (H.E.S.S.), in *33rd International Cosmic Ray Conference* (2013) arXiv:1307.4898 [astro-ph.HE] .

[527] A. A. Abdo *et al.*, Astropart. Phys. **64**, 4 (2015), arXiv:1407.1686 [astro-ph.HE] .

[528] S. Archambault (VERITAS), PoS **ICRC2017**, 691 (2018), arXiv:1709.00307 [astro-ph.HE] .

[529] M. Ackermann *et al.* (Fermi-LAT), Astrophys. J. **857**, 49 (2018), arXiv:1802.00100 [astro-ph.HE] .

[530] A. Albert *et al.* (HAWC), JCAP **04**, 026 (2020), arXiv:1911.04356 [astro-ph.HE] .

[531] P. Dave and I. Taboada (IceCube), PoS **ICRC2019**, 863 (2021), arXiv:1908.05403 [astro-ph.HE] .

[532] R. López-Coto, M. Doro, A. de Angelis, M. Mariotti, and J. P. Harding, JCAP **08**, 040 (2021), arXiv:2103.16895 [astro-ph.HE] .

[533] G. Aardsma *et al.* (SNO), Phys. Lett. B **194**, 321 (1987).

[534] E. Aslanides *et al.* (ANTARES), (1999), arXiv:astro-ph/9907432 .

[535] A. Bazarko (MiniBooNE), Nucl. Phys. B Proc. Suppl. **91**, 210 (2001), arXiv:hep-ex/0009056 .

[536] J. Ahrens *et al.* (AMANDA), Phys. Rev. D **66**, 012005 (2002), arXiv:astro-ph/0205109 .

[537] S. Fukuda, Y. Fukuda, T. Hayakawa, E. Ichihara, M. Ishitsuka, Y. Itow, T. Kajita, J. Kameda, K. Kaneyuki, S. Kasuga, *et al.*, Nuclear Instruments and Methods in Physics Research Section A: Accelerators, Spectrometers, Detectors and Associated Equipment **501**, 418 (2003).

[538] S. K. Lee, M. Lisanti, A. H. G. Peter, and B. R. Safdi, Phys. Rev. Lett. **112**, 011301 (2014), arXiv:1308.1953 [astro-ph.CO] .

[539] G. Cowan, K. Cranmer, E. Gross, and O. Vitells, Eur. Phys. J. C **71**, 1554 (2011), [Erratum: Eur.Phys.J.C 73, 2501 (2013)], arXiv:1007.1727 [physics.data-an] .

[540] L. Necib, J. Moon, T. Wongjirad, and J. M. Conrad, Phys. Rev. D **95**, 075018 (2017), arXiv:1610.03486 [hep-ph] .

[541] W. Cho, K.-Y. Choi, and S. M. Yoo, Phys. Rev. D **102**, 095010 (2020), arXiv:2007.04555 [hep-ph] .

[542] A. Granelli, P. Ullio, and J.-W. Wang, JCAP **07**, 013 (2022), arXiv:2202.07598 [astro-ph.HE] .

[543] H. An, M. Pospelov, J. Pradler, and A. Ritz, Phys. Rev. Lett. **120**, 141801 (2018), [Erratum: Phys.Rev.Lett. 121, 259903 (2018)], arXiv:1708.03642 [hep-ph] .

[544] J. Iguaz, J. Iguaz, P. D. Serpico, P. D. Serpico, T. Siegert, and T. Siegert, Phys. Rev. D **103**, 103025 (2021), [Erratum: Phys.Rev.D 107, 069902 (2023)], arXiv:2104.03145 [astro-ph.CO] .

[545] G. Elor, R. McGehee, and A. Pierce, Phys. Rev. Lett. **130**, 031803 (2023), arXiv:2112.03920 [hep-ph] .

[546] J. Liang, Z. Liu, and L. Yang, JHEP **05**, 184 (2022), arXiv:2111.15533 [hep-ph] .

[547] J. H. Chang, R. Essig, and S. D. McDermott, JHEP **09**, 051 (2018), arXiv:1803.00993 [hep-ph] .

[548] T. Li and J. Liao, Phys. Rev. D **106**, 055043 (2022), arXiv:2203.14443 [hep-ph] .

[549] A. D. Dolgov and N. A. Pozdnyakov, (2020), arXiv:2009.04361 [hep-ph] .

[550] A. D. Dolgov and N. A. Pozdnyakov, Phys. Rev. D **104**, 083524 (2021), arXiv:2107.08231 [hep-ph] .

[551] Y. F. Perez-Gonzalez and J. Turner, Phys. Rev. D **104**, 103021 (2021), arXiv:2010.03565 [hep-ph] .

[552] S. Jyoti Das, D. Mahanta, and D. Borah, JCAP **11**, 019 (2021), arXiv:2104.14496 [hep-ph] .

[553] G. Agazie *et al.* (NANOGrav), Astrophys. J. Lett. **951**, L8 (2023), arXiv:2306.16213 [astro-ph.HE] .

[554] D. J. Reardon *et al.*, Astrophys. J. Lett. **951**, L6 (2023), arXiv:2306.16215 [astro-ph.HE] .

[555] J. Antoniadis *et al.* (EPTA, InPTA:), Astron. Astrophys. **678**, A50 (2023), arXiv:2306.16214 [astro-ph.HE] .

[556] H. Xu *et al.*, Res. Astron. Astrophys. **23**, 075024 (2023), arXiv:2306.16216 [astro-ph.HE] .

[557] N. S. Pol *et al.* (NANOGrav), Astrophys. J. Lett. **911**, L34 (2021), arXiv:2010.11950 [astro-ph.HE] .

[558] H. Middleton, A. Sesana, S. Chen, A. Vecchio, W. Del Pozzo, and P. A. Rosado, Mon. Not. Roy. Astron. Soc. **502**, L99 (2021), [Erratum: Mon.Not.Roy.Astron.Soc. 526, L34 (2023)], arXiv:2011.01246 [astro-ph.HE] .

[559] V. Vaskonen and H. Veermäe, Phys. Rev. Lett. **126**, 051303 (2021), arXiv:2009.07832 [astro-ph.CO] .

[560] V. De Luca, G. Franciolini, and A. Riotto, Phys. Rev. Lett. **126**, 041303 (2021), arXiv:2009.08268 [astro-ph.CO] .

[561] K. Kohri and T. Terada, Phys. Lett. B **813**, 136040 (2021), arXiv:2009.11853 [astro-ph.CO] .

[562] G. Domènech and S. Pi, Sci. China Phys. Mech. Astron. **65**, 230411 (2022), arXiv:2010.03976 [astro-ph.CO] .

[563] K. Inomata, M. Kawasaki, K. Mukaida, and T. T. Yanagida, Phys. Rev. Lett. **126**, 131301 (2021), arXiv:2011.01270 [astro-ph.CO] .

[564] A. Talebian, S. A. Hosseini Mansoori, and H. Firouzjahi, Astrophys. J. **948**, 48 (2023), arXiv:2210.13822 [astro-ph.CO] .

[565] S. Balaji, G. Domènech, and G. Franciolini, JCAP **10**, 041 (2023), arXiv:2307.08552 [gr-qc] .

[566] A. Afzal *et al.* (NANOGrav), Astrophys. J. Lett. **951**, L11 (2023), arXiv:2306.16219 [astro-ph.HE] .

[567] J. Kopp, V. Niro, T. Schwetz, and J. Zupan, Phys. Rev. D **80**, 083502 (2009), arXiv:0907.3159 [hep-ph] .

[568] Lee, Samuel K. and Lisanti, Mariangela and Mishra-Sharma, Siddharth and Safdi, Benjamin R., Phys. Rev. D **92**, 083517 (2015), arXiv:1508.07361 [hep-ph] .

[569] C. Bunge, J. Barrientos, and A. Bunge, Atomic Data and Nuclear Data Tables **53**, 113 (1993).